DGCR8 Phosphorylation Mediates the Repair of UV-induced DNA Lesions Independently of MicroRNA Processing

Philamer Corpuz Calses

A dissertation
submitted in partial fulfillment
of the requirements for the degree of

Doctor of Philosophy

University of Washington

2015

Reading Committee:
Toshiyasu Taniguchi, Chair
Paul Nghiem
Edith Wang

Program Authorized to Offer Degree:
Molecular and Cellular Biology

University of Washington

Abstract

DGCR8 Phosphorylation Mediates the Repair of UV-induced DNA Lesions Independently of MicroRNA Processing

Philamer Corpuz Calses

Chair of the Supervisory Committee:
Affiliate Associate Professor Toshiyasu Taniguchi
Department of Pathology

Ultraviolet (UV) radiation generates toxic and mutagenic DNA lesions such as cyclobutane pyrimidine dimers (CPDs) and 6-4 pyrimidine-pyrimidone photoproducts (6-4PPs) and is a carcinogen. MicroRNAs have been implicated in cellular response to UV. However, mechanisms connecting the microRNA biogenesis machinery and UV response are unknown. Here we show a critical role of DGCR8, an RNA binding protein in the microRNA processing Drosha-DGCR8 complex, in repair of UV-induced DNA lesions. Treatment with UV (UV-C and UV-B) induced phosphorylation on Serine 153 (S153) of DGCR8 in human cells. DGCR8-deficient cells were hypersensitive to UV and deficient in removal of UV-induced CPDs and 6-4PPs. Phosphorylation of S153 was critical for removing CPDs and 6-4PPs and cellular resistance to UV, but not for microRNA expression. In contrast, the RNA-binding and the Drosha-binding activities of DGCR8 were not critical for UV resistance. DGCR8 depletion did not sensitize cells deficient in CSA, CSB or XPA, the genes involved in transcription-coupled nucleotide excision repair (TC-NER), to UV, while it sensitized wild-type or XPC-deficient cells to UV. DGCR8-depleted cells and S153A DGCR8 mutant cells showed delayed recovery of RNA

synthesis after UV exposure, further suggesting that phosphorylation of S153 is involved in TC-NER. Interestingly, Drosha-depleted cells were UV sensitive, but proficient in repairing UV-induced DNA lesions. Thus, UV-inducible phosphorylation on S153 of DGCR8 mediates TC-NER of UV-induced DNA lesions in a manner independent of microRNA processing and Drosha. Our study revealed an unexpected role of DGCR8 in TC-NER and establishes a novel UV-response signaling pathway (the DGCR8-mediated UV response pathway) that connects the microRNA biogenesis machinery and DNA repair of UV-induced DNA damage. Since both the microRNA biogenesis machinery and DNA repair have been implicated in human diseases including cancer, these findings provide novel insights into our understanding of such diseases.

TABLE OF CONTENTS

LIST OF FIGURES

LIST OF TABLES

ACKNOWLEDGEMENTS

Throughout my years in graduate school, I have been very fortunate to have worked with and mentored by outstanding scientists. I am very proud to call them my colleagues and my friends. First and foremost, I would like to thank my graduate school advisor, Toshiyasu Taniguchi, for his unwavering support, for his excellent guidance and for putting together a fun, diverse and scientifically stimulating environment this past six years. He took a chance on a nervous, fairly naïve first year graduate student to work on a risky, new project for the lab. His meticulous scientific approach is both rigorous, yet inspiring. He allowed me to explore all possibilities and new techniques for this project. I am very grateful to have been mentored by him.

I would like to extend my gratitude to my committee members, Drs. Paul Nghiem, Jonathan Cooper, Edith Wang, Alan Weiner and former committee member, Muneesh Tewari. They have provided many invaluable advice, guidance and most importantly, honestly and encouragement these past years. I would like to thank Drs. Edith Wang and Paul Nghiem for reading this dissertation and providing feedback and suggestions.

I would also like to thank the current and former members of Taniguchi lab. I am incredibly appreciative to have worked with an open-minded and intellectually stimulating group of people. First and foremost, I would like to thank my partner-in-crime, bay-mate and great friend, Dr. Kiran Dhillon for her encouragement, for her scientifically stimulating discussions and for her genuine care of my well-being these past years. I also want to thank Antonio Abeyta and Drs. Jen-Wei Huang, Maria Castella, Ronald Cheung, Celine Jacquemont and Yemin Wang for their very helpful discussions

and technical advice to complete my dissertation. They certainly have groomed me to be a successful scientist.

Last and certainly not least, I want to thank my family. My grandparents and my parents have given me so much and taught me the value of education—for that I will always be thankful. Their love, hard work, patience, support (financially and emotionally) and encouragement were my fuel to pursue a higher education. They have instilled the value of always finding happiness in whatever I do with my life. I would also like to thank my sisters for their love and support. Finally, I would like to thank my fiancé, Reed Probus, for his love, encouragement and support these past years. His patience and understanding, especially the last couple of months of my dissertation have kept me levelheaded.

DEDICATION

To my grandparents: Dominga and Loreto Corpuz
To my parents: Marilyn and Henry Malinay
To my late father: Eduardo Calses

CHAPTER ONE

Introduction

Being tanned is beautiful. Every summer, people flock to the beaches to bathe under the sun, which emits ultraviolet (UV) light that causes the skin to produce a dark pigment, melanin, resulting in a tanned skin tone[1]. While UV exposure does have its health benefits, including the production of vitamin D, over-exposure leads to sunburns, photo-aging and more serious conditions[2]. Skin cancer, the most common type of cancer in the United States, is caused by UV radiation. UV light is subdivided into three spectrum segments based on their wavelengths: UV-A (320-400nm), UV-B (295-320nm) and UV-C (100-295nm)[3, 4]. Although the earth's ozone layer can efficiently absorb wavelengths up to 310nm, progressive depletion of the ozone layer is allowing shorter wavelengths of UV light to reach the earth's surface[3]. At the DNA level, UV radiation forms DNA photoproducts that block replication, transcription, and cause DNA breaks that result in cell cycle arrest, apoptosis or proliferative transformation **(Fig 1.1)**[3]. These DNA photoproducts, namely, cyclobutane pyrimidine dimers (CPDs) and 6-4 pyrimidine-pyrimidone (6-4PPs), are efficiently produced by UV-C because DNA molecules can absorb UV irradiation up to 260nm[3-6]. CPDs arise as a result of covalent bonding between the carbon5'-carbon6'-pyrimidine to the adjacent carbon5'-carbon6'-pyrimidine, while 6-4PPs arise from covalent bonding between carbon6'-pyrimidine to the adjacent carbon4'-pyrimidine[3, 4]. These bulky DNA adducts act as a physical block for DNA polymerase during replication causing the replication fork to stall and, if left unrepaired, can cause single and double strand breaks resulting in cell cycle delay,

cellular senescence, apoptosis or proliferative transformation[3]. Likewise, active transcription can be interrupted by these DNA lesions from RNA polymerase stalling and, if left unrepaired, results in the synthesis of defective RNA molecules **[4].**

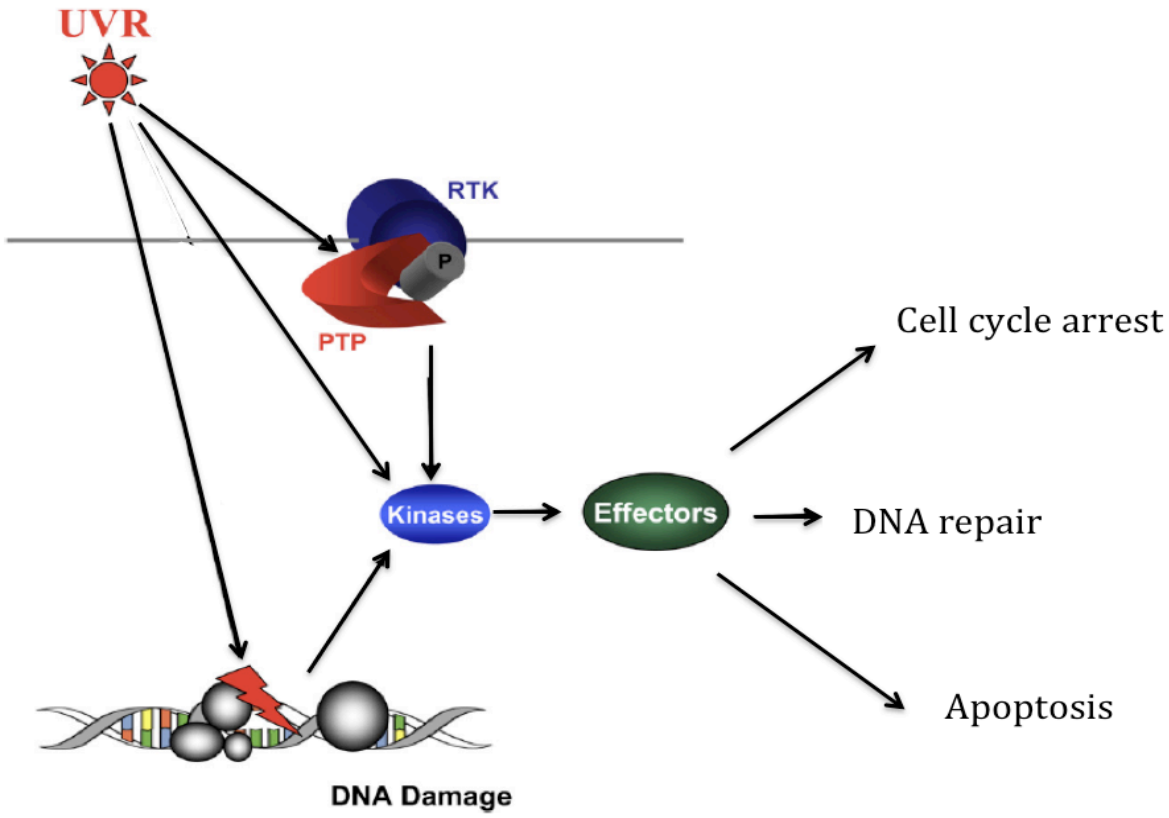

Figure 1.1. Cellular response to UV radiation.
UV irradiation (UVR) triggers at least two types of response: response from DNA damage induced by UVR and a response independent of DNA damage. DNA damage induced by UVR is recognized by sensor proteins that activate kinases that further activate effector proteins. While DNA damage independent response is induced by inactivation of phospho-tyrosine phosphatases (PTP) or by direct activation of kinases, which activates the autophosphorylation of receptor tyrosine kinases (RTK) that activate kinases that further activate effector proteins. Both pathways mediate cell cycle arrest, DNA repair and apoptosis. Adapted figure from [7].

To repair UV-induced DNA photoproducts, mammalian cells activate the nucleotide excision repair (NER) pathway **(Fig. 1.2)** [3, 8, 9]. The NER pathway operates in two subpathways: global genome repair (GGR) and transcription-coupled repair (TC-NER)[10]. GG-NER subpathway is triggered by the recognition of damage sites anywhere in the genome, while TC-NER is triggered by the recognition of DNA lesions during transcription[10]. In GG-NER, repair begins with recognition of pyrimidine dimers by DNA damage binding protein 1 and 2 (DDB1/DDB2) heterodimer along with XPE and XPC. Then, TFIIH basal transcription factor complex, which contains XPB and XPD helicases are recruited to UV-induced DNA lesions, which denatures DNA flanking the pyrimidine dimers[8]. In TC-NER, RNA polymerase I or II arrest during transcription leads to recruitment of Cockayne syndrome A (CSA) and B (CSB) proteins. GG-NER and TC-NER converge in a common downstream pathway after recognition. RPA polymerizes at the single-stranded DNA (ssDNA) exposed upon denaturation along with the independent recruitment of XPA which facilitate in stabilizing the unwound DNA[10]. Endonuclease XPF associates with XPA, to cut the 5' end of the damage site, while endonuclease, XPG, acts to cut the 3' end, releasing approximately 30bp of ssDNA. Subsequently, the ssDNA gap is filled by DNA polymerase, followed by ligation of the DNA nicks by DNA ligase[10].

In S-phase, replication can resume at this site if the barrier is excised and DNA polymerase fills the ssDNA gap. However, if the ssDNA gap is not filled and replication continues, a one-ended double strand break can form, activating ATM protein (ataxia telangiectasia mutated), which phosphorylates many substrates involved in many

biological processes such as DNA damage response and DNA repair [6].

During replication, UV-induced DNA damage activates ataxia telangiectasia-mutated and Rad3-related (ATR). ATR phosphorylates many substrates including a checkpoint kinase, CHK1, histone H2AX, RPA2 and XPA[6]. ATR phosphorylates several sites of RPA that inhibits replication[11]. In addition, ATR-mediated phosphorylation of XPA is important for cell survival after UV treatment[12]. ATR is required for UV-induced XPA foci formation[13]. These findings suggest that ATR could modulate the cellular activity of NER through phosphorylation.

Deficiencies in NER in humans are associated with an autosomal recessive genetic disorder called *Xeroderma pigmentosum (XP), Cockayne Syndrome (CS), Cerebro-oculo-facio-skeletal syndrome (COFS), UV-sensitive syndrome (UVSS) and trichothiodystrophy (TTD)*. Clinically, patients with these disorders range in phenotypic severity that is largely dependent on which NER genes are mutated in the NER pathway. For example, patients with mutations in genes only in GG-NER like XP complementation group C (XPC) and XP complementation E (XPE) are hyper-sensitive to UV and prone to skin cancers and internal tumors [3, 4, 9]. CS patients that harbor mutations in TCR genes, CSA and CSB, result in photosensitivity, severe progressive neurodevelopmental disorder, premature aging and reduced life expectancy. Mutations in genes encoding TFIIH subunits XPD and XPB results in TTD, which presents as CS with brittle nails and hair, and scaly skin. A more severe form of CS, COFS, is caused by mutations in CS genes coupled with mutation in genes in GG-NER, while UVSS patients show a milder CS phenotype with UV sensitivity, but lack the severe neurodevelopmental deficits and

predisposition to skin cancer. The spectrum of mutation in these disorders strongly suggests that proteins in the NER pathway are crucial for protection from the DNA-damaging effects of UV radiation.

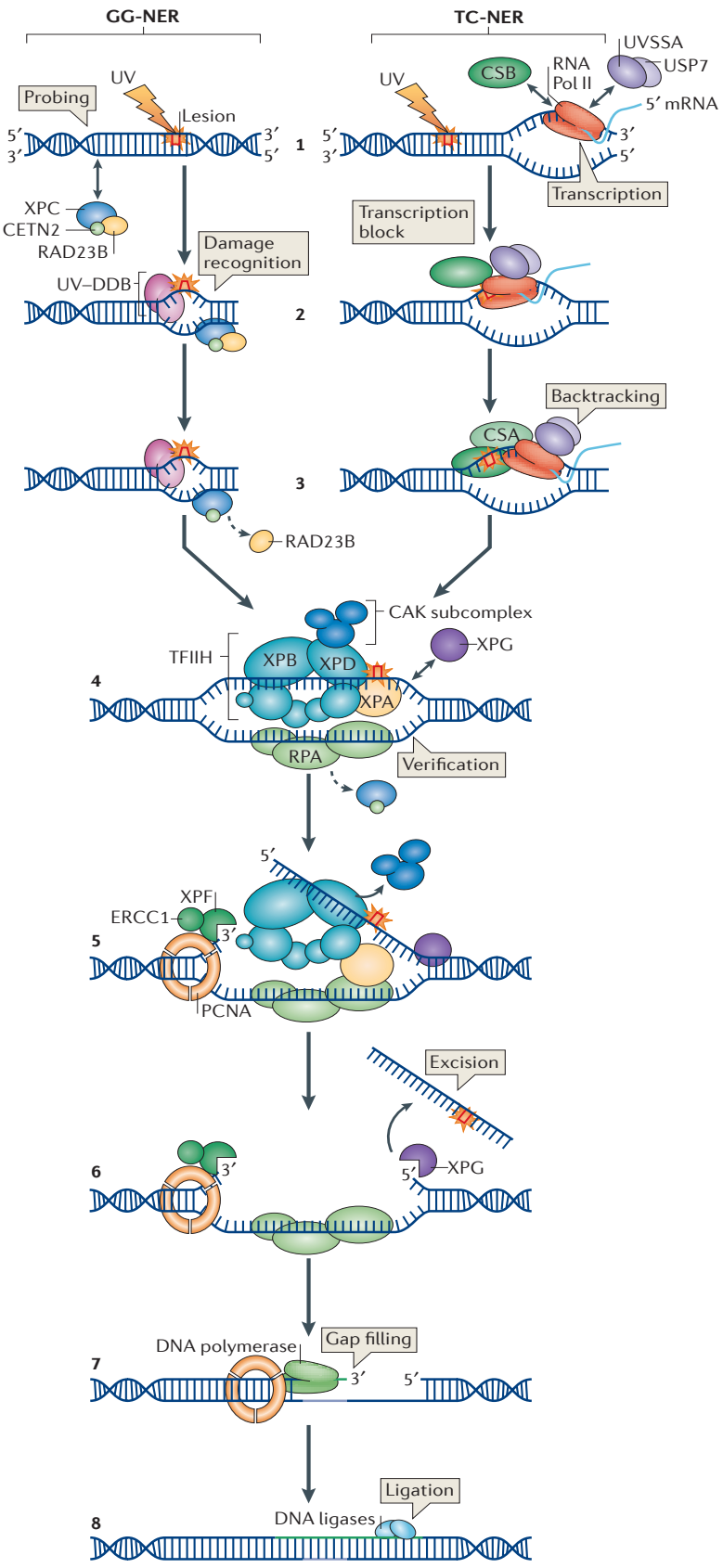

Figure 1.2. Nucleotide Excision Repair Pathway (NER) is divided into two subpathways: Global Genome Repair (GG-NER) and Transcription Coupled-Repair. In GG-NER DDB proteins along with XPC recognize UV-induced DNA lesions, while in TC-NER, RNA polymerase II stalls and recruits CSB, CSA, USSA and USP7 at UV-induced DNA lesions. Both pathways converge in a common pathway that initiates the repair. First, RPA proteins coat the single stranded DNA and recruit other XP proteins including XPA and TFIIH factors. Then, the 5'end is resected by XPF followed by 3'end resection by XPG. Once the UV-damage DNA strand is completely resected, DNA polymerase fills in the gap followed by ligation by DNA ligase. Adapted from [9].

Signal Transduction After UV Radiation Independent of DNA Damage

In addition to UV-induced DNA damage response that is mediated by the canonical ATR/CHK1 and ATM/CHK2 pathways, several other UV-induced signaling pathways are activated independent of DNA damage [14, 15]. This event is first triggered by ligand-independent auto-phosphorylation of several receptor tyrosine kinases including epidermal growth factor receptor (EGFR), which activate a network of downstream effector molecules[10].

First, general stress response pathways involving mitogen-activated protein kinases (MAPKs), including extracellular signal-regulated kinases (ERKs), c-Jun NH_2-terminal kinases (JNKs) and the p38 kinases are activated. The MAPK pathways are activated in response to extrinsic and intrinsic stimuli including, but not limited to growth factors, reactive oxygen species and DNA damage that drives cellular changes such as proliferation and apoptosis[16]. In response to UV-irradiation, JNK and p38 are activated independent of ATR, suggesting that UV irradiation can cause cellular stress or lesions other than DNA damage[3, 14, 17]. Second, p38 activates CK2, which further activates nuclear factor kappa B (NF-κB) pathway to attenuate apoptosis [17]. Third, AMP-activated protein kinase (AMPK), is activated in response to cellular stresses that deplete ATP, which mediates apoptosis in response to UV-irradiation[18]. Finally, several other kinases such as p70 S6 kinase ($p70^{S6K}$), phosphatidylinositol 3-kinase (PI3K) and protein kinase C are activated in response to UV-irradiation [16, 19]. Taken together, UV irradiation activates several kinases in addition to kinases activated by DNA damage (ATR, CHK1, ATM and CHK2) [16].

MicroRNAs

MicroRNAs (miRNAs) are short (~22nt), non-protein-encoding, single-stranded RNA molecules that have emerged as a class of post-transcriptional negative regulators of gene expression[20]. MiRNAs are widely expressed in viruses, plants and animals[21]. Most miRNAs are evolutionarily conserved but differ in the miRNA seed sequence. They have been implicated in the regulation of many biological processes such as development, differentiation and disease[20]. More than 2500 miRNAs have been identified in the human genome and have been predicted to target over 60% of the human transcriptome[22].

MicroRNAs and UV Stress Response

In spite of the growing interests in miRNAs and its role in all aspect of biology, surprisingly little is known about their role in UV stress response and how miRNA are regulated in physiological and pathological conditions. Recent miRNA profiling revealed only a subset of miRNAs change [23-25] and the pattern is distinct at different times after UV radiation[25]. Interestingly, caffeine-mediated inhibition of ATR and ATM kinases alters some of these UV-responsive miRNAs, suggesting that ATR and ATM regulated miRNA expression after UV radiation[25]. NF-kappaB transcriptionally increases miR-125b and suppresses p38α to promote cell survival after UV[26]. Additionally, miR-125b represses p53 expression and attenuates apoptosis[27]. In turn, p53 enhances the post-transcriptional processing of several miRNAs such as miR-16, -143, and -145 to subsequently regulate cell cycle and proliferation after genotoxic stress [28, 29]. The interplay between UV radiation, p53 and miRNAs remains to be

elucidated.

Additional studies show that miRNAs are emerging players in UV stress response. MiR-16 or miR-221 is induced by UVC and represses cell cycle regulator, CDC25a or cyclin-dependent kinase inhibitor p27Kip1, respectively[25]. MiR-22 is increased and represses tumor suppressor gene phosphatase and tensin homolog (PTEN) to promote cell survival after UV[30]. Overexpression of miR-638 represses BRCA1 and increases cellular sensitivity to UV and other DNA damaging agents[31]. UVA-induced expression of miR-23b directly represses related RAS vital oncogene hololog2 (RRAS2), a highly expressed gene in aggressive malignant skin cancer[32]. Importantly, depletion of Dicer and Ago2, factors required for miRNA biogenesis, leads to cellular hypersensitivity to UV [25]. These findings suggest that miRNAs play an important role in cellular response to UV. However, the mechanisms by which miRNA expression is altered upon UV irradiation are largely unknown.

MicroRNA Biogenesis

MiRNA biogenesis **(Fig. 1.3)** is initiated in the nucleus. MiRNA genes are located in intergenic and intragenic regions of the genome. They are transcribed by RNA polymerase II or III to produce long mono- or polycistronic primary miRNA (pri-miRNAs) transcripts that form a hairpin-like secondary structure that have 7-methyl guanylate cap at the 5' end and poly (A) tail at the 3' end[20, 33]. The hairpins are subsequently excised by the microprocessor complex, which consists of Drosha, an RNase III endonuclease, and DGCR8, a double-stranded RNA binding protein, to generate ~70nt precursor miRNAs [20]. More specifically, primary miRNAs are recognized by DGCR8,

which acts as a ruler to direct Drosha to cleave ~11bp away from ssRNA-dsRNA junction [34]. Then, precursor miRNAs bind to a nuclear export protein, exportin-5, and are translocated to the cytoplasm where they are cleaved near the terminal loop by another RNase III, Dicer, and its dsRNA-binding partners TRBP2 (TRBP) and PACT, to generate a ~22-nt miRNA duplex. The strand that is less thermodynamically stable (less stable base-pairing) of the miRNA duplex ends is preferentially loaded into the miRNA-induced silencing complex (miRISC), which consists of Dicer, TRBP, PACT and Argonaute proteins. The strand loaded into the miRISC complex is called the guide strand, which directs the miRISC complex to its mRNA target. The other strand, the passenger strand, is subsequently degraded by an unknown mechanism. The miRNA/miRISC complex mainly binds to the 3' untranslated region of the target mRNA in a sequence-dependent manner. The sequence complementarily of the miRNA seed sequence (5' region of the miRNA centered on nt 2-7) to its target mRNA is sufficient for translational repression, mRNA cleavage or decay [35, 36]. In a rare event, in which there is perfect complementarily between the miRNA and its target mRNA, the mRNA is cleaved by the endonuclease, Argonaute 2, a cofactor of the miRISC complex.

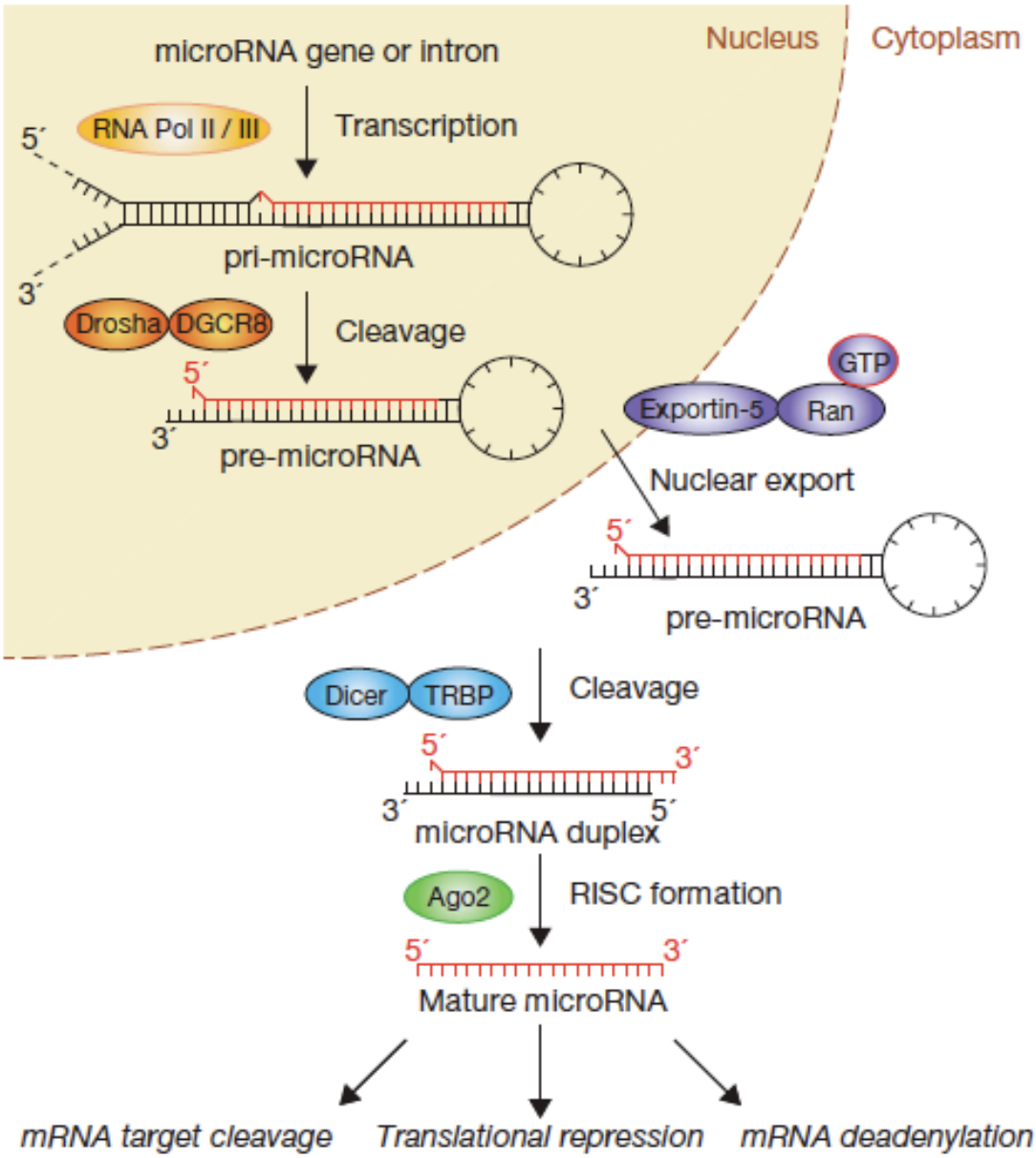

Figure 1.3 MicroRNA Biogenesis. MiRNA genes are transcribed from intergenic and intragenic regions of the genome to produce long mono- or polycistronic primary miRNA (pri-miRNAs) transcripts that form a hairpin-like secondary structure. The hairpins are subsequently excised by the microprocessor complex, which consists of Drosha, an RNase III endonuclease, and DGCR8, a double-stranded RNA binding protein, together form the microprocessor complex that generate ~70nt precursor miRNAs. Subsequently, precursor miRNAs form a complex with nuclear export protein, exportin-5, and are translocated to the cytoplasm where they are cleaved near the terminal loop by another RNase III, Dicer, and its binding partner, TAR RNA-binding protein (TRBP2), to generate a ~22-nt miRNA duplex. The miRNA duplex is loaded and unwound by Argonaute proteins forming the pre-RNA-induced silencing complex (Pre-RISC). A strand of the miRNA duplex forms the mature RISC and subsequently, targets its complementary mRNA for degradation or translational repression. Adapted from [21].

DiGeorge Syndrome Critical Region 8 (DGCR8)

DGCR8 (**Fig 1.4**) was identified as a Drosha-associated peptide that is a vital part of the microprocessor complex (DGCR8 and Drosha) for miRNA biogenesis [37]. More specifically, DGCR8 is a double stranded RNA binding protein that anchors and recognizes the stem region of pri-miRNAs and allows its RNase III binding partner, Drosha, to cleave ~11 base-pairs from the base of pri-miRNAs [38-42]. DGCR8 contains a nuclear localization signal (NLS) at the N-terminus, a WW repeat, two dsRNA binding domains (DRBD1/2) which are required for the recognition of pri-miRNAs[41], and a Drosha binding domain at the C-terminus. N-terminal region of DGCR8 is required for its nuclear localization. In addition, a heme group promotes the dimerization of DGCR8 that further promotes the cooperative trimer of DGCR8 dimers to facilitate pri-miRNA processing[42-45]. A partial crystal structure from amino acid 493-720 revealed that the DRBD1/2 is tightly packed against the C-terminal helix [41].

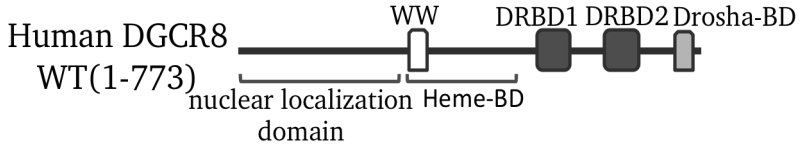

Figure 1.4 Schematic Representation of DGCR8. DGCR8 is an evolutionarily conserved protein with a N-terminal region, which is required for nuclear localization, a Heme-binding domain (Heme-BD), a tryptophan domain (WW domain), two dsRNA binding domains (DRBDs) and a Drosha binding (Drosha-BD).

Aside from the DGCR8 functions and significance in human disease and disorders highlighted above, many other studies revealed that DGCR8 is an essential gene that upon disruption leads to a dynamic range of biological consequences. To start, homozygous Dgcr8 knock-out mice die at embryonic day (E) 6.5. Embryonic stem cells

from these mice show a global loss of miRNAs, proliferation and cycle defects [46]. Dgcr8 heterozygous mice revealed partially impaired miRNA biogenesis and an accumulation of pri-miRNAs[47]. The neurons from the dgcr8 heterozygous mice have altered short-term plasticity in the prefrontal cortex and have smaller dendritic spines with reduced dendritic complexity [47, 48]. As mentioned above, monoallelic deletion on human chromosome 22q11.2 region contributes to DiGeorge syndrome, which is characterized by developmental, neurological and behavior abnormalities[49]. Interestingly in Drosophila, knockout of dgcr8, pasha in Drosophila, shows defects in neuronal morphogenesis different from drosha or ago2 knockout and independent of miRNAs, suggesting a Drosha- and miRNA- independent function of DGCR8[50]. Additionally, specific deletion of DGCR8 in mouse cardiomyocytes leads to dilated cardiomyopathy and premature death and a loss of some miRNAs[51]. Deletion of DGCR8 impairs survival and turnover of peripheral NK cells[52]. Conditional knock-out in vascular smooth muscle reveals extensive liver hemorrhage, dilated blood vessels, and embryonic mortality between E12.5 and E13.5 [53]. Conditional knock-out of Dgcr8 in mouse skin cells shows a depletion of miRNAs rather than other small RNAs including rRNAs and sn/sno-RNAs[54]. These mice survived up to 5-6 days after birth with rough skin, weight gain failure, hair follicle downgrowth into the epidermis and increased apoptosis of mature hair bulbs. Lastly, knockdown of DGCR8 in human fibroblast or murine cells leads to cellular senescence, downregulation of a subset of miRNAs and an upregulation of a cell-cycle inhibitor, p21CIP1[55]. Taken together, DGCR8 is an essential gene that regulates many biological processes.

Regulation of MicroRNA by Transcription Factors

MicroRNA biogenesis is a highly regulated process. First, transcription of miRNA genes, like protein-coding genes, is regulated at the promoter region by transcription factors, enhancers, silencing factors and chromatin modifiers to drive or repress the expression of specific miRNAs [35]. For instance, a transcription factor, Myc, regulates the expression of miRNAs that can influence growth, cell proliferation and apoptosis [56]. Myc induces expression of the miR-17-92 oncogenic cluster in lymphoma cells while inhibiting the expression of the miR-15a/16-1 tumor suppressor cluster. These Myc-induced alterations of miRNA expression can promote tumorigenesis [56, 57]. Similarly, p53 enhances the transcription of the miR-34 and miR-16 families, which induce cell cycle arrest and apoptosis [58].

Interestingly, several miRNAs and transcription factors are regulated through a feedback loop circuit. For example, during myogenesis, miR-1 is induced by Mef2/MyoD and in turn represses HDAC4, which suppresses Mef2/MyoD expression[35]. Similarly, miR-133 is induced by serum response protein (SRF) and in turn suppresses the expression of miR-133 [35]. During megakaryopoiesis, Runx1 induces miR-27a and in turn represses Rux1 expression [35].

Regulation of MicroRNA by Methylation

Promoter methylation status of miRNA genes also affects expression of miRNAs [35, 56]. For example, several miRNAs loci such as miR-193a, -203, and 34b/c, -124, 129-2 are hypermethylated, and their expression are repressed in several human cancers [59-61]. In contrast, miR-let-7a-3 gene is heavily methylated in normal human tissues,

but is re-activated by de-methylation in some lung adenocarcinomas[62]. Moreover, miRNA promoters are also regulated by histone modifications. Mammalian cells treated with histone deacetylase inhibitors change the expression of several miRNAs, suggesting that histone modification adds another layer of transcriptional control to miRNAs expression [63, 64].

Modulation of MicroRNA Biogenesis by Positive and Negative Regulators

Several factors required for miRNA biogenesis are regulated by co-factors to positively or negatively regulate miRNA production **(Fig 1.4)**. The DEAD-box RNA helicases, p68 and p72, interact with the microprocessor complex and are required for processing specific miRNAs. These proteins process one-third of murine primary miRNAs [65]. Knockout of either of these proteins is lethal and shows reduced pre-miRNAs but not pri-miRNAs, suggesting its important role in pri-miRNA processing [65] and perhaps contributing to lethality phenotype in mice. Interestingly, the tumor-suppressor p53 interacts with the microprocessor complex through the association with p68, favorably processing primary miRNAs involved in growth suppression in response to DNA damage [28]. In contrast, Hippo-signaling transducer, YAP, induces miRNA repression by sequestering p72 from binding to the microprocessor complex in a cell density dependent manner [66].

Interestingly, SMAD family proteins, signal transducers of the transforming growth factor β (TGF-β) and bone morphogenetic protein 4 (BMP4), interact with the p68/microprocessor complex, which post-transcriptionally enhance the processing of miR-21 in human primary pulmonary smooth muscle cells [67]. Regulation of these

miRNAs induced by TGF-β and BMP signaling share a conserved sequence at the stem region of primary miRNAs [68]. Similarly, the tumor suppressor, BRCA1, interacts with p68, p72, SMAD3, and p53, induces the processing of specific pri-miRNAs (let7a-1, miR-16-1, miR145 and miR34a) that function as tumor suppressors [69]. Additionally, estrogen receptor α prevents the processing of some miRNAs by interacting with p68, p72 and Drosha [70, 71].

Additionally, several splicing factors bind to conserved regions at the terminal loop of several miRNAs. Heterogeneous nuclear ribonucleoprotein (hnRNP) A1 and KH-type splicing regulatory protein (KSRP) alter the rate of cleavage by the microprocessor complex [35, 36]. Interestingly, hnRNP homolog, TAR DNA-binding protein-43 (TDP-43) [72] and fused in sarcoma/translocated in liposarcoma (FUS/TLS) [73] mediate the processing of a subset of miRNAs by interacting with Drosha in the nucleus and Dicer in the cytoplasm. These studies suggest that co-factors of miRNA biogenesis are important for precise processing of miRNAs because the slightest error in cleaving the primary miRNAs can change their stability and seed sequence that may result in improper miRNA strand incorporation into the RISC complex [35].

In addition to positive regulators, several co-factors negatively regulate miRNA production. NF90-NF45 protein complex binds to primary miRNAs and prevents the microprocessor complex from binding to primary miRNAs, including the let-7 family [74]. Interestingly, LIN-28 binds to the terminal loop of pri-let-7 blocking Drosha and Dicer from cleavage [75]. Similarly, adenosine deaminases that act on RNA (ADARs) catalyze the conversion of adenosine to inosine of many pri- or pre-miRNAs and inhibit

cleavage by Drosha or Dicer, respectively, preventing miRNA maturation[76-78]. In contrast, a recent study shows that ADAR1 interacts with DGCR8 and Drosha, which enhance miRNA production [79].

Lastly, Drosha and DGCR8 regulate each other's expression in that Drosha protein cleaves the hairpins on DGCR8 mRNA, thus destabilizing the mRNA, while the DGCR8 protein acts to stabilize the Drosha protein through protein-protein interaction [80]. Taken together, the microprocessor complex does not act alone in processing primary miRNAs. Several accessory proteins interact and influence the processing of primary miRNAs to precursor miRNAs.

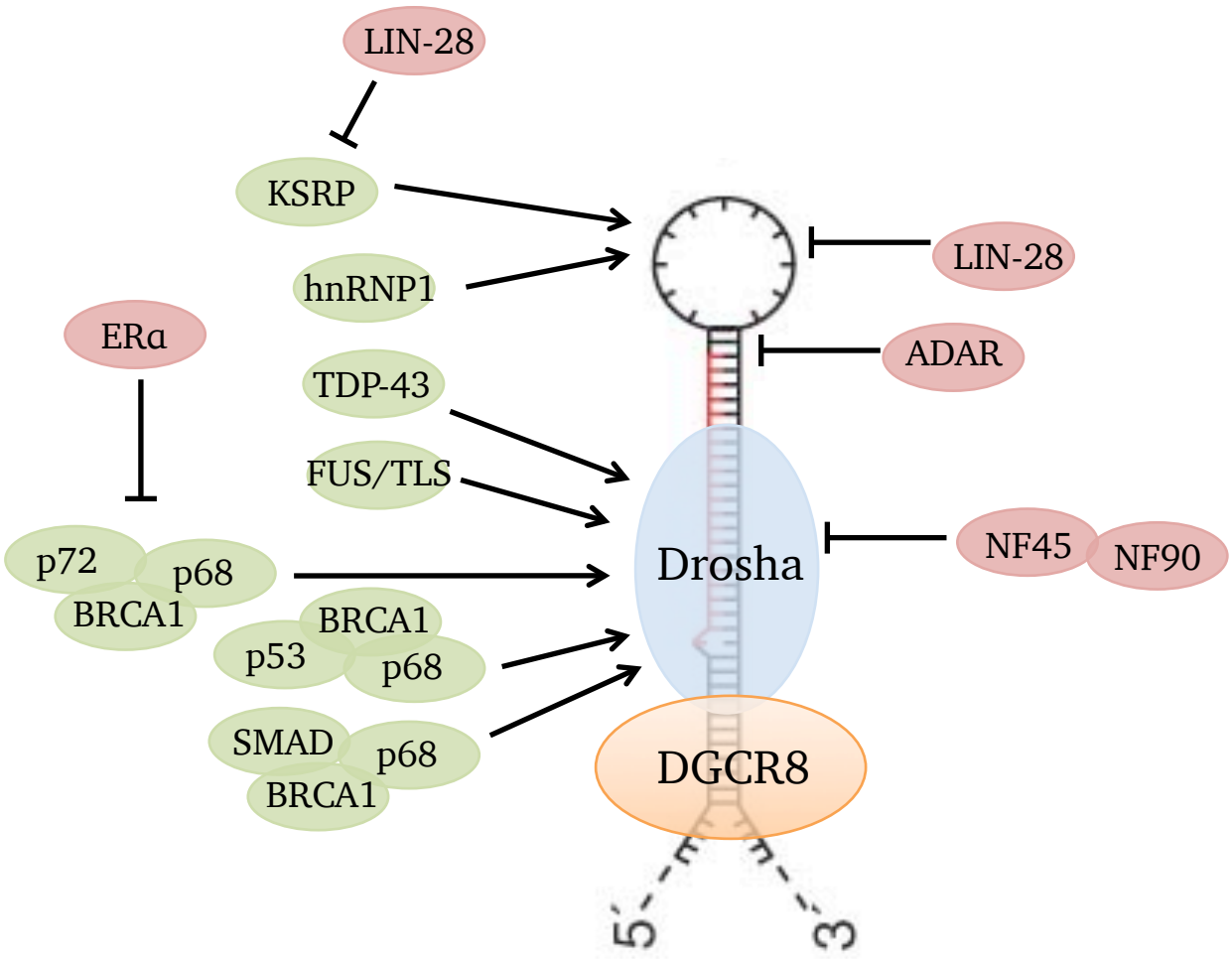

Figure 1.5 Modulation of the Microprocessor Complex by Positive and Negative Regulators. The microprocessor complex which consist of DGCR8 and Drosha catalyze the first step in miRNA maturation by cleaving ~11bp away from the base of primary miRNAs depicted above. Ellipsoids depicted in green are positive, while Ellipsoids depicted in red are negative regulators of the microprocessor complex.

Modulation of MicroRNA Biogenesis by Post-Translational Modifications

MiRNA biogenesis proteins are targeted by signaling pathways through post-translational modifications to fine-tune miRNA production from different physiological conditions **(Fig 1.5)**. DGCR8 is phosphorylated at many phosphorylation sites [81, 82] and 23 of these increases DGCR8 protein stability [83]. Phosphorylation of some these sites are mediated by MAPK/ERK pathway and increases expression of progrowth miRNAs and cellular proliferation. However, it's not clear which of these phosphorylation sites are important for DGCR8 function and activity. Deacetylation of lysine residues in the RNA binding domains of DGCR8 by histone deacetylase 1 (HDAC1) increases its affinity to primary miRNAs, thus increasing miRNA production [84]. Interestingly, phosphorylated Methyl-CpG binding protein 2 (MeCP2) binds to DGCR8, which prevents Drosha from binding resulting in the inhibition of dendritic and spine growth [85].

DGCR8 binding partner, Drosha is phosphorylated by glycogen synthase kinase 3β (GSK3β) that facilitates nuclear localization [86, 87]. Interestingly, heat and hydrogen peroxide-induced N-terminal phosphorylation of Drosha by p38 MAPK results in nuclear export and facilitates its degradation that leads to increased cell death [88]. Moreover, phosphorylation of Drosha interacting protein, p68, by p38 MAPK promotes nuclear localization of p68 and promotes the biogenesis of a subset of miRNAs [89]. TRBP2 is phosphorylated by MAPK/ERK pathway, which increases the stability of its binding partner, Dicer, and increases the expression of pro-growth miRNAs [90]. KH-type splicing regulatory protein (KSRP or KHSRP), a component of the Drosha and Dicer

complex, binds to the terminal loop of miRNAs with GGG motifs, promotes maturation of a subset of miRNAs, and is phosphorylated by a DNA damage responsive kinase, Ataxia-telangiectasia mutated (ATM) [91, 92]. High levels of LIN-28 block the association of KSRP from pri-let-7a[75]. Additionally, LIN-28 promotes the recruitment of TUT4, a terminal poly (U) polymerase that uridylate the 3'end of pre-let-7. This leads to subsequent degradation of pre-let-7 by an unknown RNase[93, 94]. These modifications have emerged as new regulators of miRNAs that affects the stability of miRNAs or impact the cleavage sites by Drosha and Dicer potentially changing the seed sequence, thus its target mRNAs[36]. In addition to uridylation by TUT4, adenylation[95] and methylation[96, 97] are implicated in modifying miRNAs. Interestingly, methyltransferase-like 3 (METTL3) has recently been implicated in methylating pri-miRNAs marking them for recognition and processing by the microprocessor complex[97]. Depletion of METTL3 represses DGCR8 binding to primary-miRNAs, subsequently reducing the miRNA production[97]. Lastly, Ago2 is phosphorylated by MAPK-activated protein kinase 2 (MAPAPK2) in response to arsenite treatment or by ATK3 by an unknown stimulus facilitates its localization to processing bodies (P-bodies)[98]. MAPAKP2-mediated phosphorylation of Ago2 facilitates Ago2 localization to processing bodies (P-bodies)[98], while ATK-3 mediated Ago2 phosphorylation increases translation repression of miRNA targets[99]. Additionally, hydroxylation of Ago2 increases its stability and localization to P-bodies[100]. Furthermore, hypoxia-induced phosphorylation of Ago2 by epidermal growth factor receptor (EGFR) removes Ago2 from Dicer and reduces pre-miRNA processing[101]. In mouse, Ago2 is targeted by

ubiquitylation-mediated proteasomal degradation by LIN41[102]. Taken together, these studies suggest that posttranslational modifications of factors in miRNA biogenesis are integral components in the regulation of miRNAs in response to various stimuli.

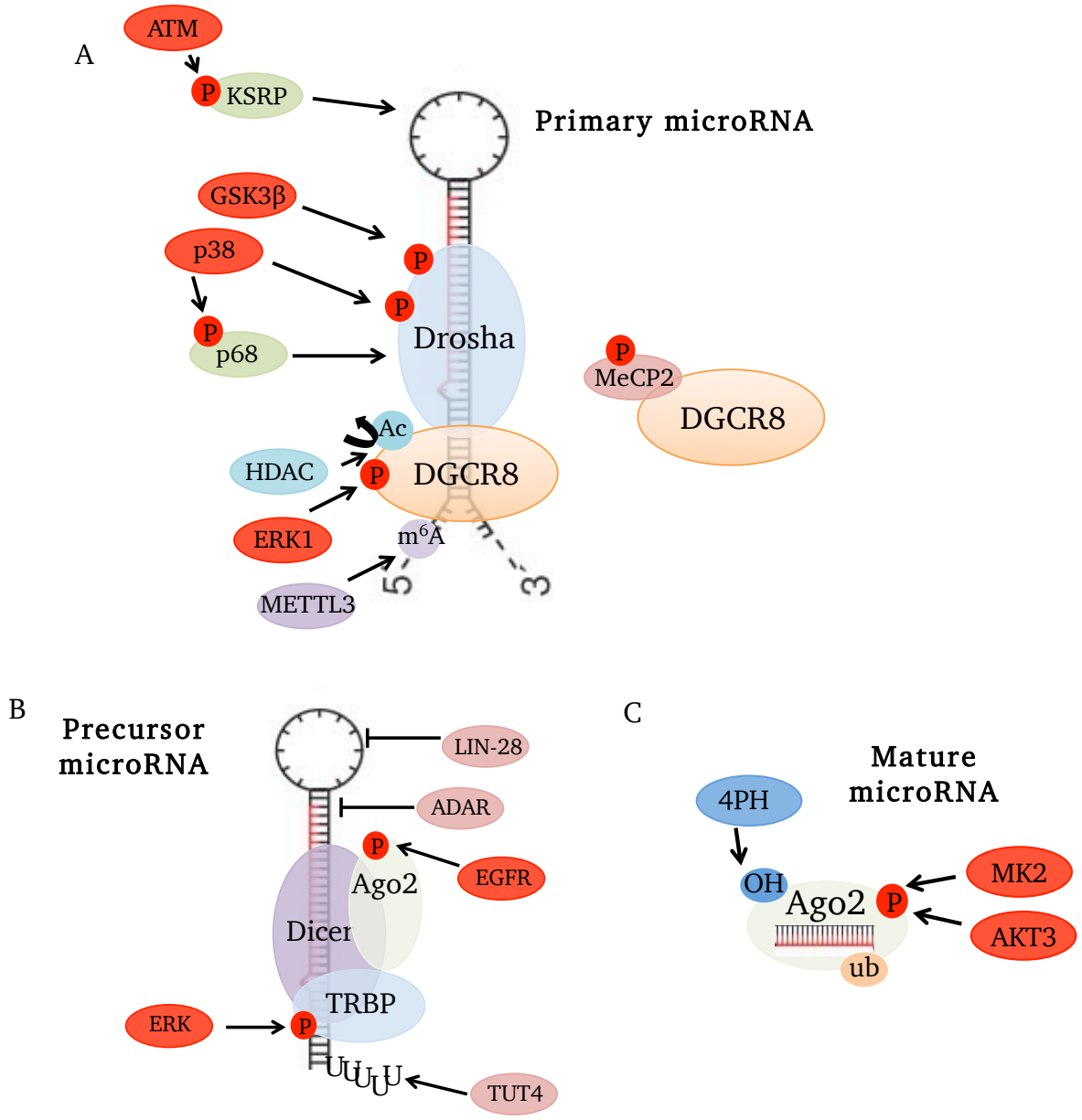

Figure 1.6 Post-translational Modifications of factors involved in microRNA biogenesis. **A.** The microprocessor complex, DGCR8 and Drosha, which cleaves pri-miRNAs are phosphorylated **(P)** by several kinases depicted in red ellipsoids. Histone deacetylase 1 deacetylates **(Ac)** DGCR8 depicted in blue ellipsoid and methyltransferase-like 3 methylates **(m^6A)** pri-miRNAs depicted in purple ellipsoid. Green ellipsoids are co-factors of the microprocessor complex. **B.** Dicer, TRBP and Ago2 bind to pre-miRNAs and are phosphorylated **(P)** by kinases (red ellipsoids). Terminal uridylyltransferase 4 (TUT4) (light red ellipsoids) uridylates pre-miRNAs. Factors that negatively regulate pre-miRNAs are depicted in light red ellipsoids. **C.** Ago2 binds to mature miRNAs and is phosphorylated **(P)** by kinases depicted in red ellipsoids. Type I collagen prolyl-4-hydroxylase (4-PH) hydroxylate Ago2 depicted in blue ellipsoid. Additionally, Ago2 is also ubiquitylated **(ub)**.

Non-canonical Functions of MicroRNA Biogenesis Factors

Although most of the research is focused on clarifying the activity of factors in miRNAs biogenesis and the involvement of miRNAs in many biological processes, some evidence indicates that factors in miRNA biogenesis have non-canonical functions. Drosha recognizes and cleaves the stem loop structures of mRNAs. The first example of this is the autoregulation of the microprocessor complex (Drosha and DGCR8). Drosha cleaves the stem-loop structures at the 5' UTR and destabilizes DGCR8 mRNA, while DGCR8 protein stabilizes Drosha[80]. Similarly, in neurons, Drosha binds and cleaves the stem-loop structures at the 3' UTR of a preneuronal transcription factor, Neurogenin 2 (Ngn2)[103]. The loss of Drosha leads to increased Ngn2 expression that results in neuronal degeneration and interestingly, without the loss of miRNAs [103], suggesting that this phenotype is Drosha-dependent, but miRNA-independent. A global approach revealed that miRNAs are not the most abundant targets of DGCR8 and Drosha, and that many different types of RNAs including mRNAs and long non-coding RNAs (lncRNAs) are targets of DGCR8 and Drosha[104]. Importantly, the study revealed that DGCR8 binds to small nucleolar RNAs (snoRNAs) independently of Drosha and regulates alternative splicing[104]. These studies strongly suggest a miRNA biogenesis-independent activity of the microprocessor complex and that other nucleases other than Drosha may be functionally important for this function.

Interestingly, the microprocessor complex is recruited to chromatin during transcription and processes pri-miRNA co-transcriptionally [105, 106]. Additionally, DGCR8/Drosha along with transcription termination factors, Setx, Xrn2 and Rrp6

induces RNAPII pausing and premature termination at the HIV-1 promoter [107]. Lastly, DNA damage leads to generation of RNA products in a manner dependent on Dicer and Drosha. These RNA products regulate DNA damage-induced foci formation of several DNA repair proteins, cell cycle and cellular senescence[108]. Taken together, these studies suggest a miRNA-independent function of factors involved in the miRNA biogenesis and reveal activities in RNA metabolism.

Components in MicroRNA Biogenesis are Involved in Human Disorders

Defects of the microRNA biogenesis machinery have been implicated in several human diseases. Perhaps the best known and well studied is in the context of cancer where global miRNAs are repressed in cancer tissues relative to normal tissues[109], which highlights the significance of miRNAs in the development and progression of cancer. In fact, some miRNAs have been labeled as drivers in cancer development termed as oncomiRs [109]. For example, the first transgenic mouse overexpressing miR-155 revealed its contribution in the development of high-grade lymphoma[110]. In addition to lymphoma, miR-155 is upregulated in other cancers including lung and breast cancer[109]. In contrast, several miRNAs, including miR-143/145, miR-34a, miR-25 and let-7, function as tumor suppressors miRNAs, because they inhibit tumor progression and are repressed in cancer[109]. These studies suggest that these miRNAs could be clinically relevant targets for cancer therapy. In fact, ongoing research are determining several ways to effectively deliver miRNAs or miRNA inhibitors, using viral vectors[111, 112], cationic lipoplexes[113] and nanoparticles[114, 115] for cancer therapy. Interestingly, miRNAs can be detected in several bodily fluids, including saliva, urine,

serum and plasma that could potentially be useful as biomarkers for some cancers[116, 117]. Arroyo et al. revealed that miRNAs are stabilized in human plasma when in complex with Ago2 [118].

Expression of factors in miRNA biogenesis, including Drosha, DGCR8, XPO5, Dicer, Ago2 and TRBP, are associated with cancer development and progression[119]. Drosha and Dicer expression is associated with poor clinical outcomes in patients in many types of cancers, including ovarian cancer [120], neuroblastoma[121], endometrial cancer[122] and nasopharyngeal carcinoma[123]. DGCR8 is overexpressed in colorectal cancer[124], skin cancer[125], and ovarian cancer[126]. Knockdown of DGCR8 increases ovarian cancer cells sensitivity to cisplatin and reduces proliferation, migration and invasion[126]. Similarly, other factors such as Ago2, TRBP and XPO5 are upregulated in multitude of cancers types[119]. It remains to be determined how these factors are deregulated, and whether they play a direct role in cancer development.

Mutations in some miRNA biogenesis factors have been discovered in human cancer. First, there are multiple nonsynonymous polymorphisms including missense, frameshift and stop variants in DGCR8 and Drosha with some on functional protein domains have been reported[127]. Analyses of patients with Wilms tumor, the most common type of childhood kidney cancer, revealed somatic mutations in Drosha[128-131], DGCR8[128, 129] and Dicer[131]. Some of these mutations lead to reduction of processing of multiple miRNAs[128-131], including the let-7 family, which plays a critical role in regulating MYCN and LIN28 in Wilms tumor[131]. Moreover, inactivating truncation mutations of exportin-5 have been identified in colon cancer, resulting in the

accumulation of precursor-miRNAs in the nucleus [132]. Similarly, inactivating truncation mutations of TRBP have been identified in colon cancer, resulting in the decrease of mature miRNAs, along with Dicer destabilization [133]. These studies suggest that miRNAs and factors in miRNA biogenesis contribute to the development and progression of cancer, have the potential of being a diagnostic tools and targets for therapy in cancer.

The microprocessor complex has been implicated in several behavioral and neurological disorders. First, DGCR8 is one of several genes associated with a human genetic disorder called DiGeorge syndrome with a heterozygous micro-deletion in chromosome 22q11.2 characterized by developmental, cardiac and cognitive deficits[49]. While mouse model for this deletion showed similar phenotypes to the human disorder, changes in miRNAs was minimal, suggesting that DGCR8 may function in an alternative pathway[47]. These mice resulted in altered short-term plasticity and increase risk for schizophrenia[48, 134]. In humans, single-nucleotide polymorphisms (SNPs) in the microprocessor complex genes is associated with increased risk for schizophrenia[135]. Expansion of 55-200 CGG repeats in the 5'UTR of the fragile X mental retardation (FMR1) mRNA is sequestered by the microprocessor complex, resulting in reduced miRNA processing and neuronal cell death in patients with an inherited neurodegenerative disorder called Fragile X-associated tremor/ataxia syndrome (FXTAS)[136]. It remains to be determined which deregulated miRNAs are responsible for this phenotype or whether the microprocessor complex acts as barrier for the expanded FMR1 gene from decay. Mutated microprocessor complex cofactors,

TDP43 and FUS/TLS, cause Amyotrophic Lateral Sclerosis (ALS) and are mislocalized to the cytoplasm[137].

Dissertation Overview

The overall goal of my dissertation was to characterize a discovery of a novel UV inducible phosphorylation site on DGCR8. In chapter two, I describe the identification of several phosphorylation sites on DGCR8. More specifically, I demonstrated that phosphorylation on Serine 153 (S153) on DGCR8 is induced by UV and other cellular stresses in multiple human cell lines. With a phospho-specific antibody that we generated, I found that phosphorylation of S153 on DGCR8 was induced in the nucleus and on chromatin. UV-induced S153 phosphorylation was localized diffusely in the nucleus and not UV-induced DNA damage spots. In chapter three, I describe that DGCR8 and Drosha is essential for cellular resistance to UV radiation. Importantly, phosphorylation on S153 of DGCR8 is required for UV resistance independently of RNA binding and Drosha binding activities of DGCR8. In contrast, DGCR8 binding or RNA binding activities of Drosha is not required for UV resistance. Lastly, I describe that phosphorylation on S153 of DGCR8 is not important for miRNA expression. In chapter four, I describe the role of DGCR8 in removing UV-induced DNA lesions and a link to transcription-coupled nucleotide excision repair. More specifically, I show that phosphorylation on S153 of DGCR8 is required for the removal of UV-induced DNA lesions and is required for efficient recovery of RNA synthesis after UV radiation. Furthermore, I describe that DGCR8 is functionally linked to transcription-coupled nucleotide excision repair, but not global-genome nucleotide excision repair.

Interestingly, phosphorylation on S153 of DGCR8 is not important of microRNA processing. These data suggest that DGCR8 phosphorylation is important for the removal of UV-induced DNA lesions through transcription-coupled repair independently of microRNAs. In chapter five, I describe a global approach in identifying the kinase(s) that phosphorylate S153 of DGCR8 by performing a high-content immunofluorescence screen of a siRNA library that contains over 700 kinases known in the human genome. Similarly, I screened a siRNA library against over 300 DNA damage responsive genes to identify modifiers of S153 phosphorylation. In chapter six, I describe the final conclusion and future directions of my dissertation.

CHAPTER TWO

Identification of UV-induced DGCR8 Phosphorylation Sites

Abstract

Post-translational modifications of proteins play a major role in cellular response to DNA damaging agents, including UV radiation. Here, we describe a novel finding that DGCR8, a critical factor for processing primary-microRNAs (pri-miRNAs), is phosphorylated in response to UV radiation. We identified nine phosphorylation sites on DGCR8 using mass spectrometry. Site-directed mutagenesis of these sites revealed two possible UV-induced phosphorylation sites on DGCR8 (Serine S153 and Serine 377). Using phospho-specific antibodies (anti-phospho S153-human DGCR8 and anti-phospho S377-human DGCR8) we generated, we found that phosphorylation at S153, but not S377 is induced by UV radiation. Phosphorylation at S153 was induced early in response to UV in a time and dose dependent manner in multiple cell lines including human primary fibroblast and keratinocytes. Phosphorylation at S153 was also induced by other cellular stress. These data suggest a role of phosphorylation at S153 in cellular response to UV.

Introduction

MicroRNAs are short, non-coding RNAs that negatively regulate gene expression post-transcriptionally[37]. First, miRNAs are transcribed by RNA polymerase II and produce a large stem-loop structure called primary (pri)-microRNAs[138]. The stem region of these structures are recognized and cleaved ~11 base-pairs from the base by the microprocessor complex, which consists of the double-stranded RNA binding protein, DGCR8, and an RNase III, Drosha. The microprocessor complex generates ~70 nucleotide excised stem-loop, or precursor microRNA (pre-microRNA)[34].

Many proteins are post-transnationally modified by many cellular stresses, including UV radiation. Interestingly, several factors required for miRNA biogenesis are regulated by post-translational modifications. DGCR8 is multiply phosphorylated [81, 82] that functions to increase protein stability [83]. The phosphorylation of some of these sites is mediated by MAPK/ERK pathway and leads to increased expression of progrowth miRNAs and cellular proliferation. However, none of these phosphorylation sites are critical for pri-miRNA processing activity of DGCR8. Deacetylation of lysine residues in the RNA binding domains of DGCR8 by histone deacetylase 1 (HDAC1) increases its affinity to pri-miRNAs, thus increasing miRNA production[84]. DGCR8 binding partner, Drosha is phosphorylated by glycogen synthase kinase 3 β (GSK3 β), and this phosphorylation facilitates nuclear localization of Drosha [86, 87]. Interestingly, heat and hydrogen peroxide-induced N-terminal phosphorylation of Drosha by p38 MAPK results in nuclear export of Drosha and facilitates its degradation, which leads to increased cell death [88]. These data suggest that different signaling pathways may

regulate Drosha in response to different stimuli. However, it was not known whether posttranslational modifications of DGCR8 or Drosha is involved in cellular response to UV. Here, we reveal a novel UV inducible phosphorylation site for DGCR8.

Results

Initially we performed DGCR8 western blotting of cells untreated or treated with UVC and realized that two isoforms of DGCR8 (upper and lower bands) exist in human and murine cells (**Fig 2.1A and 2.1B**). The upper band was upregulated in UVC-treated cells compared to untreated cells (**Fig 2.1A**). This upper band disappeared after treatment with lambda phosphatase and addition of phosphatase inhibitors restored the upper band, suggesting that the upper band represents a phosphorylated isoform and that DGCR8 is phosphorylated after UVC radiation (**Fig 2.1A**). UV-induced phosphorylation on DGCR8 occurred in a time and dose dependent manner (**Fig 2.1C**). To determine which regions of DGCR8 are phosphorylated, we generated several truncation mutants and tested the presence of the upper band after UV radiation by western blotting (**Fig 2.1D**). The appearance of the upper band was observed in the wild-type DGCR8, Δ275, Δ276-773, Δ483, but not Δ484-773 mutants of DGCR8, after UV radiation, suggesting that UV-induced phosphorylation sites were within amino acid 1-483 DGCR8 (**Fig 2.1D**).

To identify sites of phosphorylation, we performed mass spectrometry analysis of immuno-purified DGCR8 protein from UV irradiated or non-irradiated human cells (HeLa cells transduced with FLAG-tagged DGCR8), and identified nine phosphorylation sites (S95, S153, S271, S275, T371, S373, S377, S434 and S619)(**Fig 2.2A-K**). Among

them, phosphorylation of serine 153 (S153) was detected only in the upper band (**Fig 2.2B**) and not the lower band in UV-treated samples, while the other sites were detected in the lower and upper band in untreated and UV-treated samples. We validated each of these sites by generating phospho-mutants using site-directed mutagenesis. The upper band was absent in Δ275-S153A and Δ276-773-S377A UV radiation, suggesting that S153 and S377 are phosphorylated in response to UV in these DGCR8 fragments (**Fig 2.3A**). Next we introduced S153A and/or S377A mutations in full length DGCR8 and tested the effect on the appearance of the upper band of DGCR8. We found that the upper band was absent in S153A and S153A-S377A mutants, but present in S377A mutant (**Fig 2.3B**). This suggests that the upper band of the full length DGCR8 was S153 phosphorylated isoform. Additionally, the lower bands in the S377A and S153A-S377A mutants migrated faster than the lower bands of wild-type DGCR8 and S153A mutant in the western blot, suggesting that phosphorylation at S377 occurred in the lower band (**Fig 2.3B**). S153 or S377 is conserved among mammals or vertebrates, respectively, but not in other eukaryotes (**Fig 2.3C**).

Next, we generated phospho-specific antibodies using a 10 amino-acid peptide flanking S153 or S377 as an immunogen (**Fig 2.3C**). The antibody for S153 recognized the upper band of wild type DGCR8, but not S153A mutant DGCR8, in western blotting (**Fig 2.3D**). Likewise, the antibody for S377 recognized mainly the lower band of wild type DGCR8, but not S377A mutant DGCR8, by western blotting (**Fig 2.3D**). These data indicate that the antibodies are specific. Phosphorylation at S153 was robustly induced in the wild-type cells after UV radiation, while the signal was absent in the S153A

mutant cells (**Fig 2.3D**). In contrast, S377 was basally phosphorylated and not induced by UV in wild type cells, while the signal was absent in the S377A mutant cells (**Fig 2.3D**). Interestingly, in S153A mutant cells, S377 phosphorylation increased after UV treatment, while in S377A mutant cells, S153 phosphorylation was not increased after UV radiation. These results suggest that basal phosphorylation at S377 facilitates the UV-induced phosphorylation at S153 and that S153 phosphorylation in turn attenuates the UV-induced S377 phosphorylation (**Fig 2.3D and 2.3E**). While basal phosphorylation of S377 may play a role in DGCR8 activity, we decided to focus on UV-induced phosphorylation on S153 for further studies, since S153 was the UV-induced phosphorylation site in wild type cells.

S153 of DGCR8 was slightly phosphorylated in untreated cells and the phosphorylation of S153 was increased in response to UVC radiation in a time- and dose-dependent manner (**Fig 2.4A**) in multiple human cell lines, including primary fibroblast and keratinocytes (**Fig 2.4B**). Interestingly, phosphorylation on S153 of DGCR8 was not induced by UVC radiation in a melanoma cells line, Mel-624, and UVC-induced phosphorylation of S153 was delayed in another melanoma cell line, A375 (**Fig 2.4C**). The mechanism behind this phosphorylation defects in melanoma cells remains to be elucidated. Phosphorylation at S153 was also induced by treatments with UVB, and some other chemicals including, 4-nitroquinoline-1-oxide (which mimics UV), hydrogen peroxide, potassium bromate, melphalan, but not with other DNA damaging agents such as cisplatin, mitomycin C, AZD2281 (PARP inhibitor), etoposide and hydroxyurea, and a mitotic inhibitor, paclitaxel (**Fig 2.4D, 2.4E and 2.4F**). This suggest that S153

phosphorylation is induced by bulky DNA adducts and cellular oxidizers.

Subcellular fractionation experiments revealed that S153-phosphorylated DGCR8 was detected in the nuclear soluble and chromatin fractions and was increased after UVC irradiation (**Fig 2.5A**). Next, we performed immunocytochemical analyses of S153 phosphorylation using the S153-DGCR8 phosphospecific antibody we generated (**Fig 2.5B and C**). The S153 phosphorylation signal was weakly detected in untreated cells transfected with control siRNA, while the signal was not detected in DGCR8 siRNA-transfected cells, indicating the specificity of the antibody for immunocytochemistry. After treatment with UVC, the S153 phosphorylation signal was significantly increased (**Fig 2.5B**). The S153 phosphorylation signal was induced diffusely in the nucleus (**Fig 2.5B**) even after localized UV irradiation through a micropore filter (**Fig 2.5C**) indicating that the distribution of S153-phosphorylated DGCR8 is not limited to sites of UV induced DNA lesions.

Discussion

In this study, we discovered that DGCR8 is phosphorylated in response to UV radiation in human and murine cells. Mass spectrometry analysis revealed nine phosphorylation sites of DGCR8 after UV radiation. S153 and S377 on DGCR8 appeared to be the possible sites for UV-induced phosphorylation. Generation of phospho-specific antibodies to these sites revealed interesting kinetics and inter-dependent dynamics between these sites. First, S153 phosphorylation is weakly detected in untreated cells and increased in response to UV radiation in a time and dose dependent manner. In contrast, S377 is basally phosphorylated, but S377 phosphorylation was not increased in

response to UV radiation in wild type cells. Interestingly, these sites appear to regulate each other after UV radiation. Basal phosphorylation on S377 facilitates the phosphorylation on S153 after UV radiation. Conversely, S153 phosphorylation attenuates the induction of phosphorylation on S377 after UV radiation. We speculate that S377 phosphorylation may act as priming site for S153 phosphorylation. Further tests are needed to address the importance of this phosphorylation dynamics.

Since S377 phosphorylation was not induced by UV radiation in wild type cells, we focused on S153 for the remainder of this study. UV-induced S153 phosphorylation occurred in multiple cell lines including primary fibroblast and keratinocytes. Additionally, we found that S153 phosphorylation was induced by other cellular stresses including chemical UV-mimetic, 4NQO[139], and oxidizers such as hydrogen peroxide and potassium bromate.

Subcellular fractionation revealed that DGCR8 and Drosha are mostly localized in the nuclear soluble and chromatin fractions. Furthermore, phosphorylation of S153 was induced in these fractions, suggesting a role of S153 phosphorylated DGCR8 in the nucleus and chromatin. Consistent with this subcellular localization of DGCR8 we observed, it has been reported that the microprocessor complex (DGCR8-Drosha complex) is recruited to chromatin during transcription of the host transcript and process primary-miRNA co-transcriptionally [105, 106]. We also found that phospho-S153 was localized diffusely in the nucleus and not limited to localized UV-induced DNA damage. This suggest that S153 phosphorylation may occur globally in the nucleus, or that the phosphorylation may occur at sites of DNA damage and the phosphorylated DGCR8 may

spread rapidly in the nucleus. These possibilities remain to be tested.

Interestingly, S153 phosphorylation was not induced in a melanoma cell line, Mel-624 or delayed in another melanoma cell line, A375, after UVC radiation. We have not investigated the mechanisms behind these defects, but speculate that they include the defective signaling pathway upstream of the S153 DGCR8 phosphorylation and DGCR8 mutations that affect UV-induced S153 phosphorylation in these melanoma cell lines. cBioPortal for Cancer Genomics revealed several missense and nonsense mutation throughout DGCR8 in several different types of cancers, including melanoma. Specifically, several missense mutations flank S153 of DGCR8 including L152F, S156N (melanoma) and G149C (stomach and lung cancer)[140, 141]. It remains to be tested whether these mutations alter phosphorylation of S153 on DGCR8.

To date, this study is the first to demonstrate that DGCR8 is phosphorylated after UV radiation at a specific site. A study by the Steitz lab revealed 23 phosphorylation sites of DGCR8, including S153 [83]. Interestingly, mutations of all of these sites together does not affect pri-microRNA processing activity of DGCR8 [83], suggesting that DGCR8 phosphorylation is not required miRNA processing and perhaps plays an alternative role independent of the miRNA processing. Since we found that S153 phosphorylation was increased in response to UV treatment, we speculate that S153 phosphorylation may have a role in cellular survival or repair of UV-induced lesions, which may not be mediated by pri-microRNA processing activity of DGCR8.

Materials and Methods

Cell lines, UV and chemical treatments. HeLa, HCT-116 and U2OS cells

were obtained from ATCC. Mouse embryonic fibroblasts were a gift from the Clurman lab (FHCRC). Immortal human keratinocytes (HaCaT) were a gift from the Nghiem lab (UW-SLU). Primary human foreskin fibroblast (HFF) was a gift from the Galloway lab (FHCRC). Melanoma cell lines (Mel-624 and A375) were a gift from the Nelson lab (FHCRC). To detect UV induced phosphorylation at S153, cell were treated with UVC (254nm) was from a UV stratalinker 1800 (Stratagene), UVB (output range 280-320nm) at indicated doses from method previously described[142], hydrogen peroxide (95321, Sigma-Aldrich), 4-Nitroquinoline N-oxide (4NQO) (N8141, Sigma-Aldrich), potassium bromate (309087, Sigma-Aldrich), Cisplatin (P4394, Sigma-Aldrich), AZD2281-Parp inhibitor (S1060, Selleckchem), Paclitaxel (T1912, Sigma-Aldrich), hydroxyurea (H8627, Sigma-Aldrich).

Plasmids, shRNA and viral productions. Full-length and truncated human DGCR8 (Δ 275, Δ 276-773, Δ 483 and Δ 484-773) were cloned into the Nco1 and BamH1 sites of pMMP-IRES-puro retroviral vector [143]. Phosphomutant (S153A, S377A or S153AS377A) of DGCR8 was generated using the QuikChange XL Site-Directed Mutagenesis kit (200514-5, Agilent Technologies). Lenti-virus containing shDGCR8-1 (TRCN0000166035) was purchased from Sigma. Lenti- and Retro-viruses were produced as previous described [144]. All constructs were verified by direct sequencing.

Antibodies. Rabbit polyclonal antibodies against phosho-S153 DGCR8 (5126 and 6131) or phospho-377 DGCR8 (5628 and 5629) were generated by PhosphoSolutions. DGCR8 (10996-1-AP, Proteintech), FLAG (F1804, Sigma-Aldrich), CPD (CAC-NM-DND-001, Cosmo Bio Co.), vinculin (V9131, Sigma-Aldrich).

Western blot analysis and immunoprecipitation. Whole-cell lysates were prepared using sample buffer (0.05 mol/L Tris-HCl (pH 6.8), 2% SDS, 6% β-mercaptoethanol), resolved by polyacrylamide gel (NuPage, Life Technologies) electrophoresis and transferred onto nitrocellulose membranes. Subcellular fractionation was performed using a published protocol [145]. For λ phosphatase treatment, cells were lysed with lysis buffer (50nM Tris pH 7.4, 150nM NaCl, 1% Triton-X100, protease inhibitor (04693116011, Roche) on ice for 15 minutes. After centrifugation at 4 °C at 13.2K rpm for 15minutes, the supernatant was collected and incubated with 100 units of λ phosphatase supplemented with 1mM $MnCl_2$ (P0753, New England BioLabs) and with or without phosphatase inhibitors (50mM NaF and 10mM $NaVO_4$). After incubation for 1 hour at 30 °C, samples were boiled in sample buffer for 5 minutes. To detect the UV-induced DGCR8 upward shift shown in **Fig. 2.1 A-C and Fig 2.3A-B**, large 7.5% SDS-PAGE gels were used. Chemiluminescence was used for detection, and membranes were digitally scanned by Imagequant LAS 4000 (GE Biosciences).

Immunofluorescent microscopy and micropore UV irradiation. To detect pS153 DGCR8 by immunofluorescence, cells were treated with 60 J/m^2 UVC. After one hour, cells were fixed with 4% paraformaldehyde (Santa Cruz Biotechnology) for 10 minutes at room temperature and subsequently permeabilized with PBS containing 0.5% Tween-20 (Fisher Scientific) for 10 minutes at room temperature. After several washes with PBS containing 0.5% Tween-20 (washing buffer), cells were incubated over night at 4 °C with anti-phosphoS153 (1:1000). After several washes with PBS containing 0.5% Tween-20, cells were incubated with Alexa-fluor 488 goat anti-

rabbit (A11034, Life Technologies) secondary antibody for one hour. Nuclei were counterstained with 4,6-diami- dino-2-phenylindole (DAPI, 1 µg/mL). Coverslips were mounted on slides in Vectashield (Vector Laboratories). To determine whether pS153-DGCR8 was localized at UV-induced CPDs, cells were plated onto coverslips, covered with a 5 µm micropore filter (TMTP01300, Millipore) and treated with 100 J/m^2 UVC. After one hour, cells were fixed and permeabilized as described above. Then, cells were treated with 2M HCl to denature DNA for 30 minutes at room temperature. After several washes with washing buffer, cells were blocked with 3% BSA in PBS for 20 minutes at room temperature and then incubated with anti-CPDs and anti-pS153 DGCR8 overnight at 4 °C. After several washes with washing buffer, cells were incubated for one hour at room temperature with Alexa-fluor 488 goat anti-rabbit (A11034, Life Technologies) and Alexa-fluor 594 donkey anti-mouse (A21203, Life Technologies) secondary antibodies. Subsequent steps were done as described above. Image acquisitions were made with a TE2000 Nikon microscope equipped with a 20x immersion objective and a CCD camera (CoolSNAP ES, Photometrics).

Mass spectrometry. HeLa cells stably infected with pMMPpuroFLAG-DGCR8 were treated with 60 J/m^2 of UV-C and 1 hour later, whole-cell extracts were prepared in lysis buffer. IP was performed using monoclonal antibody against FLAG (M2, Santa Cruz) and the IP product was separated by 7.5% SDS-PAGE. Gel pieces corresponding to FLAG-DGCR8 bands were cut from a Coomassie stained gel and subjected to tryptic digestion [146]. Tryptic peptides were concentrated and desalted using a C18micro ZipTip (Millipore) following the manufacturer's instructions. The eluted peptides were

dried by vacuum centrifugation, resuspended in 7 μL of 2% acetonitrile/0.1% formic acid and 5 μL was analyzed by liquid chromatography coupled to tandem mass spectrometry (LC-MS/MS) with a nanoLC 2D (Eksigent) coupled to an OrbiTrap mass spectrometer (ThermoScientific) using an instrument configuration [147]. In-line de-salting was accomplished using a reversed-phase trap column (100 µm × 20 mm) packed with Magic C_{18}AQ (5-µm 200Å resin; Michrom Bioresources, Auburn, CA) followed by peptide separations on a reversed-phase column (75 µm × 250 mm) packed with Magic C_{18}AQ (5-µm 100Å resin; Michrom Bioresources, Auburn, CA) directly mounted on the electrospray ion source. Chromatographic separations were conducted at a flowrate of 300 nL/min with a elution profile from 2%B to 2%B in 5 min, 2%B to 10%B in 3 min, 10%B to 40%B in 60 min, 40%B to 80%B in 2 min, and 80%B to 80%B in 10 min using 0.1% formic acid in water (A) and 0.1% formic acid in acetonitrile (B) as solvents. Data were collected in a data-dependent mode in which a high mass resolution/high mass accuracy scan (in the FT part of the instrument) was followed by low resolution/low mass accuracy MS/MS scans of the five most abundant ions from the preceding MS scan (in the LTQ part of the instrument). The FT part of the instrument was set at a target resolution of 60,000 at m/z 400, an AGC target value of 1e6, and a maximum ion time of 150 ms while the ion trap was set to a MSn AGC target value of 1e4 and a MSn maximum ion time of 50 ms. The data-dependent method triggered a MS3 (MS/MS/MS) analysis on an MS2 (MS/MS) ion species if an MS2 ion species differed from the precursor ion species by m/z 98.0, 49.0, or 32.7, the neutral loss of phosphoric acid for a singly-, doubly-, or triply-charged ion species, respectively. Normalized collision energy

of 35% and isolation widths of 2.0 were used for both MS2 and MS3 events. Dynamic exclusion was enabled with a repeat count of 1, a repeat duration of 15 seconds, an exclusion duration of 15 seconds, a low exclusion mass width of 0.55 and a high exclusion mass width of 1.55. Raw MS/MS data were submitted to the Computational Proteomics Analysis System (CPAS) [148] and searched using the X! Tandem search engine[149] against the IPI human protein database (v3.59). Cys -17.027 Da, Glu -18.011 Da, Met +15.995, Gln -17.027, Ser +79.966, Thr +79.966, and Try +79.966 were set as variable modifications. The mass tolerances were set ±2 Da and ±0.5 Da for precursor and fragment ions, respectively. The enzyme was set to Trypsin, and up to 2 missed cleavages were permitted. Peptide validation was conducted with Peptide Prophet[150] and peptide identification results were filtered with false discovery rate of less than 5%.

Figures and Legends

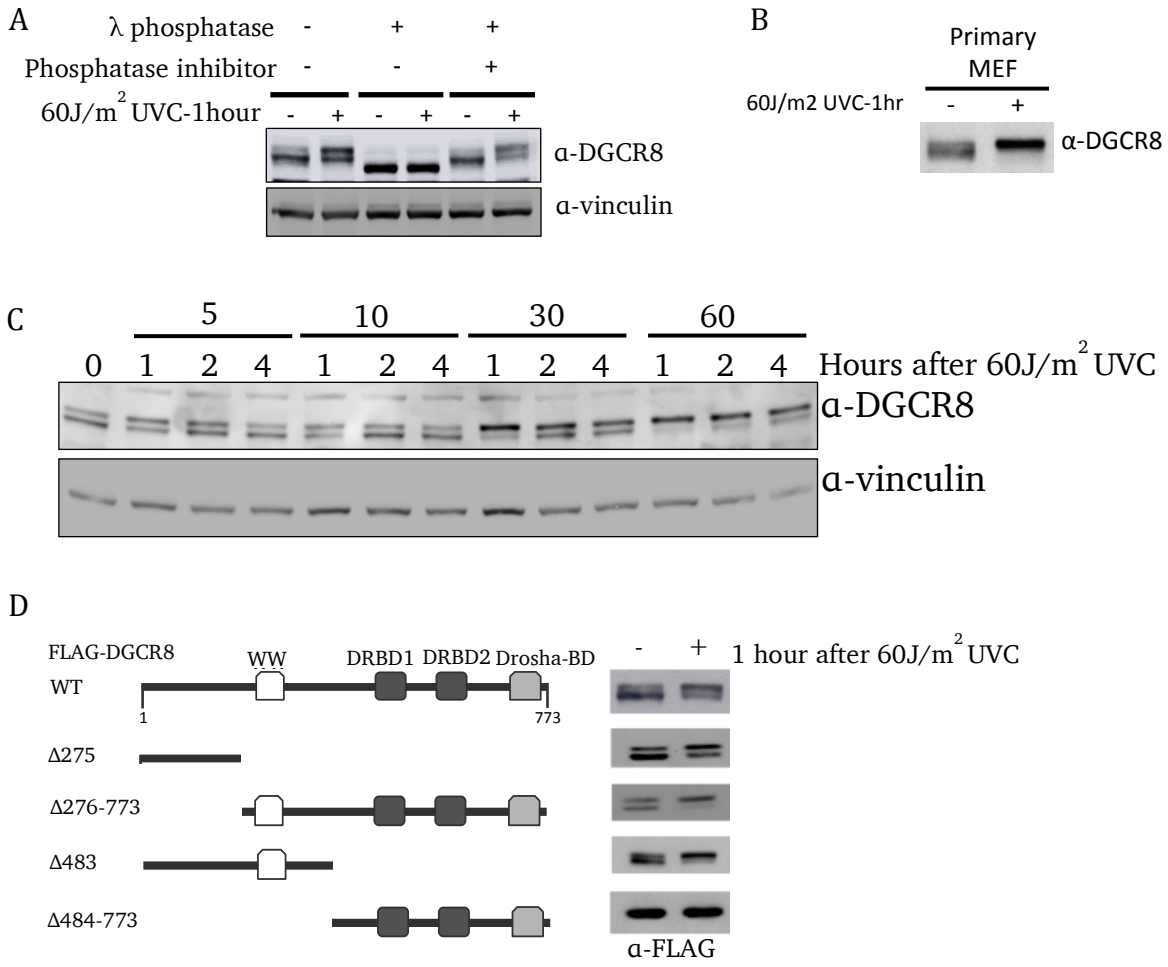

Figure 2.1 DGCR8 is phosphorylated by UV radiation. **A.** Cell lysates from U2OS cells treated with UV were treated with lambda phosphatase and phosphatase inhibitors and immunoblotted for DGCR8. **B.** Cell lysates from murine primary embryonic fibroblasts treated with UV and immunoblotted for DGCR8. **C.** Cell lysates from U2OS cells treated with UV at indicated doses and times then, were immunoblotted for DGCR8. **D.** Cell lysates from U2OS cells expressing several FLAG-tagged truncated DGCR8 mutants treated with UV and were immunoblotted for FLAG.

A

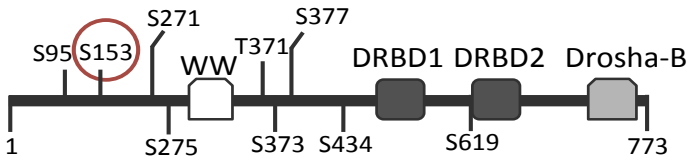

B

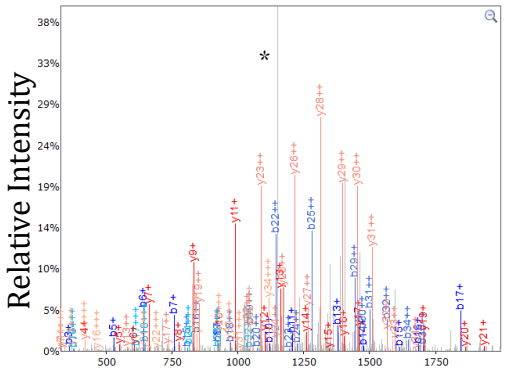

C

b+	b2+	b3+	#	Seq	#	y+	y2+	y3+
72.0444	36.5258	24.6863	1	A	36			
201.0870	101.0471	67.7005	2	E	35	3480.5448	1740.7760	1160.8531
361.1177	181.0625	121.0441	3	C	34	3351.5022	1676.2547	1117.8389
418.1391	209.5732	140.0512	4	G	33	3191.4715	1596.2394	1064.4953
531.2232	266.1152	177.7459	5	L	32	3134.4500	1567.7287	1045.4882
644.3073	322.6573	215.4406	6	L	31	3021.3660	1511.1866	1007.7935
757.3913	379.1993	253.1353	7	L	30	2908.2819	1454.6446	970.0988
924.3897	462.6985	308.8014	8	S	29	2795.1978	1398.1026	932.4041
1021.4424	511.2248	341.1523	9	P	28	2628.1995	1314.6034	876.7380
1120.5108	560.7591	374.1751	10	V	27	2531.1467	1266.0770	844.3871
1207.5429	604.2751	403.1858	11	S	26	2432.0783	1216.5428	811.3643
1264.5643	632.7858	422.1930	12	G	25	2345.0463	1173.0268	782.3536
1379.5913	690.2993	460.5353	13	D	24	2288.0248	1144.5161	763.3465
1478.6597	739.8335	493.5581	14	V	23	2172.9979	1087.0026	725.0041
1615.7186	808.3629	539.2444	15	H	22	2073.9295	1037.4684	691.9813
1686.7557	843.8815	562.9234	16	A	21	1936.8706	968.9389	646.2950
1846.7864	923.8968	616.2670	17	C	20	1865.8335	933.4204	622.6160
1943.8392	972.4232	648.6179	18	P	19	1705.8028	853.4050	569.2724
2090.9076	1045.9574	697.6407	19	F	18	1608.7500	804.8786	536.9215
2147.9290	1074.4682	716.6479	20	G	17	1461.6816	731.3444	487.8987
2204.9505	1102.9789	735.6550	21	G	16	1404.6601	702.8337	468.8916
2291.9825	1146.4949	764.6657	22	S	15	1347.6387	674.3230	449.8844
2391.0509	1196.0291	797.6885	23	V	14	1260.6066	630.8070	420.8737
2448.0724	1224.5398	816.6957	24	G	13	1161.5382	581.2727	387.8509
2563.0993	1282.0533	855.0380	25	D	12	1104.5168	552.7620	368.8438
2620.1208	1310.5640	874.0451	26	G	11	989.4898	495.2485	330.5015
2719.1892	1360.0982	907.0679	27	V	10	932.4684	466.7378	311.4943
2776.2107	1388.6090	926.0751	28	G	9	833.3999	417.2036	278.4715
2889.2947	1445.1510	963.7698	29	I	8	776.3785	388.6929	259.4643
2946.3162	1473.6617	982.7769	30	G	7	663.2944	332.1508	221.7697
3003.3377	1502.1725	1001.7841	31	G	6	606.2729	303.6401	202.7625
3132.3803	1566.6938	1044.7983	32	E	5	549.2515	275.1294	183.7553
3219.4123	1610.2098	1073.8089	33	S	4	420.2089	210.6081	140.7411
3290.4494	1645.7283	1097.4880	34	A	3	333.1769	167.0921	111.7305
3405.4764	1703.2418	1135.8303	35	D	2	262.1397	131.5735	88.0514
			36	K	1	147.1128	74.0600	49.7091

Figure 2.2 Mass spectrometry spectra of DGCR8 phosphorylation sites. A. Nine phosphorylation sites of DGCR8 identified by mass spectrometry. Encircled in red is S153, the only site that was identified to be phosphorylated in the upper band. The DGCR8 protein contains a WW domain, two dsRNA binding domains (DRBD1 and DRBD2) and a Drosha binding domain (Drosha-BD). **B.** Phosphosite identification of S153 in DGCR8**.** A gel band of DGCR8 subjected to UV light exposure was digested with trypsin and subjected to tandem mass spectrometry. The "*" in the spectrum labels a peak corresponding to the neutral loss of m/z 32.7 from the precursor ion equaling the loss of H_3PO_4, which is a common occurrence during the tandem mass analysis of phosphopeptides. **C.** The tandem mass spectrum from panel B was subjected to phosphopeptide identification using the database search algorithm X!Tandem. The algorithm identified the peptide A146 to K181 containing a single phosphate group located to S153 as shown (highlighted in yellow). The panel displays all predicted fragment ions for the identified peptide and highlights in red and blue the y-ions and b-ions, respectively, that were identified in the tandem mass spectrum in panel A. The m/z difference between the predicted triply-charged ion species (m/z 1184.5321) for singly phosphorylated A146 to K181 peptide and the measured triply-charged ion species (m/z 1184.5325) is 0.0004.

D

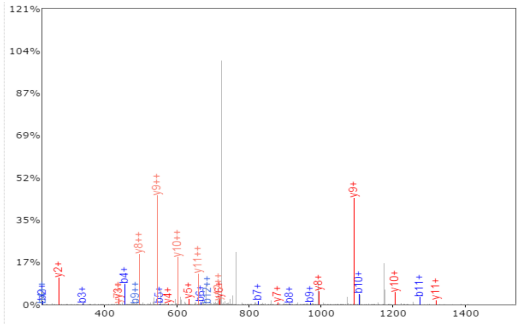

b+	b2+	#	Seq	#	y+	y2+
114.0913	57.5493	1	L	13		
227.1754	114.0913	2	L	12	1432.6039	716.8056
340.2595	170.6334	3	I	11	1319.5198	660.2636
455.2864	228.1468	4	D	10	1206.4358	603.7215
552.3392	276.6732	5	P	9	1091.4088	546.2080
666.3821	333.6947	6	N	8	994.3561	497.6817
826.4128	413.7100	7	C	7	880.3131	440.6602
913.4448	457.2260	8	S	6	720.2824	360.6449
970.4663	485.7368	9	G	5	633.2504	317.1288
1107.5252	554.2662	10	H	4	576.2290	288.6181
1274.5235	637.7654	11	S	3	439.1700	220.0887
1371.5763	686.2918	12	P	2	272.1717	136.5895
		13	R	1	175.1190	88.0631

E

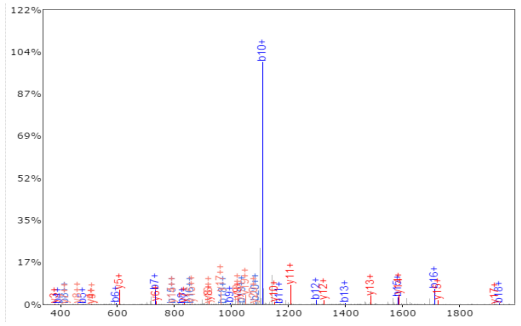

b+	b2+	#	Seq	#	y+	y2+
164.0706	82.5389	1	Y	21		
221.0921	111.0497	2	G	20	2155.8308	1078.4190
278.1135	139.5604	3	G	19	2098.8093	1049.9083
393.1405	197.0739	4	D	18	2041.7878	1021.3976
480.1725	240.5899	5	S	17	1926.7609	963.8841
595.1994	298.1034	6	D	16	1839.7289	920.3681
732.2584	366.6328	7	H	15	1724.7019	862.8546
829.3111	415.1592	8	P	14	1587.6430	794.3251
996.3095	498.6584	9	S	13	1490.5902	745.7988
1111.3364	556.1718	10	D	12	1323.5919	662.2996
1168.3579	584.6826	11	G	11	1208.5650	604.7861
1297.4005	649.2039	12	E	10	1151.5435	576.2754
1398.4481	699.7277	13	T	9	1022.5009	511.7541
1485.4802	743.2437	14	S	8	921.4532	461.2303
1584.5486	792.7779	15	V	7	834.4212	417.7142
1712.6071	856.8072	16	Q	6	735.3528	368.1800
1809.6599	905.3336	17	P	5	607.2942	304.1507
1940.7004	970.8538	18	M	4	510.2415	255.6244
2071.7409	1036.3741	19	M	3	379.2010	190.1041
2172.7886	1086.8979	20	T	2	248.1605	124.5839
		21	K	1	147.1128	74.0600

F

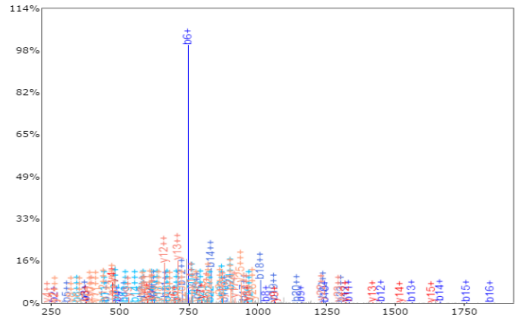

b+	b2+	b3+	#	Seq	#	y+	y2+	y3+
132.0478	66.5275	44.6874	1	M	27			
260.1427	130.5750	87.3858	2	K	26	2950.3789	1475.6931	984.1312
375.1697	188.0885	125.7281	3	D	25	2822.2840	1411.6456	941.4328
489.2126	245.1099	163.7424	4	N	24	2707.2570	1354.1322	903.0905
618.2552	309.6312	206.7566	5	E	23	2593.2141	1297.1107	865.0762
747.2978	374.1525	249.7708	6	E	22	2464.1715	1232.5894	822.0620
903.3989	452.2031	301.8045	7	R	21	2335.1289	1168.0681	779.0478
1032.4415	516.7244	344.8187	8	E	20	2179.0278	1090.0175	727.0141
1160.5001	580.7537	387.5049	9	Q	19	2049.9852	1025.4962	683.9999
1247.5321	624.2697	416.5155	10	S	18	1921.9266	961.4670	641.3137
1334.5641	667.7857	445.5262	11	S	17	1834.8946	917.9509	612.3031
1449.5911	725.2992	483.8685	12	D	16	1747.8626	874.4349	583.2924
1562.6751	781.8412	521.5632	13	L	15	1632.8356	816.9215	544.9501
1663.7228	832.3650	555.2458	14	T	14	1519.7516	760.3794	507.2554
1760.7756	880.8914	587.5967	15	P	13	1418.7039	709.8556	473.5728
1847.8076	924.4074	616.6074	16	S	12	1321.6511	661.3292	441.2219
1904.8291	952.9182	635.6145	17	G	11	1234.6191	617.8132	412.2112
2019.8560	1010.4316	673.9569	18	D	10	1177.5976	589.3025	393.2041
2118.9244	1059.9658	706.9797	19	V	9	1062.5707	531.7890	354.8617
2285.9227	1143.4650	762.6458	20	S	8	963.5023	482.2548	321.8389
2382.9755	1191.9914	794.9967	21	P	7	796.5039	398.7556	266.1728
2482.0439	1241.5256	828.0195	22	V	6	699.4512	350.2292	233.8219
2610.1389	1305.5731	870.7178	23	K	5	600.3828	300.6950	200.7991
2707.1917	1354.0995	903.0687	24	P	4	472.2878	236.6475	158.1008
2820.2757	1410.6415	940.7634	25	L	3	375.2350	188.1212	125.7499
2907.3077	1454.1575	969.7741	26	S	2	262.1510	131.5791	88.0552
			27	R	1	175.1190	88.0631	59.0445

Figure 2.2 Mass spectrometry spectra for phospho-S95, -S275 and –S377. **D.** Spectrum of a phosphopeptide containing pS95. The X!Tandem algorithm identified a single phosphate group located on S95 as shown (highlighted in yellow). **E.** Spectrum of a phosphopeptide containing pS275. The X!Tandem algorithm identified a single phosphate group located on S275 as shown (highlighted in yellow). **F.** Spectrum of a phosphopeptide containing pS377. The X!Tandem algorithm identified a single phosphate group located on S377 as shown (highlighted in yellow).

G

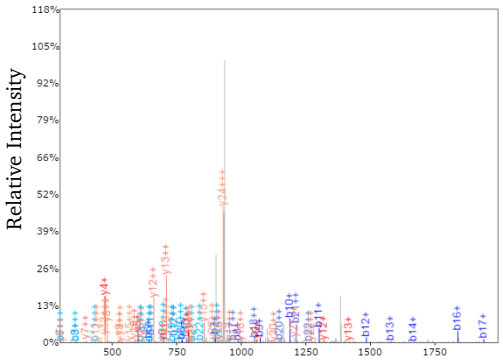

b+	b2+	b3+	#	Seq	#	y+	y2+	y3+
116.0342	58.5207	39.3496	1	D	25			
230.0771	115.5422	77.3639	2	N	24	2787.2233	1394.1153	929.7460
359.1197	180.0635	120.3781	3	E	23	2673.1804	1337.0938	891.7317
488.1623	244.5848	163.3923	4	E	22	2544.1378	1272.5725	848.7175
644.2634	322.6354	215.4260	5	R	21	2415.0952	1208.0512	805.7033
773.3060	387.1567	258.4402	6	E	20	2258.9941	1130.0007	753.6696
901.3646	451.1859	301.1264	7	Q	19	2129.9515	1065.4794	710.6554
988.3966	494.7020	330.1371	8	S	18	2001.8929	1001.4501	667.9692
1075.4287	538.2180	359.1477	9	S	17	1914.8609	957.9341	638.9585
1190.4556	595.7314	397.4901	10	D	16	1827.8289	914.4181	609.9478
1303.5397	652.2735	435.1847	11	L	15	1712.8019	856.9046	571.6055
1484.5537	742.7805	495.5227	12	T	14	1599.7179	800.3626	533.9108
1581.6064	791.3068	527.8737	13	P	13	1418.7039	709.8556	473.5728
1668.6384	834.8229	556.8843	14	S	12	1321.6511	661.3292	441.2219
1725.6599	863.3336	575.8915	15	G	11	1234.6191	617.8132	412.2112
1840.6869	920.8471	614.2338	16	D	10	1177.5976	589.3025	393.2041
1939.7553	970.3813	647.2566	17	V	9	1062.5707	531.7890	354.8617
2106.7536	1053.8804	702.9227	18	S	8	963.5023	482.2548	321.8389
2203.8064	1102.4068	735.2736	19	P	7	796.5039	398.7556	266.1728
2302.8748	1151.9410	768.2964	20	V	6	699.4512	350.2292	233.8219
2430.9697	1215.9885	810.9948	21	K	5	600.3828	300.6950	200.7991
2528.0225	1264.5149	843.3457	22	P	4	472.2878	236.6475	158.1008
2641.1066	1321.0569	881.0404	23	L	3	375.2350	188.1212	125.7499
2728.1386	1364.5729	910.0510	24	S	2	262.1510	131.5791	88.0552
			25	R	1	175.1190	88.0631	59.0445

H

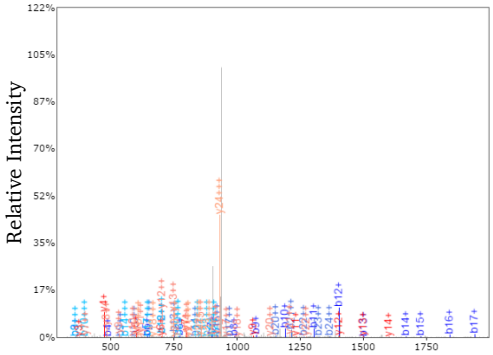

b+	b2+	b3+	#	Seq	#	y+	y2+	y3+
116.0342	58.5207	39.3496	1	D	25			
230.0771	115.5422	77.3639	2	N	24	2787.2233	1394.1153	929.7460
359.1197	180.0635	120.3781	3	E	23	2673.1804	1337.0938	891.7317
488.1623	244.5848	163.3923	4	E	22	2544.1378	1272.5725	848.7175
644.2634	322.6354	215.4260	5	R	21	2415.0952	1208.0512	805.7033
773.3060	387.1567	258.4402	6	E	20	2258.9941	1130.0007	753.6696
901.3646	451.1859	301.1264	7	Q	19	2129.9515	1065.4794	710.6554
988.3966	494.7020	330.1371	8	S	18	2001.8929	1001.4501	667.9692
1075.4287	538.2180	359.1477	9	S	17	1914.8609	957.9341	638.9585
1190.4556	595.7314	397.4901	10	D	16	1827.8289	914.4181	609.9478
1303.5397	652.2735	435.1847	11	L	15	1712.8019	856.9046	571.6055
1404.5874	702.7973	468.8673	12	T	14	1599.7179	800.3626	533.9108
1501.6401	751.3237	501.2182	13	P	13	1498.6702	749.8387	500.2282
1668.6384	834.8229	556.8843	14	S	12	1401.6174	701.3124	467.8773
1725.6599	863.3336	575.8915	15	G	11	1234.6191	617.8132	412.2112
1840.6869	920.8471	614.2338	16	D	10	1177.5976	589.3025	393.2041
1939.7553	970.3813	647.2566	17	V	9	1062.5707	531.7890	354.8617
2106.7536	1053.8804	702.9227	18	S	8	963.5023	482.2548	321.8389
2203.8064	1102.4068	735.2736	19	P	7	796.5039	398.7556	266.1728
2302.8748	1151.9410	768.2964	20	V	6	699.4512	350.2292	233.8219
2430.9697	1215.9885	810.9948	21	K	5	600.3828	300.6950	200.7991
2528.0225	1264.5149	843.3457	22	P	4	472.2878	236.6475	158.1008
2641.1066	1321.0569	881.0404	23	L	3	375.2350	188.1212	125.7499
2728.1386	1364.5729	910.0510	24	S	2	262.1510	131.5791	88.0552
			25	R	1	175.1190	88.0631	59.0445

Figure 2.2 Mass spectrometry spectra for phospho-T371/S377, -S373/S377.
G. Spectrum of a phosphopeptide containing pT371 and S377. The X!Tandem algorithm identified a single phosphate group located on T371 and S377 as shown (highlighted in yellow). **H.** Spectrum of a phosphopeptide containing pS373 and S377. The X!Tandem algorithm identified a single phosphate group located on S373 and S377 as shown (highlighted in yellow).

I

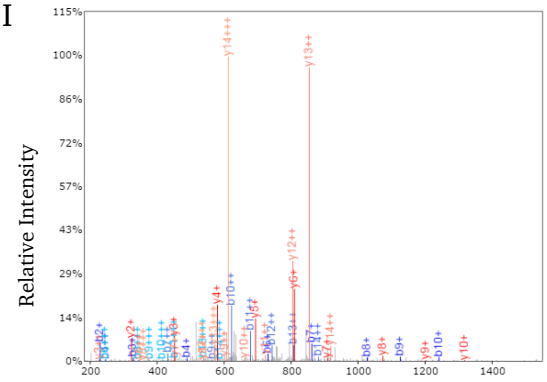

b+	b2+	b3+	#	Seq	#	y+	y2+	y3+
100.0757	50.5415	34.0301	1	V	15			
229.1183	115.0628	77.0443	2	E	14	1834.7565	917.8819	612.2570
328.1867	164.5970	110.0671	3	V	13	1705.7139	853.3606	569.2428
488.2174	244.6123	163.4106	4	C	12	1606.6455	803.8264	536.2200
616.3123	308.6598	206.1090	5	K	11	1446.6148	723.8110	482.8765
731.3393	366.1733	244.4513	6	D	10	1318.5198	659.7636	440.1781
860.3819	430.6946	287.4655	7	E	9	1203.4929	602.2501	401.8358
1027.3802	514.1937	343.1316	8	S	8	1074.4503	537.7288	358.8216
1126.4486	563.7279	376.1544	9	V	7	907.4520	454.2296	303.1555
1241.4756	621.2414	414.4967	10	D	6	808.3836	404.6954	270.1327
1354.5596	677.7835	452.1914	11	L	5	693.3566	347.1819	231.7904
1483.6022	742.3047	495.2056	12	E	4	580.2726	290.6399	194.0957
1612.6448	806.8260	538.2198	13	E	3	451.2300	226.1186	151.0815
1759.7132	880.3603	587.2426	14	F	2	322.1874	161.5973	108.0673
			15	R	1	175.1190	88.0631	59.0445

J

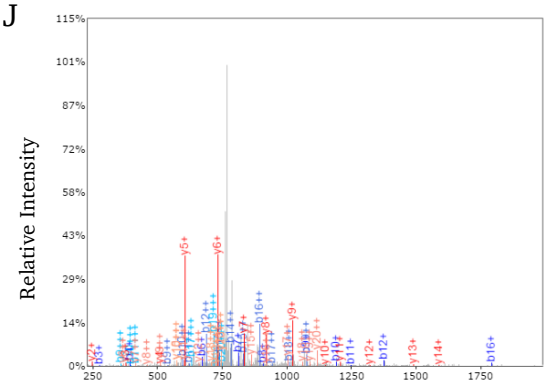

b+	b2+	b3+	#	Seq	#	y+	y2+	y3+
164.0706	82.5389	55.3617	1	Y	21			
221.0921	111.0497	74.3689	2	G	20	2235.7971	1118.4022	745.9372
278.1135	139.5604	93.3760	3	G	19	2178.7756	1089.8914	726.9300
393.1405	197.0739	131.7183	4	D	18	2121.7541	1061.3807	707.9229
560.1388	280.5730	187.3845	5	S	17	2006.7272	1003.8672	669.5806
675.1657	338.0865	225.7268	6	D	16	1839.7289	920.3681	613.9145
812.2247	406.6160	271.4131	7	H	15	1724.7019	862.8546	575.5722
909.2774	455.1423	303.7640	8	P	14	1587.6430	794.3251	529.8859
1076.2758	538.6415	359.4301	9	S	13	1490.5902	745.7988	497.5349
1191.3027	596.1550	397.7724	10	D	12	1323.5919	662.2996	441.8688
1248.3242	624.6657	416.7796	11	G	11	1208.5650	604.7861	403.5265
1377.3668	689.1870	459.7938	12	E	10	1151.5435	576.2754	384.5194
1478.4144	739.7109	493.4763	13	T	9	1022.5009	511.7541	341.5052
1565.4465	783.2269	522.4870	14	S	8	921.4532	461.2303	307.8226
1664.5149	832.7611	555.5098	15	V	7	834.4212	417.7142	278.8119
1792.5734	896.7904	598.1960	16	Q	6	735.3528	368.1800	245.7891
1889.6262	945.3167	630.5469	17	P	5	607.2942	304.1507	203.1029
2020.6667	1010.8370	674.2271	18	M	4	510.2415	255.6244	170.7520
2151.7072	1076.3572	717.9072	19	M	3	379.2010	190.1041	127.0718
2252.7549	1126.8811	751.5898	20	T	2	248.1605	124.5839	83.3917
			21	K	1	147.1128	74.0600	49.7091

Figure 2.2 Mass spectrometry spectra for phospho-S434, -S271/S275.
I. Spectrum of a phosphopeptide containing pS434. The X!Tandem algorithm identified a single phosphate group located on S434 as shown (highlighted in yellow). **J.** Spectrum of a phosphopeptide containing pS271 and pS275. The X!Tandem algorithm identified a single phosphate group located on S271 and S275 as shown (highlighted in yellow).

K

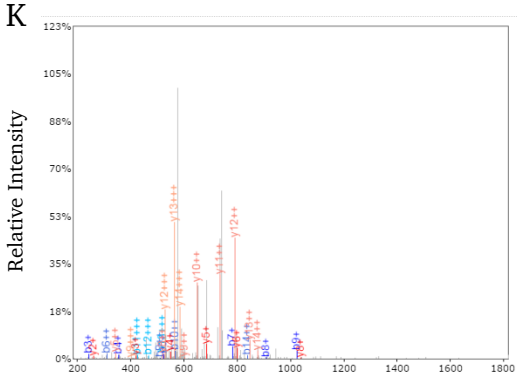

b+	b2+	b3+	#	Seq	#	y+	y2+	y3+
72.0444	36.5258	24.6863	1	A	15			
129.0659	65.0366	43.6935	2	G	14	1750.8598	875.9335	584.2914
242.1499	121.5786	81.3882	3	L	13	1693.8383	847.4228	565.2843
355.2340	178.1206	119.0828	4	L	12	1580.7542	790.8808	527.5896
522.2323	261.6198	174.7490	5	S	11	1467.6702	734.3387	489.8949
619.2851	310.1462	207.0999	6	P	10	1300.6719	650.8396	434.2288
782.3484	391.6778	261.4543	7	Y	9	1203.6191	602.3132	401.8779
910.4070	455.7071	304.1405	8	Q	8	1040.5558	520.7815	347.5234
1023.4910	512.2492	341.8352	9	I	7	912.4972	456.7522	304.8372
1136.5751	568.7912	379.5299	10	L	6	799.4131	400.2102	267.1426
1273.6340	637.3206	425.2162	11	H	5	686.3291	343.6682	229.4479
1402.6766	701.8419	468.2304	12	E	4	549.2701	275.1387	183.7616
1562.7073	781.8573	521.5739	13	C	3	420.2276	210.6174	140.7474
1675.7914	838.3993	559.2686	14	L	2	260.1969	130.6021	87.4038
			15	K	1	147.1128	74.0600	49.7091

Figure 2.2 Mass spectrometry spectra for phospho-S619.

K. Spectrum of a phosphopeptide containing pS619. The X!Tandem algorithm identified a single phosphate group located on S619 as shown (highlighted in yellow).

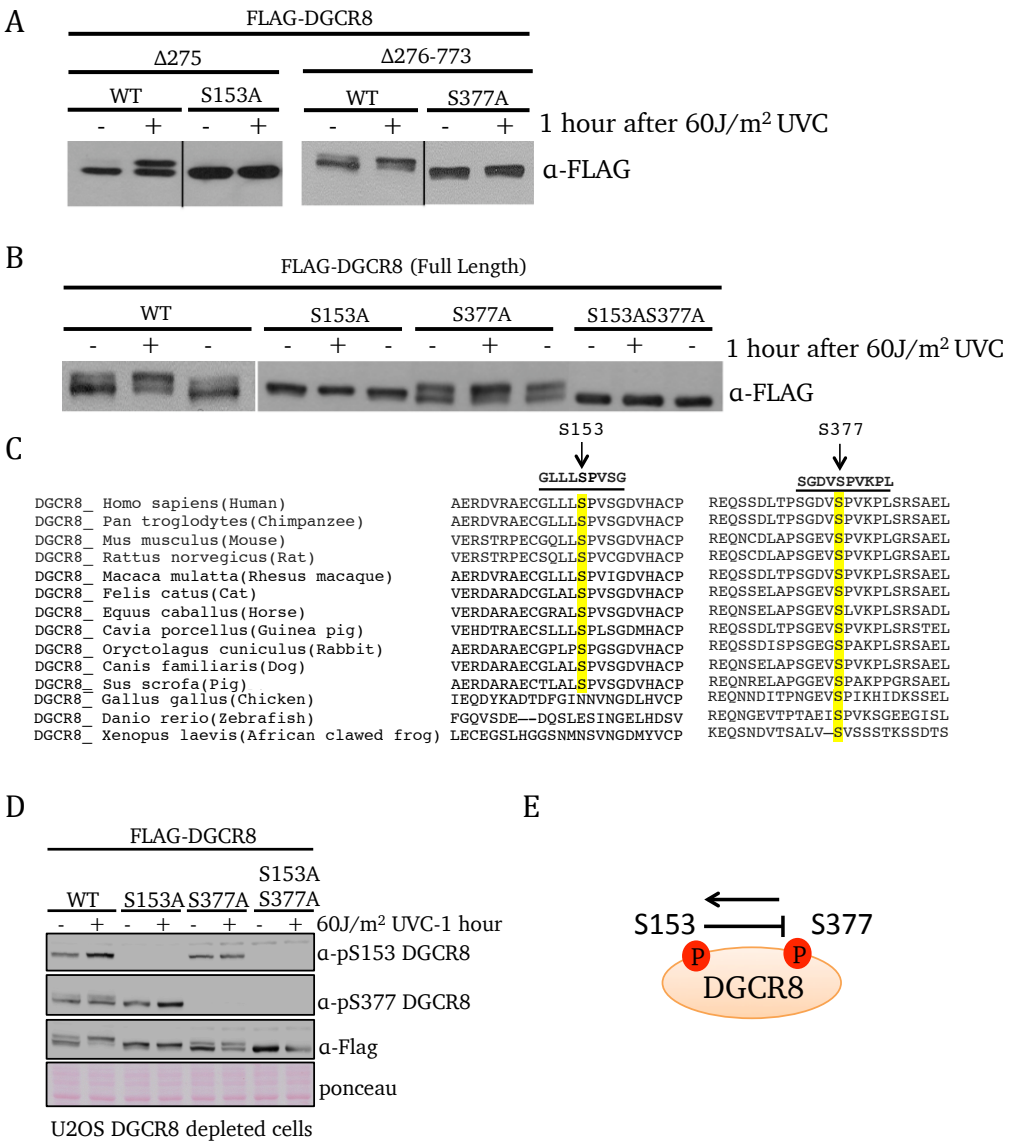

Figure 2.3 Serines 153 and 377 on DGCR8 are phosphorylated. A. Cell lysates from U2OS cells expressing FLAG-Δ 275 wild-type, FLAG-Δ 275 S153A, FLAG-Δ 276-773 wild-type or FLAG-Δ 276-773 S377A treated with UV and were immunoblotted for FLAG. **B.** Cell lysates from U2OS cells expressing full-length FLAG-wild-type DGCR8 or FLAG-S153A or FLAG-S377A treated with UV were immunoblotted for FLAG. **C.** DGCR8 S153 and S377 sequence alignment. S153 or S377 is conserved among mammals or vertebrates, respectively, but not in other eukaryotes. **D.** Cell lysates from U2OS cells depleted of endogenous DGCR8 by shDGCR8 expressing several shDGCR8 resistant FLAG-tagged full-length DGCR8 wild-type, S153A, S377A or S153AS377A treated with UV and were immunoblotted for phospho-S153, phospho-S377 or anti-FLAG. **E.** Model: the phosphorylation dynamics on DGCR8.

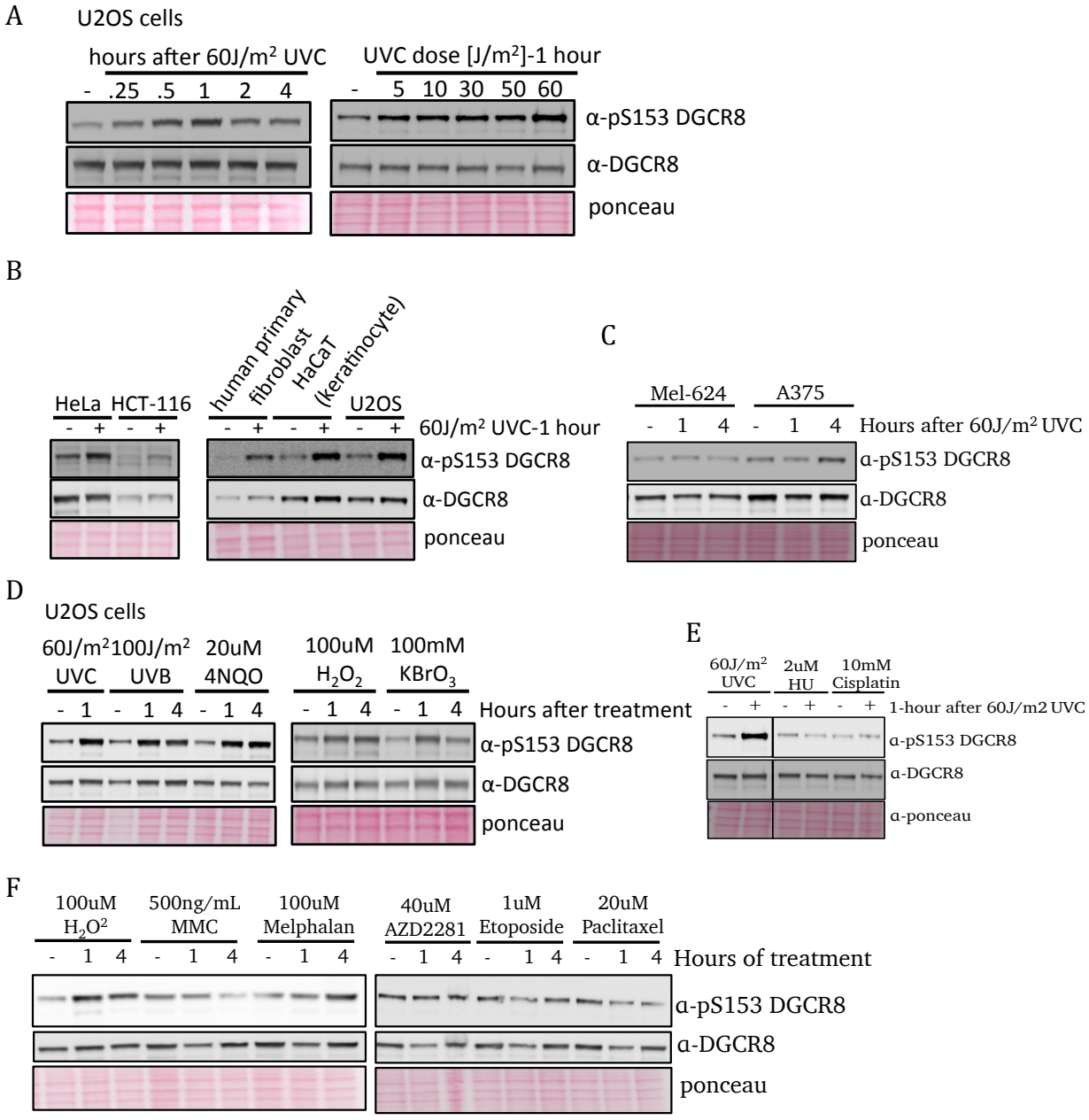

Figure 2.4 Serine S153 on DGCR8 is phosphorylated in response to UV and other cellular stresses in multiple cell lines. **A.** Cell lysates from U2OS cells expressing full-length FLAG-tagged wild-type DGCR8 treated with UV at the indicated dose or time and were immunoblotted for phospho-S153 or DGCR8. **B & C.** Cell lysates from several cell lines expressing full-length FLAG-tagged wild-type DGCR8 treated with UV and were immunoblotted for phospho-S153 or DGCR8. **D, E & F.** Cell lysates from U2OS cells expressing full-length FLAG-tagged wild-type DGCR8 treated with UV and other cellular stresses were immunoblotted for phospho-S153 or DGCR8. Mitomycin C (MMC), Hydroxyurea (HU), Potassium Bromate ($KBrO_3$), Hydrogen Peroxide (H_2O_2), 4-nitroquinoline-1-oxide (4-NQO) and PARP inhibitor (AZD2281).

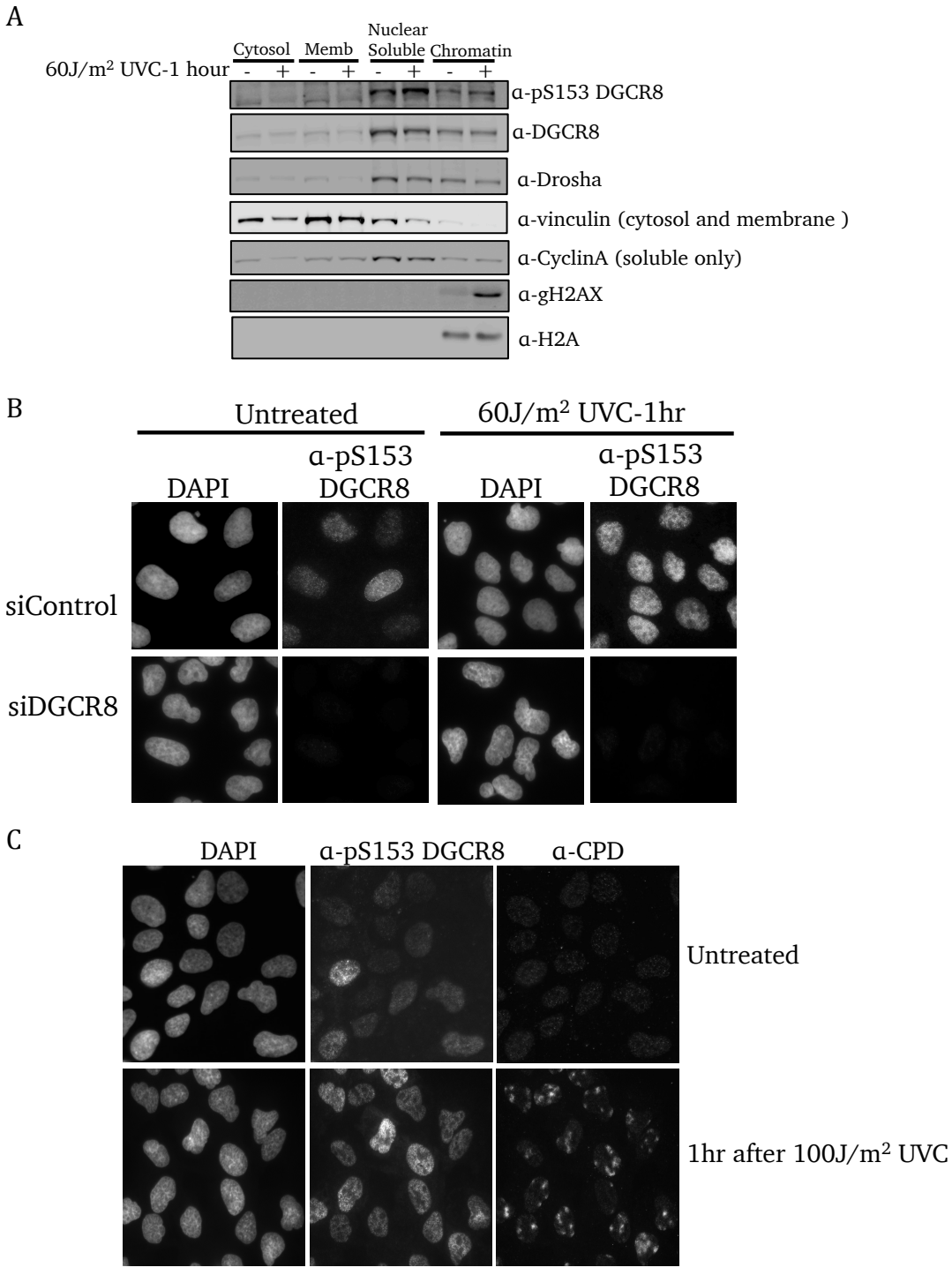

Figure 2.5 Cellular localization of S153 phosphorylation. A. Cell lysates from U2OS cells untreated and treated with UVC were subjected to subcellular fractionation followed by immunoblotting. **B.** Immuno-cytochemistry. U2OS cells transfected with indicated siRNAs and treated with UV were subjected to immunocytochemistry with phosho-S153 antibody. **C.** Micropore UV irradiation and immunofluorescent microscopy. U2OS cells were UV treated through a micropore filter (5 μm pore diameter). Cells were double immunostained with phosphoS153-DGCR8 and CPD antibodies.

CHAPTER THREE

Phosphorylation of DGCR8 Regulates Cellular Survival After UV Radiation Independently of Drosha and microRNA Processing

Abstract

In chapter two, we showed that treatment with UV and other cellular stresses induced phosphorylation on Serine 153 (S153) of DGCR8 in human cells. However, the functional significance of the S153 phosphorylation was not clear. Here, in chapter three, we show a critical role of DGCR8 in cellular resistance to UV radiation. DGCR8-depleted cells were hypersensitive to UV and the re-introduction of wild-type or phospho-mimetic (S153D) DGCR8 restored UV resistance in DGCR8-depleted cells, while phospho-mutant (S153A) failed to restore UV resistance, suggesting that S153 phosphorylation is critical for cellular resistance to UV. Interestingly, the RNA-binding domain mutant of DGCR8 and the Drosha binding domain mutant of DGCR8 restored UV resistance of DGCR8-depleted cells, suggesting that microRNA processing function or Drosha binding of DGCR8 is not important for UV resistance. Additionally, we found that depletion of Drosha led to cellular hypersensitive to UV radiation and that re-introduction of wild-type, RNA binding mutant, or DGCR8 binding mutant of Drosha restored UV resistance in Drosha-depleted cells, suggesting that Drosha is required for cellular resistance UV independent of its RNA binding and DGCR8 binding activities. Lastly, microRNA expression was not significantly different between wild-type DGCR8 expressing cells and S153A-DGCR8 expressing cells, suggesting S153 phosphorylation is not critical for microRNA processing function of DGCR8. Taken together, these findings suggest that

DGCR8 has two independent functions: 1) S153 phosphorylation-mediated cellular resistance to UV, and 2) RNA binding- and Drosha binding-domains–mediated RNA (primary microRNA) processing.

Introduction

Ultraviolet (UV) radiation forms cytotoxic DNA pyrimidine dimers and if, left unrepaired cause mutations or genomic instability that can lead to cellular transformation. In contrast, UV-induced DNA dimers can cause cell death or senescence that can lead to ageing. Mammalian cells activate an elaborate DNA damage response signaling in which post-translational modifications, such as phosphorylation, play a critical layer of regulation in safeguarding the genome from the negative effects of UV radiation. MicroRNAs have emerged as another layer of regulation in response to UV. First, the expression of a subset of microRNAs is altered in response to UV[151]. Second, depletion of Dicer and Ago2, factors required for microRNA biogenesis, leads to cellular hypersensitivity to UV[151]. However, the mechanisms connecting the miRNA biogenesis machinery and UV response remain unclear.

The microprocessor complex which consists of DGCR8 and Drosha, are critical proteins for pri-miRNA processing[37]. More specifically, DGCR8 anchors pri-miRNAs which allow Drosha to cleave ~11bp from the base of pri-miRNAs[34]. DGCR8 and Drosha contain several functional domains required for pri-mRNA processing. DGCR8 contains two double-stranded-RNA binding, a heme-binding, and a Drosha binding-domains[38]. Drosha contains two RNase III domains, a double-stranded-RNA binding and a DGCR8-binding domains[39].

DGCR8[46] or Drosha[152] knock-out models in mice show to reduced production of global miRNAs. Interestingly, conditional knock-out of Dgcr8 in mouse skin cells shows a depletion of miRNAs rather than other small RNAs including rRNAs and sn/sno-RNAs[54]. These mice survived up to 5-6 days after birth with rough skin, weight gain failure, hair follicle downgrowth into the epidermis and increased apoptosis of mature hair bulbs. Additionally, knockdown of DGCR8 in human primary fibroblast or murine cells leads to cellular senescence and reduced miRNA expression[55]. These studies warrant further investigation to whether S153 phosphorylation contributes to these phenotypes.

Interestingly, DGCR8[83] and Drosha[88] are reported to be phosphorylated, however, it's unclear whether these phosphorylation events are functionally important for miRNA processing in response to UV radiation. Furthermore, it's unclear whether the functional domains of DGCR8 and Drosha are important for cellular response to UV. In this study, we present that phosphorylation on S153 of DGCR8 is required for cellular resistance to UV radiation independent of microRNA processing.

Results

To test the functional significance of UV-induced phosphorylation of S153, we examined UV sensitivity of DGCR8-deficient cells. We depleted DGCR8 in human colorectal cancer cell line (HCT-116) using three independent shRNAs. DGCR8-depleted cells were hypersensitive to UVC **(Fig. 3.1A)** and UVB **(Fig. 3.2A)**. Re-introduction of shRNA-resistant wild-type DGCR8 or the S153D phospho-mimetic mutant into DGCR8-depleted HCT116 cells restored UVC resistance, while the S153A phospho-mutant failed

to restore UVC (**Fig. 3.1B & 3.1C**) and UVB **(Fig. 3.2A)** resistance suggesting that S153 phosphorylation is critical for cellular resistance to UV. Similarly, DGCR8-depleted cells were hypersensitive to hydrogen peroxide, and reintroduction of wild-type and S153D mutant of DGCR8 into DGCR8-depleted cells restored resistance to hydrogen peroxide, but that of S153A mutant did not **(Fig. 3.2B)**.

Mutations introduced into two dsRNA-binding domains of DGCR8 almost completely abolish microRNA processing activity [38]. Surprisingly, complementation of DGCR8-depleted cells with the dsRNA binding domains mutant (mDRBD1/2) restored UVC (**Fig. 3.1B & 3.1C**) and UVB **(Fig. 3.2A)** resistance, indicating that RNA binding activity and microRNA processing function of DGCR8 are not required for UV resistance.

Among the various deletion mutants we tested **(Fig. 3.1C & 3.2C)** the Δ 692 (Drosha-binding deficient) mutant [38] restored UVC resistance in DGCR8-depleted cells **(Fig. 3.1C)**, while other mutants with large deletions (Δ 275, Δ 483, and Δ 276-773) [38] failed to do so **(Fig. 3.2D & 3.2E)**. In contrast, the Δ 692 S153A mutant failed to restore UV resistance in DGCR8-depleted cells **(Fig. 3.1C)**. The Δ 692 or the Δ 692 S153A mutant proteins were not co-immunoprecipitated with Drosha as expected, while wild type DGCR8 and the DGCR8 S153A mutant were co-immunoprecipitated with Drosha **(Fig. 3.1D)**. Altogether, these findings indicate that S153 phosphorylation is critical for UV resistance, while DGCR8-Drosha interaction is not.

Interestingly, Drosha depletion led to hypersensitivity to UVC and UVB **(Fig. 3.3A)**. Reintroduction of wild type Drosha, the Δ C114 (miRNA processing-deficient) or

Δ N490 (miRNA processing-deficient and DGCR8 binding-deficient) mutants of Drosha [39] into Drosha-depleted cells restored cellular resistance to UVC and UVB **(Fig. 3.3B & 3.3C)**, suggesting that DGCR8 binding or microRNA processing activities of Drosha are not required for UV resistance. Furthermore, UV-induced phosphorylation of S153 on DGCR8 occurred normally in Drosha-depleted cells (**Fig. 3.3D).** These findings collectively suggest that DGCR8 and Drosha are independently required for UV resistance and that microRNA processing activity of the Drosha-DGCR8 microprocessor complex is not important for UV resistance.

Next, to determine whether S153 on DGCR8 is critical for miRNA expression, we conducted a miRNA profiling using quantitative RT-PCR of 372 human miRNAs in DGCR8-depleted HCT116 cells transduced with empty vector, wild-type DGCR8, or the S153A mutant. DGCR8-depleted cells transduced with empty vector showed reduction of microRNA expression compared to other cells, but there was no clear difference of microRNA expression profiles between the wild-type and S153A DGCR8 cells **(Fig. 3.4-3.5, Table 3.1-3.2)**, suggesting that S153 is not critical for microRNA processing. This is consistent with a recent report that many phosphorylation sites on DGCR8 (including S153) are not critical for its microRNA processing activity[83].

Taken together, these finding suggest that DGCR8 has two independent functions: 1) S153 phosphorylation-mediated cellular resistance to UV, and 2) RNA binding- and Drosha binding-domains-mediated RNA (pri-miRNA) processing.

Discussion

In this study, we describe a new function of DGCR8 in cellular response to UV

radiation. In chapter two, we revealed that DGCR8 is phosphorylated on S153 after UV radiation. Here, we demonstrate that DGCR8 and Drosha are required for cellular resistance to UV radiation, consistent with previous report showing that miRNA biogenesis factors such as Dicer and Ago2 are required for UV resistance[151]. Importantly, we found that phosphorylation on S153 of DGCR8 was critical for cellular survival after UV radiation and hydrogen peroxide treatment. Furthermore, the RNA binding- and Drosha-binding domains of DGCR8 was not required for UV resistance, suggesting that S153 phosphorylation was required for UV resistance independent of its RNA binding- and RNA processing activities. Additionally, the RNA binding and DGCR8 binding domains of Drosha was not required for UV resistance. Altogether, these data indicates that S153 phosphorylation is critical for UV resistance, while DGCR8-Drosha interaction and its RNA binding activities are not important. It's been reported that DGCR8 contains a heme-binding domain that is required for efficient pri-miRNA processing[45]. This domain remains to be tested whether it's functionally important for UV resistance. Additionally, Drosha is phosphorylated at its N-terminus[88] and several mutations have been identified in Wilms tumor [130]. It remains to be determined whether these phosphorylation sites or mutations on Drosha contribute to the DGCR8-independent mechanism for UV resistance.

Reports of DGCR8 knock-out models indicate that DGCR8 is an essential gene that is involved in cellular proliferation and miRNAs processing. For instance, knock-out of DGCR8 in mouse embryonic stem cells shows a global loss of miRNAs, and defects in proliferation [46]. Conditional knock-out of DGCR8 in mouse skin cells shows a

depletion of a subset of miRNAs, results in early post-natal death and abnormal skin and hair development [54]. Additionally, specific deletion of DGCR8 in mouse cardiomyocytes leads to dilated cardiomyopathy and premature death and a loss of some miRNAs[51]. Deletion of DGCR8 impairs survival and turnover of peripheral NK cells[52]. It is possible that some of the phenotypic defects in DGCR8 knock-out models are a result of defects in miRNA-processing-independent functions of DGCR8. It will be important to determine whether S153 phosphorylated DGCR8 play a role in some of the defects.

Previous reports suggest that DGCR8 form an alternative complex consisting of other proteins including endonucleases[104, 153]. Additionally, DGCR8 is targeted by caspase-3 mediated cleavage, consequently reducing miRNA expression[154]. It is possible that DGCR8 functions through separate sub-complexes, one containing DGCR8 and Drosha that functions in miRNA processing, while UV-induced phosphorylated DGCR8 form another complex that participate in cellular resistance to UV radiation.

Lastly, a previous study shows that DGCR8 phosphorylation did not alter global miRNA expression[83], suggesting that phosphorylation of DGCR8 is not crucial for miRNA processing. Consistent with this observation, we found that majority of miRNAs were decreased by DGCR8 depletion and the reintroduction of either the wild-type or phospho-mutant (S153A) restored miRNA expression with no significant statistical difference, suggesting that S153 phosphorylation is not important for miRNA expression. In summary, we found that S153 phosphorylation is required for cellular resistance to UV independently of Drosha and miRNA processing.

Materials and Method

Cell lines. U2OS and HCT116 were obtained from the American Type Culture Collection (ATCC) and were grown in DMEM with 10% FBS, L-glutamine and Pen/strep.

Plasmids, siRNAs, shRNAs and virus production. Human full-length and DGCR8 truncated human DGCR8 (Δ 275, Δ 276-773, Δ 483 and Δ 484-773) were cloned into the Nco1 and BamH1 sites of pMMP-IRES-puro retroviral vector [143]. A phosphomutant (S153A) and a phosphomimic mutant (S153D) of DGCR8 were generated using the QuikChange XL Site-Directed Mutagenesis kit (200514-5, Agilent Technologies). The double-stranded RNA binding domain mutant A568K, A569K, A676K, S677K (mDRBD1/2) of DGCR8 was subcloned into pMMP-IRES-puro using the aforementioned sites from pcDNA-mDRBD1/2 DGCR8 [38], a gift from the Narry Kim lab (Seoul National University). FLAG-DGCR8 WT and mutants were mutated using QuikChange XL Site-Directed Mutagenesis kit with primers (1. Forward 5'CTCCCTGCTGAGGACCCTTTTAATTTTTATGGGGCCTCCCTTCTCTCCAA AGGA-3' 2. Reverse 5'TCCTTTGGAGAGAAGGGAGGCCCCATAAAAATTAAAAGGGTC CTCAGCAGGGAG -3') to generate shDGCR8-1 resistant constructs. The Drosha-binding domain mutant (FLAG-Δ692 WT and FLAG-Δ692 S153A) of DGCR8 was also subcloned into pMMP-IRES-puro. FLAG-wild-type-, FLAG-ΔC114- and FLAG-ΔN490-Drosha were subcloned into pBABE puro retroviral vector (a gift from the Clurman lab, FHCRC) using BamH1 and Sal1 sites from plasmids [155] provided by the Narry Kim lab. siDGCR8 (5'CCUU CAACUUCUACGGAGCUUC-3'), siDrosha-1 (5' AACGAGUAGGCUUCGUGACUU-3') and siDrosha-2 (5'-AAGUCACGAAGCCUACUCG-3') -3') were used. Lentiviral constructs containing shRNAs for DGCR8 (shRNA1: TRCN0000166035, shRNA2: TRCN0000165324, shRNA3: TRCN0000162331), Drosha (shRNA1: TRCN0000022249, shRNA2: TRCN000002

2250), or XPC (shRNA1: TRCN0000083119, shRNA2: TRCN0000083118) were purchased from Sigma. Retroviruses and lentiviruses were produced as described [144]. All constructs were verified by direct sequencing.

Antibodies. A rabbit polyclonal antibody against phosho-S153 DGCR8 (#5126) was generated by PhosphoSolutions. DGCR8 (10996-1-AP, Proteintech), Drosha (#3364, Cell Signaling), XPC (A301-122A, Bethyl Lab) and FLAG (F1804, Sigma-Aldrich) antibodies were used.

Western blot analysis and Immunoprecipitation. Whole-cell lysates were prepared using sample buffer (0.05 mol/L Tris-HCl (pH 6.8), 2% SDS, 6% β-mercaptoethanol), resolved by polyacrylamide gel (NuPage, Life Technologies) electrophoresis and transferred onto nitrocellulose membranes. For the immunoprecipitation, cells were lysed with lysis buffer (20mM Tris-HCl pH 7.4, 150mM NaCl, 0.5% NP40, 2mM $MgCl_{2,}$ 125units/mL Universal Nuclease (88702, Thermo Scientific) on ice for 30 minutes. After centrifugation at 4 °C at 13.2K rpm for 5 minutes, the supernatant was collected. One mg of protein lysate was pre-cleared in lysis buffer with protein A/G Plus-Agarose (sc-2003, Santa Cruz Biotechnology) incubated for 30 minutes at 4 °C on a shaker. After centrifugation at 4 °C at 2K rpm for 5 minutes, 2 µg of anti-FLAG antibody (F1804, Sigma-Aldrich) or normal mouse IgG (sc-2025, Santa Cruz Biotechnology) was added in the pre-cleared protein lysates. After an overnight incubation at 4 °C on a shaker, protein A/G Plus-Agarose was added into the mix and incubated at 4 °C on a shaker for 2 hours. Then, the lysates were washed 3 times with lysis buffer. After the last wash, lysates were boiled at 95°C in sample buffer. The

western blot was done as described above. Chemiluminescence was used for detection, and membranes were digitally scanned by Imagequant LAS 4000 (GE Biosciences).

Cell survival assay. Transduced or transfected HCT116 cells were seeded into 12-well plates at 8 x10^3/well and treated with UVC (254nm) from a UV stratalinker 1800 (Stratagene), UVB (output range 280-320nm) indicated doses from method previously described[142] or hydrogen peroxide (95321, Sigma-Aldrich). After incubation for 5-7days, cells were stained with crystal violet as described[144].

MicroRNA profiling. RNA from stable isogenic cell lines (HCT-116) depleted of endogenous DGCR8 by shDGCR8-1, transduced with shRNA-resistant FLAG-WT, FLAG-S153A DGCR8 or empty vector, were extracted using RNeasy mini kit (Qiagen). RNA from four biological replicates were submitted to Exiqon for miRNA real-time PCR using miRCURY LNA™ Universal RT microRNA PCR human panel 1 which contains 372 human miRNAs. Differential Expression: Raw Ct values were generated for four biological replicates. Samples were from two batches (two replicates per batch). MiRNAs with Ct values available for at least 3 replicates were analyzed for differential expression (117 miRNAs out of 257 non-control miRNAs) (n = 4 for 86 miRNAs, n = 3 for 31 miRNAs). SNORD38b snoRNA was used as an internal control. Ct values of SNORD38b snoRNA were subtracted from all raw Ct values for the 117 miRNAs respectively for each sample, per replicate, to obtain DCt values. Mean DCt values from at least 3 biological replicates were used to carry out pairwise DDCt calculation using either mean DCt from control untreated or mean DCt from control UV-treated cells as basis for comparison. DDCt values were log transformed. Heatmaps were generated in R using the 'gplots'

package. **Statistical Testing:** DCt values (from at least 3 biological replicates) were log transformed prior to pairwise statistical testing with Student's t-test. MiRNAs with $p < 0.05$ were considered to be statistically significantly differentially expressed. Relative expression was calculated for individual miRNAs with statistically significant differential expression in DGCR8-depleted cells relative to control or DGCR8-depleted cells complimented with wildtype DGCR8, untreated and 24 hours after $20J/m^2$ UVC treatment. DCt values of control or control +UVC were used as a baseline for pairwise comparison across 3 to 4 biological replicates. Relative expression was calculated by taking the inverse mean DCt relative to control or control +UVC across replicates.

Statistics. All statistical analyses (except for microRNA profiling) were done using Student's t-test (2-tail). P value < 0.05 was considered significant.

Figures and Legends

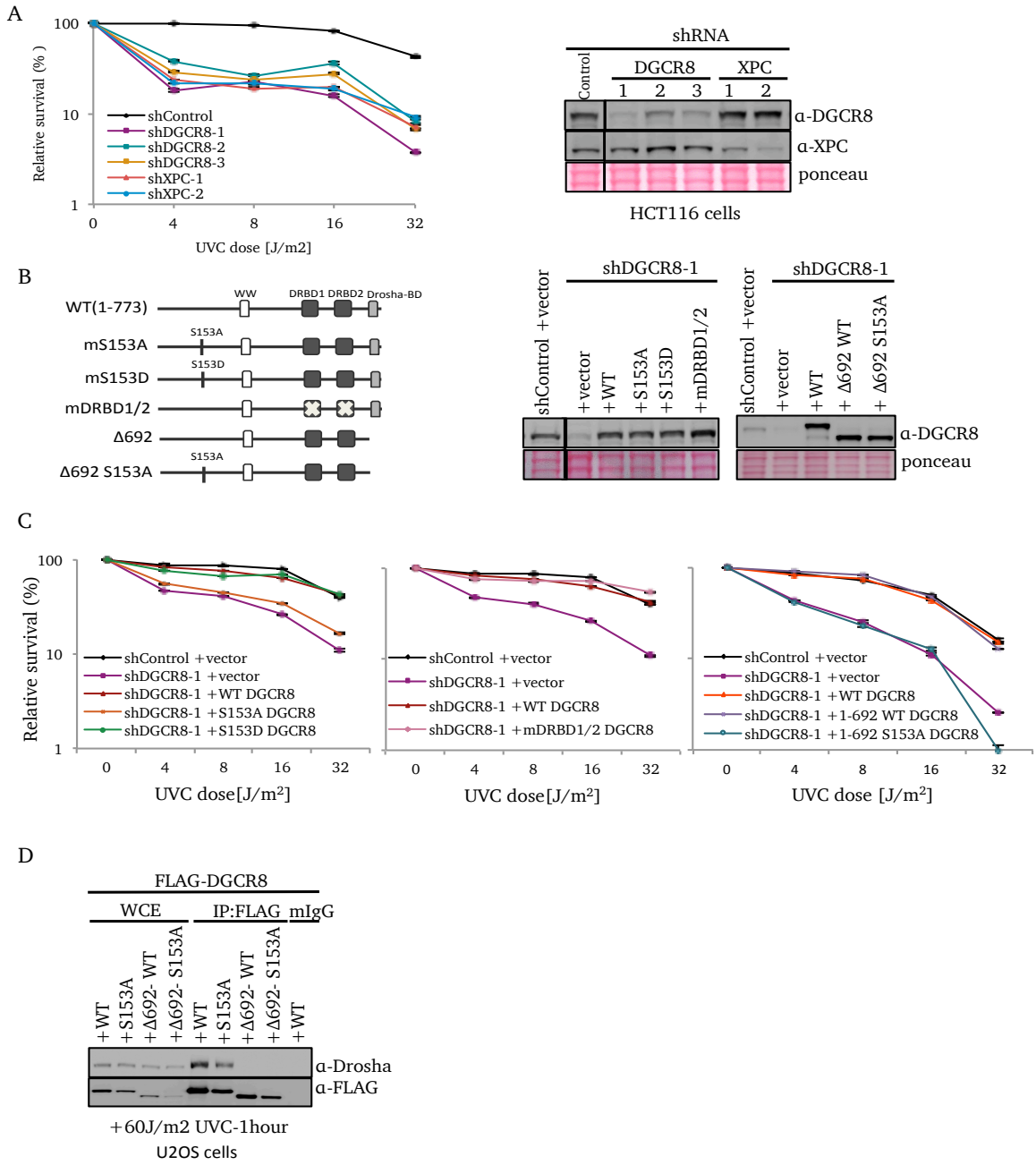

Figure 3.1 Phosphorylation of S153 on DGCR8 is critical for cellular resistance to UVC. **A.** UVC sensitivity assay. HCT116 cells were depleted of DGCR8 or XPC and subjected to the assay. Immunoblot confirmed DGCR8 and XPC depletion. **B.** Schematic presentation of DGCR8 mutants. Immunoblot confirmed expression of the indicated shRNA-resistant DGCR8 constructs in DGCR8-depleted HCT116 cells. **C.** UVC sensitivity assay. DGCR8-depleted HCT116 cells were transduced with the indicated DGCR8 constructs and subjected to the assay. All UVC sensitivity data represent mean values +/- SEM of three independent experiments. **D.** IP-western. Cell lysate of UV-treated U2OS cells transduced with the indicated FLAG-tagged DGCR8 constructs were immunoprecipitated with anti-FLAG. Immunoblot was done using the indicated antibodies.

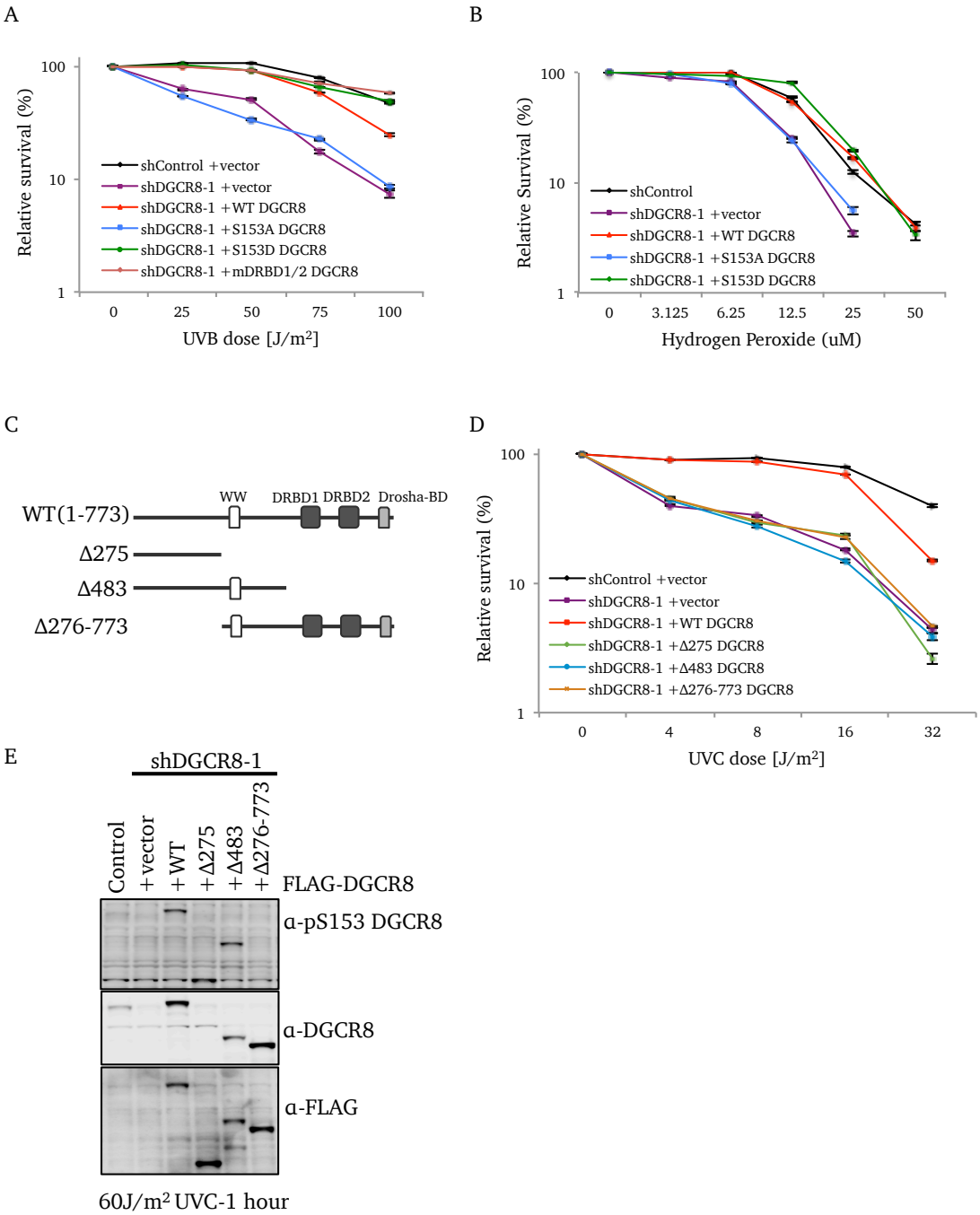

Figure 3.2 Phosphorylation of S153 of DGCR8 is critical for cellular resistance to UVB and hydrogen peroxide **A.** UVB sensitivity assay of DGCR-depleted HCT116 cells transduced with the indicated DGCR8 constructs. **B.** Hydrogen peroxide sensitivity assay of DGCR-depleted HCT116 cells transduced with the indicated DGCR8 constructs. **C.** Schematic presentation of DGCR8 deletion mutants. **D.** UVC sensitivity assay. DGCR8-depleted HCT116 cells were transduced with the indicated DGCR8 constructs and subjected to the assay. **E.** Immunoblot confirmed expression of the indicated shRNA-resistant DGCR8 deletion mutants and wild-type DGCR8 in DGCR8-depleted HCT116 cells. DGCR8 antibody does not detect Δ275-DGCR8. All UV sensitivity data represent mean values +/- SEM of three independent experiments.

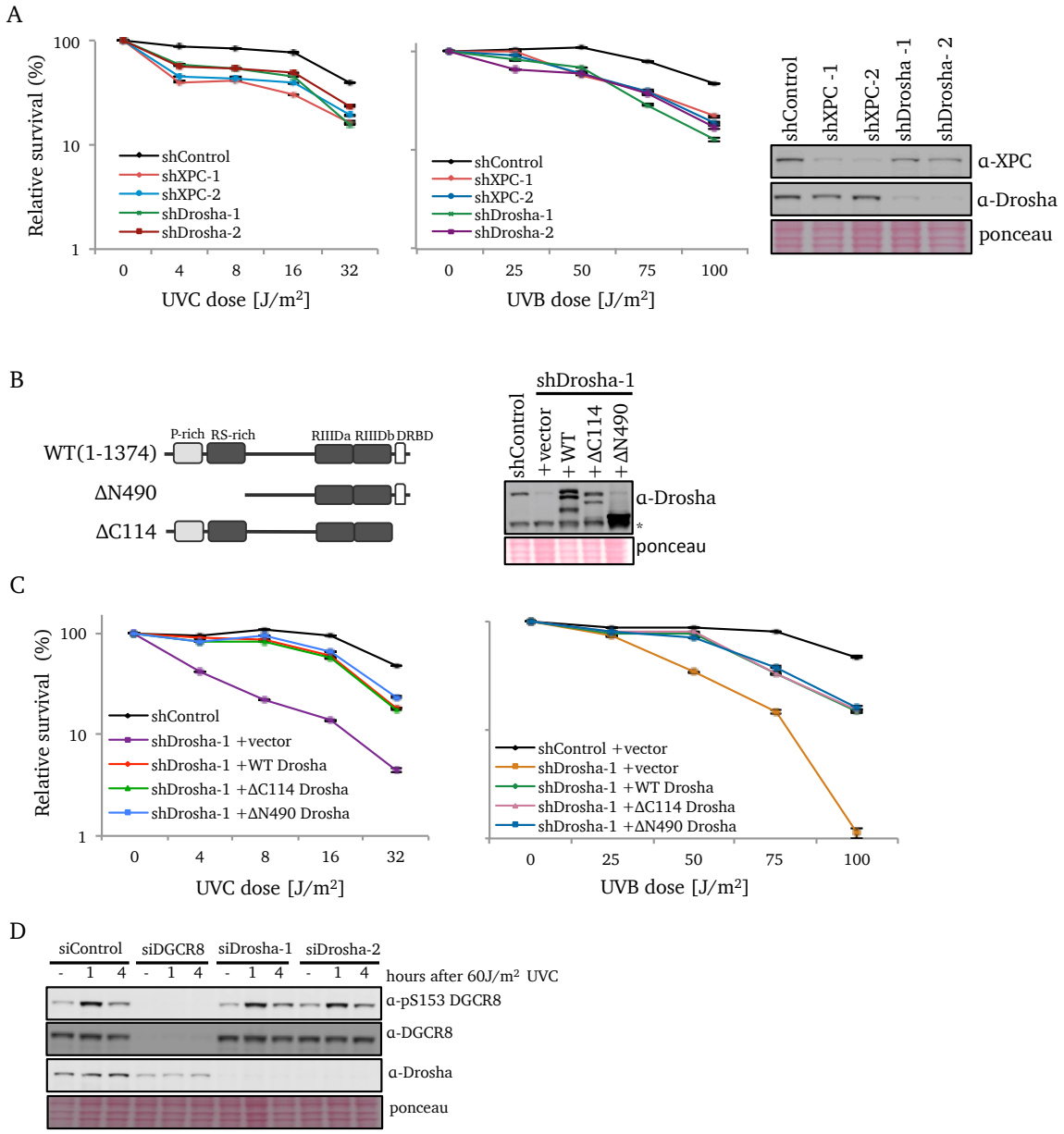

Figure 3.3 Drosha is required for UV resistance independently of DGCR8.
A. UVC and UVB sensitivity assay. HCT116 cells were depleted of Drosha or XPC, and subjected to the assay. Immunoblot confirmed the depletion. **B.** Schematic presentation of Drosha mutants. Immunoblot confirmed expression of the indicated Drosha constructs in Drosha-depleted HCT116 cells. **C.** Drosha depleted HCT116 cells were transduced with the indicated Drosha constructs and subjected to the UVC and UVB sensitivity assay. All UVC and UVB sensitivity data represent mean values +/- SEM of three independent experiments. **D.** U2OS cells depleted of DGCR8 or Drosha were UV irradiated and subjected to immunoblot with the indicated antibodies.

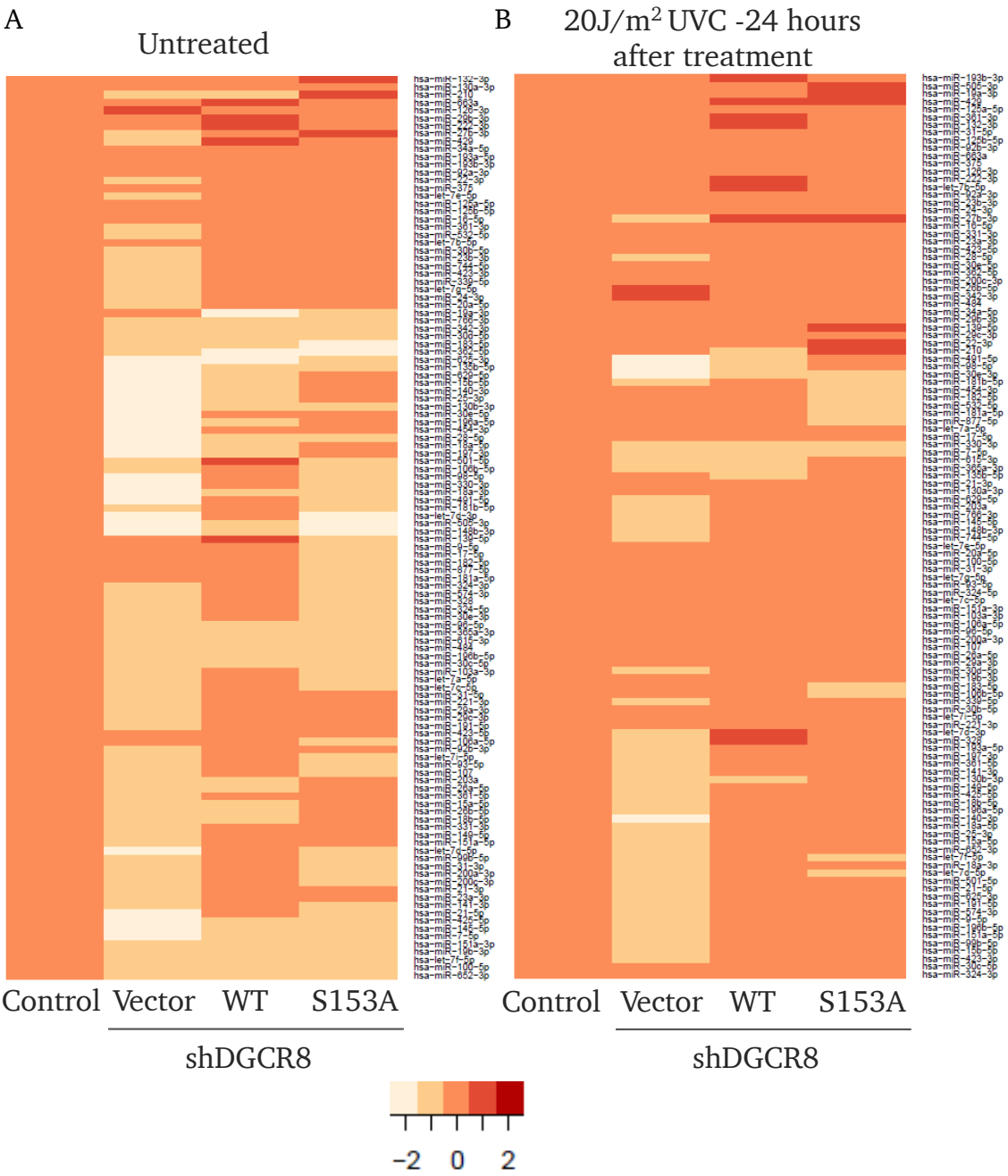

Figure 3.4 S153 phosphorylation is not critical for miRNA expression.
Heatmaps of differential expression of DGCR8-dependent miRNAs. Downregulation of a subset of miRNAs that occurred upon DGCR8 depletion was rescued by expression of either wildtype or DGCR8 153A mutant protein in DGCR8-depleted HCT116 cells. Expression of miRNA's in untreated DGCR8-depleted cells (+Vector) relative to untreated control cells is shown. **A**. Untreated control and DGCR8-depleted cells expressing empty vector, wild-type DGCR8, or DGCR8 153A-mutant and for **B.** UV-treated control and DGCR8- depleted cells expressing empty vector, wild-type DGCR8, or DGCR8 153A-mutant are shown. Decreased expression is indicated in shades of lighter shades of orange/red, while increased relative expression is indicated in darker shades of red. Clustering by rows (miRNAs) has been applied to heatmaps for better visualization. The values were normalized so that those of control cells transduced with empty vector are set to zero.

miRNAs	shDGCR8		
	+Vector	+WT- DGCR8	+S153A DGCR8
hsa-let-7a-5p	-0.620	-0.268	-0.478
hsa-let-7b-5p	-0.332	0.180	-0.128
hsa-let-7c-5p	-0.658	-0.362	-0.476
hsa-let-7d-3p	-1.314	-0.106	-1.316
hsa-miR-140-3p	-2.00	-0.619	0.365
hsa-let-7e-5p	-0.443	-0.226	-0.045
hsa-let-7f-5p	-0.995	-0.668	-0.550
hsa-let-7g-5p	-0.518	0.006	-0.318
hsa-let-7i-5p	-0.525	-0.393	-0.472
hsa-miR-100-5p	-0.862	-0.662	-0.596
hsa-miR-103a-3p	-0.705	-0.288	-0.594
hsa-miR-106a-5p	-0.411	-0.114	-0.502
hsa-miR-106b-5p	-1.096	0.095	-0.718
hsa-miR-107	-0.530	-0.318	-0.533
hsa-miR-125a-5p	-0.172	-0.242	-0.207
hsa-miR-125b-5p	-0.395	-0.167	-0.249
hsa-miR-126-3p	0.779	0.115	-0.106
hsa-miR-130a-3p	-0.143	-0.244	0.397
hsa-miR-130b-3p	-1.678	-0.609	-0.675
hsa-miR-132-3p	-0.407	-0.296	0.802
hsa-miR-135b-5p	-1.447	-1.264	-0.445
hsa-miR-139-5p	-0.222	0.537	-0.576
hsa-miR-25-3p	-1.93	-0.635	-0.375
hsa-miR-141-3p	-1.058	-0.140	-0.453
hsa-miR-197-3p	-1.66	-0.579	-0.298
hsa-miR-148b-3p	-1.529	-0.634	-1.499
hsa-miR-18a-3p	-1.52	-0.444	-1.042
hsa-miR-196a-5p	-1.46	-0.428	-0.086
hsa-miR-425-5p	-1.38	-0.450	-0.748
hsa-miR-145-5p	-1.34	-0.663	-0.449
hsa-miR-15b-5p	-1.545	-0.855	-0.276
hsa-miR-16-5p	-0.403	-0.229	-0.240
hsa-miR-17-5p	-0.361	-0.138	-0.733
hsa-miR-181a-5p	-0.207	-0.256	-1.041
hsa-miR-181b-5p	-1.039	-0.408	-1.149
hsa-miR-182-5p	-0.268	-0.284	-0.699
hsa-miR-183-5p	-1.039	-1.228	-1.572
hsa-miR-98-5p	-1.29	0.231	-0.720
hsa-miR-18a-5p	-1.569	-0.588	-0.236
hsa-miR-18b-5p	-1.030	-0.557	-0.150
hsa-miR-191-5p	-0.639	-0.367	-0.151
hsa-miR-193a-5p	-0.154	0.040	0.082
hsa-miR-193b-3p	-0.095	0.173	-0.145
hsa-let-7d-5p	-1.28	-0.159	-0.454
hsa-miR-196b-5p	-0.727	-0.505	-0.444
hsa-miR-766-3p	-1.24	-1.050	-1.007
hsa-miR-19a-3p	-0.071	-2.110	-0.563
hsa-miR-19b-3p	-1.058	-0.846	-0.684
hsa-miR-200a-3p	-1.054	-0.164	-0.695
hsa-miR-200c-3p	-0.845	-0.127	-0.461
hsa-miR-203a	-0.953	-0.467	0.221
hsa-miR-20a-5p	-0.617	0.007	-0.377
hsa-miR-210	-0.765	-1.134	0.666
hsa-miR-21-3p	-0.918	-0.238	-0.344
hsa-miR-21-5p	-1.403	-0.352	-0.572
hsa-miR-221-3p	-0.685	-0.210	-0.354
hsa-miR-222-3p	-0.157	0.489	0.023
hsa-miR-22-3p	-0.533	-0.177	0.134
hsa-miR-23a-3p	-1.049	-0.166	-0.336
hsa-miR-23b-3p	-0.807	0.262	-0.227
hsa-miR-24-3p	-0.558	0.098	-0.365

miRNAs	shDGCR8		
	+Vector	+WT- DGCR8	+S153A DGCR8
hsa-miR-149-5p	-1.22	-0.343	-0.407
hsa-miR-26a-5p	-0.898	-0.437	-0.151
hsa-miR-26b-5p	-1.003	-0.535	-0.143
hsa-miR-27b-3p	-0.629	0.392	0.494
hsa-miR-28-5p	-1.553	-0.508	-0.449
hsa-miR-29a-3p	-0.595	-0.374	-0.222
hsa-miR-29b-3p	-0.398	0.613	0.189
hsa-miR-29c-3p	-0.623	-0.304	-0.167
hsa-miR-30b-5p	-0.649	0.220	-0.053
hsa-miR-30c-5p	-0.849	-0.440	-0.492
hsa-miR-30d-5p	-0.601	-0.741	-1.179
hsa-miR-30e-3p	-0.572	-0.163	-0.972
hsa-miR-30e-5p	-1.540	-0.326	-0.075
hsa-miR-31-3p	-0.930	-0.056	-0.611
hsa-miR-31-5p	-0.578	-0.167	-0.260
hsa-miR-324-3p	-0.604	0.053	-0.704
hsa-miR-324-5p	-0.571	-0.170	-0.912
hsa-miR-328	-0.714	0.031	-0.930
hsa-miR-330-3p	-1.837	-0.228	-0.719
hsa-miR-331-3p	-1.060	-0.153	-0.146
hsa-miR-339-5p	-0.568	0.002	-0.242
hsa-miR-342-3p	-0.738	-0.670	-0.945
hsa-miR-34a-5p	0.025	0.261	0.151
hsa-miR-361-3p	-0.884	0.040	0.178
hsa-miR-361-5p	-0.836	-0.389	-0.270
hsa-miR-362-5p	-1.013	-1.613	-1.905
hsa-miR-365a-3p	-0.650	-0.964	-0.657
hsa-miR-375	-0.420	-0.194	-0.031
hsa-miR-151a-5p	-1.20	-0.165	-0.414
hsa-miR-423-5p	-0.397	-0.112	-0.391
hsa-miR-151a-3p	-1.16	-0.563	-0.714
hsa-miR-429	-0.731	0.760	0.190
hsa-miR-454-3p	-1.690	-0.311	-0.265
hsa-miR-484	-0.490	-0.555	-0.746
hsa-miR-491-5p	-1.722	-0.417	-1.070
hsa-miR-501-5p	-1.097	0.553	-1.155
hsa-miR-505-3p	-1.363	-0.685	-1.411
hsa-miR-532-5p	-0.431	0.342	-0.125
hsa-miR-574-3p	-0.687	-0.005	-0.841
hsa-miR-615-3p	-0.669	-0.984	-0.621
hsa-miR-625-3p	-1.923	-1.427	-0.444
hsa-miR-629-5p	-1.269	-0.910	-0.286
hsa-miR-652-3p	-0.906	-0.602	-0.680
hsa-miR-663a	0.357	0.585	0.102
hsa-miR-744-5p	-0.759	0.095	-0.222
hsa-miR-7-5p	-1.315	-0.611	-0.580
hsa-miR-15a-5p	-1.04	-0.474	-0.159
hsa-miR-877-5p	-0.026	-0.103	-0.890
hsa-miR-92a-3p	-0.095	-0.021	-0.129
hsa-miR-92b-3p	-0.424	-0.322	-0.389
hsa-miR-93-5p	-0.495	-0.252	-0.484
hsa-miR-9-5p	-0.196	0.121	-0.615
hsa-miR-96-5p	-0.506	-0.780	-0.428
hsa-miR-423-3p	-0.74	0.045	-0.202
hsa-miR-99b-5p	-0.952	-0.273	-0.576

Table 3.1 S153 phosphorylation is not critical for miRNA expression in untreated condition. List of differential expression of DGCR8-dependent miRNAs from the heatmap above for the untreated condition. Downregulation of a subset of miRNAs that occurred upon DGCR8 depletion was rescued by expression of either wildtype or DGCR8 153A mutant protein in DGCR8-depleted HCT116 cells. Highlighted in "green" indicates miRNAs that are statistically significant expression ($p < 0.05$) from three to four biological replicates.

miRNAs	shDGCR8		
	+Vector	+Wildtype DGCR8	+S153A
hsa-let-7a-5p	-0.234	0.207	-0.416
hsa-let-7b-5p	0.182	0.673	-0.287
hsa-let-7c-5p	-0.064	0.114	-0.253
hsa-let-7d-3p	-1.137	0.819	-0.311
hsa-let-7d-5p	-0.986	-0.166	-0.614
hsa-let-7e-5p	-0.211	0.192	0.053
hsa-let-7f-5p	-0.754	-0.085	-0.629
hsa-let-7g-5p	-0.027	0.264	-0.084
hsa-let-7i-5p	-0.387	-0.135	-0.434
hsa-miR-100-5p	-0.119	-0.025	0.029
hsa-miR-103a-3p	-0.172	0.183	-0.111
hsa-miR-106a-5p	-0.285	0.208	-0.184
hsa-miR-106b-5p	-0.280	-0.246	-0.593
hsa-miR-107	-0.277	-0.013	-0.205
hsa-miR-125a-5p	0.320	0.499	0.452
hsa-miR-125b-5p	-0.017	0.459	0.067
hsa-miR-126-3p	-0.092	0.398	-0.194
hsa-miR-130a-3p	-0.463	-0.406	0.161
hsa-miR-130b-3p	-1.049	-0.605	-0.246
hsa-miR-132-3p	0.074	1.137	0.482
hsa-miR-135b-5p	-0.471	-0.626	0.217
hsa-miR-139-5p	0.268	0.073	0.605
hsa-miR-140-3p	-1.540	-0.137	-0.469
hsa-miR-141-3p	-0.939	0.369	-0.076
hsa-miR-145-5p	-0.755	-0.124	-0.089
hsa-miR-148b-3p	-0.843	-0.102	-0.104
hsa-miR-149-5p	-1.102	-0.159	-0.150
hsa-miR-151a-3p	-0.246	0.241	-0.059
hsa-miR-151a-5p	-0.761	0.130	-0.086
hsa-miR-15a-5p	-0.821	-0.400	-0.359
hsa-miR-15b-5p	-0.709	-0.067	-0.196
hsa-miR-16-5p	-0.131	0.201	0.187
hsa-miR-17-5p	-0.385	0.313	-0.468
hsa-miR-181a-5p	-0.128	0.047	-0.666
hsa-miR-181b-5p	-0.776	-0.227	-1.289
hsa-miR-182-5p	-0.389	0.285	-0.689
hsa-miR-183-5p	-0.195	-0.314	-0.569
hsa-miR-18a-3p	-1.006	-0.218	-0.431
hsa-miR-18a-5p	-1.537	-0.132	-0.246
hsa-miR-18b-5p	-1.267	-0.003	-0.399
hsa-miR-191-5p	-0.584	0.182	-0.054
hsa-miR-193a-5p	-0.545	0.448	0.060
hsa-miR-193b-3p	0.093	0.525	0.470
hsa-miR-196a-5p	-1.195	-0.223	-0.365
hsa-miR-196b-5p	-0.718	0.060	-0.056
hsa-miR-197-3p	-0.960	0.374	0.083
hsa-miR-19a-3p	0.104	0.331	0.758
hsa-miR-19b-3p	-0.091	-0.311	-0.347
hsa-miR-200a-3p	-0.434	-0.327	-0.168
hsa-miR-200c-3p	-0.501	0.404	-0.183
hsa-miR-203a	-0.910	0.045	0.066
hsa-miR-20a-5p	-0.191	0.099	-0.032
hsa-miR-210	0.315	-0.933	0.519
hsa-miR-21-3p	-0.462	-0.450	0.215
hsa-miR-21-5p	-0.931	0.229	-0.223
hsa-miR-221-3p	-0.484	-0.116	-0.500
hsa-miR-222-3p	0.313	0.704	0.049
hsa-miR-22-3p	-0.270	-0.063	0.584
hsa-miR-23a-3p	-0.296	0.318	0.120
hsa-miR-23b-3p	-0.147	0.499	0.353
hsa-miR-24-3p	-0.100	0.512	0.225
hsa-miR-25-3p	-1.483	-0.150	-0.316
hsa-miR-26a-5p	-0.286	-0.101	-0.143
hsa-miR-26b-5p	0.945	0.467	0.152
hsa-miR-27b-3p	-0.523	0.515	0.554
hsa-miR-28-5p	-0.515	0.133	0.317
hsa-miR-29a-3p	-0.427	-0.039	0.075
hsa-miR-29b-3p	0.217	-0.026	-0.233
hsa-miR-29c-3p	0.168	-0.170	0.486
hsa-miR-30b-5p	-0.507	-0.185	-0.353
hsa-miR-30c-5p	-0.442	-0.007	-0.144
hsa-miR-30d-5p	-0.513	-0.143	-0.010
hsa-miR-30e-3p	-1.875	-0.805	-0.858
hsa-miR-30e-5p	-0.279	0.393	-0.136
hsa-miR-31-3p	-0.137	-0.010	-0.014
hsa-miR-31-5p	-0.032	0.449	0.170
hsa-miR-324-3p	-0.401	-0.011	-0.298
hsa-miR-324-5p	-0.025	0.080	-0.241
hsa-miR-328	-0.725	0.705	0.027
hsa-miR-330-3p	-0.890	-1.437	-0.760
hsa-miR-331-3p	-0.209	0.232	0.183
hsa-miR-339-5p	-0.555	-0.310	-0.467
hsa-miR-342-3p	0.624	-0.496	0.018
hsa-miR-34a-5p	0.147	-0.183	-0.003
hsa-miR-361-3p	0.337	0.944	0.491
hsa-miR-361-5p	-0.839	0.291	-0.036
hsa-miR-362-5p	-0.458	0.312	-0.077

miRNAs	shDGCR8		
	+Vector	+Wildtype DGCR8	+S153A
hsa-miR-365a-3p	-0.540	-0.623	-0.048
hsa-miR-375	0.035	0.467	-0.241
hsa-miR-423-3p	-0.529	0.101	-0.245
hsa-miR-423-5p	-0.345	0.204	0.116
hsa-miR-425-5p	-1.329	-0.315	-0.189
hsa-miR-429	0.411	0.623	0.612
hsa-miR-454-3p	0.082	0.043	-1.173
hsa-miR-484	0.262	-0.171	-0.072
hsa-miR-491-5p	-2.565	-0.663	-0.372
hsa-miR-501-5p	-0.750	0.453	-0.474
hsa-miR-505-3p	0.055	0.401	0.526
hsa-miR-532-5p	-0.416	0.315	-0.896
hsa-miR-574-3p	-0.687	0.172	-0.077
hsa-miR-615-3p	-1.206	-0.964	-0.508
hsa-miR-625-3p	-0.893	0.206	-0.449
hsa-miR-629-5p	-0.965	-0.018	0.210
hsa-miR-652-3p	-0.726	-0.443	-0.486
hsa-miR-663a	0.213	0.373	0.095
hsa-miR-744-5p	-0.925	-0.079	-0.121
hsa-miR-7-5p	-0.815	-0.787	-0.563
hsa-miR-766-3p	-0.876	-0.104	-0.295
hsa-miR-877-5p	-0.404	0.098	-0.584
hsa-miR-92a-3p	0.198	0.423	-0.189
hsa-miR-92b-3p	-0.079	0.506	-0.040
hsa-miR-93-5p	-0.126	0.292	-0.100
hsa-miR-9-5p	-0.700	0.174	-0.159
hsa-miR-96-5p	-0.138	-0.337	0.006
hsa-miR-98-5p	-1.612	-0.528	-0.363
hsa-miR-99b-5p	-0.607	-0.095	-0.249

Table 3.2 S153 phosphorylation is not critical for miRNA expression in UV treated condition. List of differential expression of DGCR8-dependent miRNAs from the heatmap above for the UV-treated condition. Downregulation of a subset of miRNAs that occurred upon DGCR8 depletion was partially rescued by expression of either wildtype or DGCR8 153A mutant protein in DGCR8-depleted HCT116 cells. Highlighted in "green" indicates miRNAs that are statistically significant expression ($p < 0.05$) from three to four biological replicates.

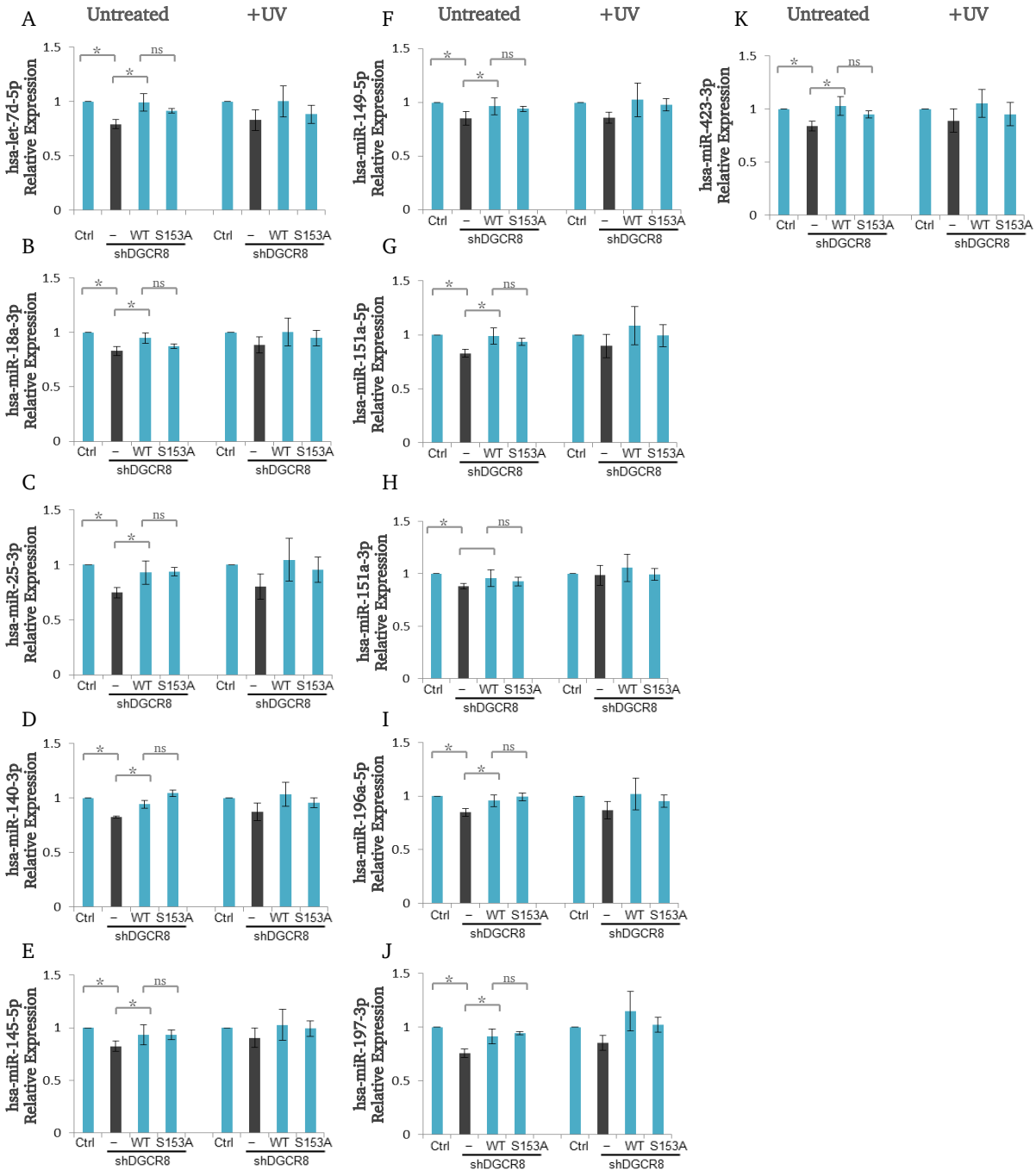

Figure 3.5 **S153 phosphorylation is not critical for miRNA expression.**
A-K. Relative expression is shown for miRNAs with statistically significant differential expression in DGCR8-depleted cells relative to control or DGCR8-depleted cells complimented with wild-type DGCR8, untreated and 24 hours after 20J/m^2 UVC . Relative expression shown is the inverse mean of ΔCt values relative to control across 3 to 4 replicates. Error bars indicate SEM across biological replicates. An "*" indicates statistically significant differential expression ($p < 0.05$) and an "ns" indicates a non-significant result. None of the UV treated samples showed statistically significant results.

CHAPTER FOUR

Phosphorylation of DGCR8 is Required for the Repair of UV-induced DNA Lesions by Transcription-coupled Nucleotide Excision Repair

Abstract

The nucleotide excision repair (NER) pathway, which operates through two subpathways: global genome nucleotide excision repair (GG-NER) and transcription-coupled repair (TC-NER) protects the mammalian genome from the UV-induced DNA lesions, including cyclobutane pyrimidine dimers (CPDs) and 6-4 pyrimidine-pyrimidone (6-4PPs). Here, we describe a novel microRNA independent function of DGCR8 in TC-NER. DGCR8 depletion, but not Drosha depletion, led to impaired removal of UV-induced DNA lesions (CPDs and 6-4PPs). Reintroduction of wild-type DGCR8 rescued this delay. In contrast, reintroduction of phospho-mutant (S153A) failed to rescue the repair of CPDs and 6-4PPs, suggesting that phosphorylation on S153 of DGCR8 is required for the efficient repair of UV-induced DNA lesions.

DGCR8 depletion was functionally linked to defects in XPA, CSA and CSB, but not in XPC, suggesting that DGCR8 functions in TC-NER but not in GG-NER. DGCR8-depleted cells and S153A DGCR8 phospho-mutant cells showed delayed recovery of RNA synthesis after UV exposure, further suggesting that phosphorylation of S153 is required for TC-NER. Treatment with a transcription elongation inhibitor, 5,6-Dichlorobenzimidazole 1-β-D-ribofuranoside (DRB), also induced S153 phosphorylation, consistent with the idea that stalled RNA Polymerase II (the first step in TC-NER) triggers the phosphorylation. These data suggest that phosphorylation on S153 of DGCR8 is critical in removing UV-induced DNA lesions through TC-NER.

Introduction

UV irradiation generates DNA photoproducts, mainly cyclobutane pyrimidine dimers (CPDs) and 6-4 pyrimidine-pyrimidone (6-4PPs), and causes cell cycle arrest, apoptosis, mutagenesis and proliferative transformation [7]. These DNA lesions are repaired by nucleotide excision repair (NER) in mammalian cells [156]. Deficiencies in NER are associated with human genetic disorders, such as xeroderma pigmentosum (XP), Cockayne syndrome (CS), cerebro-oculo-facio-skeletal syndrome (COFS), UV-sensitive syndrome (UVSS) and trichothiodystrophy (TTD) [156]. The NER pathway operates through two subpathways: global genome nucleotide excision repair (GG-NER) and transcription-coupled nucleotide excision repair (TC-NER) **(Fig 1.2)** [156]. In GG-NER, XPC and UV-DDB recognize damage sites throughout the genome, while TC-NER is initiated by RNA polymerase II (RNAPII) blocked by DNA lesions during transcription [156]. These subpathways converge on a common downstream pathway to resolve the DNA lesions [156].

MiRNAs are initially transcribed as long primary miRNAs (pri-miRNAs) [20]. Pri-miRNAs are processed by the microprocessor complex, consisting of Drosha (an RNase III-type enzyme), and DGCR8, a double-stranded RNA-binding protein, to generate ~70-nt precursor miRNAs (pre-miRNAs) [20]. Pre-miRNAs are exported to the cytoplasm where they are cleaved by another RNase III, Dicer, to generate a ~22-nt mature miRNA duplexes. Apart from its critical role in miRNA biogenesis [157], DGCR8 also regulates the stability of some mRNAs and snoRNAs [104]. The two dsRNA-binding domains of DGCR8 are required for the recognition of the RNA substrates [38, 41, 104].

Interestingly, the microprocessor complex is recruited to chromatin during transcription of the host transcript and process primary-miRNA co-transcriptionally [105, 106]. Additionally, DGCR8/Drosha along with transcription termination factors, Setx, Xrn2 and Rrp6 induces RNAPII pausing and premature termination at the HIV-1 promoter [107]. Moreover, UV and transcriptional inhibitors induced DGCR8 localization to distinct speckles in the nucleoplasm[153, 158]. In a recent study, Drosha was found to bind to RNAPII and at promoter regions of transcribed human genes independent of its RNA cleavage and miRNA processing activities that resulted in efficient transcription elongation and increased gene expression[159]. Since RNAPII stalls after UV-induced DNA lesions, it's an intriguing possibility that phosphorylated DGCR8 is involved in the removal of UV-induced DNA lesions by interacting with RNA pol II and factors in the TC-NER.

Results

We found that depletion of DGCR8 delayed the repair of CPDs **(Fig 4.1)** and 6-4PPs **(Fig 4.2)** similar to XPC depletion, and re-introduction of wild-type DGCR8 into DGCR8-depleted cells restored efficient removal of CPDs and 6-4 PPs, suggesting that DGCR8 is required for the repair of UV-induced DNA lesions. Importantly, the reintroduction of S153A-DGCR8 failed to restore the efficient repair of UV-induced DNA lesions, suggesting that UV-induced phosphorylation of DGCR8 at S153 is required for the efficient repair of UV-induced DNA lesions **(Fig 4A & 4B)**. Interestingly, depletion of Drosha did not delay the repair of UV-induced DNA lesions (**Fig 4A & 4B**), suggesting that Drosha is not involved in the DNA repair of the UV-induced DNA lesions

and again suggesting that the mechanisms by which Drosha functions in UV resistance is different from that the mechanisms by which DGCR8 functions in UV resistance.

UV-induced DNA lesions are detected and repaired by the NER pathway, which consists of two sub-pathways, GG-NER and TC-NER. XPC is involved in GG-NER, while RNA polymerase II (RNAP II), Cockayne syndrome A (CSA) and Cockayne syndrome B (CSB) are involved in TCR-NER. Some of other NER factors, including xeroderma pigmentosum complementation A (XPA), are involved in the common downstream events of the both sub-pathways [160]. To determine the role of DGCR8 in NER, we depleted DGCR8 in human patient-derived fibroblast deficient in XPC, XPA, CSA or CSB and their corrected counterparts. XPC, XPA, CSA and CSB deficient cells were hypersensitive to UVC compared to controls as previously reported[161].

DGCR8 depletion in XPA, CSB and CSA-deficient cells did not further sensitize these cells to UVC (**Fig 4.3A-C**), indicating that XPA, CSA and CSB are epistatic with DGCR8 terms of UV sensitivity. In contrast, DGCR8 depletion further sensitized XPC-deficient cells to UVC radiation (**Fig 4.4**), indicating that DGCR8 and XPC are not epistatic. These data suggest that DGCR8 functions in TC-NER, but not in GG-NER.

Since RNAPII stalling is presumed to be the initial step for TC-NER [162], we hypothesized that RNAPII stalling triggers S153 phosphorylation. To test this, we treated human cells with a transcription inhibitors, actinomycin D and 5,6-Dichlorobenzimidazole 1-β-D-ribofuranoside (DRB). Actinomycin D or DRB treatment led to increased S153 phosphorylation even in the absence of UV treatment **(Fig 4.6A-B)**. Depletion of CDK9, a kinase involved in transcription elongation and a target of

DRB, also led to increased phosphorylation of S153 **(Fig 4.6C)**. These findings suggest that RNAPII stalling caused either by UV-induced DNA lesions or by other mechanisms stimulates S153 phosphorylation. Furthermore, DGCR8 was co-immunoprecipitated with RNAPII and CSB, and the interaction was increased after UV treatment **(Fig 4.7A),** consistent with the notion that DGCR8 plays a role in TC-NER. However, DGCR8 depletion did not affect expression of CSA, CSB, or RNAPII, **(Fig 4.7B)** and CSA or CSB deficiency did not affect UV-induced phosphorylation of S153 of DGCR8 **(Fig 4.7C)**, indicating that S153 phosphorylation is not downstream of CSB or CSA.

Discussion

In the previous chapters, we described the discovery of UV-induced S153 phosphorylation on DGCR8. This phosphorylation is required for cellular resistance to UV radiation independently of Drosha binding and miRNA processing. In this chapter, we describe that UV-induced S153 phosphorylation on DGCR8 mediates the removal of UV-induced DNA lesions by TC-NER. More specifically, first, we show that S153 phosphorylation was important for the removal of UV-induced CPDs and 6-4PPs. Second, we found that DGCR8 is epistatic with factors in TC-NER (CSA, CSB, and XPA), but not with XPC, which is a factor specifically involved in GG-NER. Third, S153 phosphorylation mediated recovery of RNA synthesis after UV radiation. Fourth, S153 phosphorylation was induced by transcription inhibition even without UV radiation, suggesting that RNAPII stalling caused either by UV-induced DNA lesions or by other mechanisms stimulates S153 phosphorylation. Finally, we found that DGCR8 was co-immunoprecipitated with RNA polymerase II and CSB, and the interaction increased

after UV radiation, consistent with notion that DGCR8 participates in transcription-coupled repair initiation. Altogether, these data indicate that S153 phosphorylation mediates he removal of UV-induced DNA lesions through TC-NER pathway.

These findings uncover a novel, unexpected function of DGCR8 in TC-NER. This function of DGCR8 may make sense, considering, the fact that the microprocessor complex is recruited to chromatin during transcription and processes pri-miRNA co-transcriptionally [105, 106], and that Drosha binds to RNAPII at promoter regions of transcribed genes, resulting in efficient transcription elongation and increased gene expression [159]. Perhaps by proximity, it is possible that DGCR8 is recruited along with CSB after RNA polymerase II stalling and participate in TC-NER. Another intriguing possible mechanism is the S153 phosphorylation is involved in R-loop dynamics and regulations. R-loops are RNA-DNA hybrid displaced by single-stranded DNA formed during transcription when RNA emerges from the transcription machinery and hybridized with the DNA template and causes double-strand breaks[163]. Most recently, this process has been shown to involve transcription-coupled repair factor, CSB, and not global genome repair factor, XPC[164]. It would be of great interest to determine whether S153 phosphorylation DGCR8 participates in the process since we found that DGCR8 are functionally linked to defects in TC-NER and not GG-NER.

Materials and Methods

Cell lines: U2OS and HCT116 were obtained from the American Type Culture Collection (ATCC). XPA deficient (GM04312), XPA corrected (GM15876), CSA (GM16094) and CSB (GM16095) deficient human fibroblasts were purchased from

Coriell Cell Repositories. These cells were grown in DMEM with 10% FBS, L-glutamine and Pen/strep. XPC deficient cells (XP4PASV) and XPC corrected human fibroblasts (XP4PASV/FLAG-XPC(wt)) were described [161].

Plasmids, siRNAs, shRNAs and virus production. Human DGCR8 and CSA cDNA were cloned into the Nco1 and BamH1 sites of pMMP-IRES-puro retroviral vector [143]. A phosphomutant (S153A) and a phosphomimic mutant (S153D) of DGCR8 were generated using the QuikChange XL Site-Directed Mutagenesis kit (200514-5, Agilent Technologies). FLAG-DGCR8 WT and mutants were mutated using QuikChange XL Site-Directed Mutagenesis kit with primers (1. Forward 5'ctccctgctgaggacccttttaatttttatggggcc tcccttctctccaaagga-3' 2. Reverse 5'tcctttggagagaagggaggccccataaaaattaaaagggtcctcagcagg gag -3') to generate shDGCR8-1 resistant constructs. CSB construct (pBR-CSB) was a gift from Weiner lab (University of Washington) and was used to subclone FLAG-CSB into pBABE-puro retroviral vector using BamH1 and Sal1 sites. siDGCR8 (5'-ccuucaacuucuacg gagcuuc-3'), siDrosha-1 (5'-aacgaguaggcuucgugacuu-3'), siDrosha-2 (5'-aagucacgaagcc uacucg-3') and siCSB (5'-caggacucgugguucaaauua-3') were used. Lentiviral constructs containing shRNAs for DGCR8 (shRNA1: TRCN0000166035, shRNA2: RCN0000165324, shRNA3: TRCN0000162331), Drosha (shRNA1: TRCN0000022249, shRNA2: TRCN0000022250), or XPC (shRNA1: TRCN0000083119, shRNA2: TRCN0000083118) were purchased from Sigma. Retroviruses and lentiviruses were produced as described [144]. All constructs were verified by direct sequencing.

Antibodies: A rabbit polyclonal antibody against phosho-S153 DGCR8 (#5126) was generated by PhosphoSolutions. DGCR8 (10996-1-AP, Proteintech), Drosha (#3364,

Cell Signaling), ERCC8 (CSA) (15921-1-AP, Proteintech), FLAG (F1804, Sigma-Aldrich), CSB (sc-25370, Santa Cruz Bio.), XPA (sc-853, Santa Cruz Bio.), XPC (A301-122A, Bethyl Lab.), CDK9 (C12F7) (2316, Cell signaling), CPD (CAC-NM-DND-001, Cosmo Bio Co.) and 6-4PP (CAC-NM-DND-002, Cosmo Bio Co.) antibodies were used.

Western blot analysis. Whole-cell lysates were prepared using sample buffer (0.05 mol/L Tris-HCl (pH 6.8), 2% SDS, 6% β-mercaptoethanol), resolved by polyacrylamide gel (NuPage, Life Technologies) electrophoresis and transferred onto nitrocellulose membranes. Chemiluminescence was used for detection, and membranes were digitally scanned by Imagequant LAS 4000 (GE Biosciences).

Cell survival assay. XP and CS cells were seeded into 12-well plates at 1 x 10^4/well and treated with UVC (254nm) from a UV Stratalinker 1800 (Stratagene). After incubation for 5-7 days, cells were stained with crystal violet as described [144].

Flow cytometry. Cells were treated with UVC (12 J/m^2 for detection of CPDs, or 60 J/m^2 for detection of 6-4PPs) and fixed with 2% paraformaldehyde at 37 °C for 10 minutes. Then, cells were treated with cold 90% methanol for 30 minutes at -20 °C and treated with DNase (Promega) for 1 hour at 37 °C. After blocking with PBS containing 1% BSA for 10 minutes at room temperature, cells were incubated with anti-CPD (1:1000) or anti-6-4PPs (1:1000) diluted in PBS containing 1% BSA and 0.25% Tween 20 overnight at 4 °C. After washing with PBS containing 1% BSA and 0.05% Tween 20, cells were incubated with fluorescein-conjugated anti-mouse antibody (1:1000) (715-095-151, Jackson ImmunoResearch) for 1 hour in the dark at room temperature. Nuclei were counterstained with propidium iodide (2 µg/mL) (P1470, Sigma-Aldrich) and

treated with RNase A (100 µg/mL) (Invitrogen) for 20 minutes at 37°C. Flow cytometric analyses were conducted with a BD FACS Canto II analyzer and the FlowJo software.

Recovery of RNA synthesis (RRS) assay. RRS assays were done as described with some modifications [165, 166]. U2OS cells stably expressing siRNA resistant FLAG-WT DGCR8, FLAG-S153A DGCR8 or FLAG-S153D-DGCR8 were transfected with siRNA against endogenous DGCR8. Forty-eight hours after transfection of siRNAs, cells were irradiated with UVC (16 J/m^2) and immediately incubated with 5'-ethynyuridine (EU) (50 µM, Life Technologies) for 2 hours [165, 166]. Then, cells were fixed and permeabilized at the indicated time points. After blocking with PBS containing 10% FBS, cells were incubated for 1 hour at room temperature with Alexa-fluor 488 goat anti-rabbit (A11034, Life Technologies) secondary antibody. Nuclei were counterstained with DAPI (1 µg/mL). Coverslips were mounted on slides with Vectashield (Vector Laboratories). Image acquisitions were made with a TE2000 Nikon microscope with a 20x immersion objective, a CCD camera (CoolSNAP ES) and MetaVue software (Universal Imaging). EU signal intensity was measured by Cellomics software (Thermo Scientific). Cells without EU incubation were used as a negative control to subtract background signal.

Statistics. All statistical analyses were done using Student's t-test (2-tail). P value < 0.05 was considered significant.

Figures and Legends:

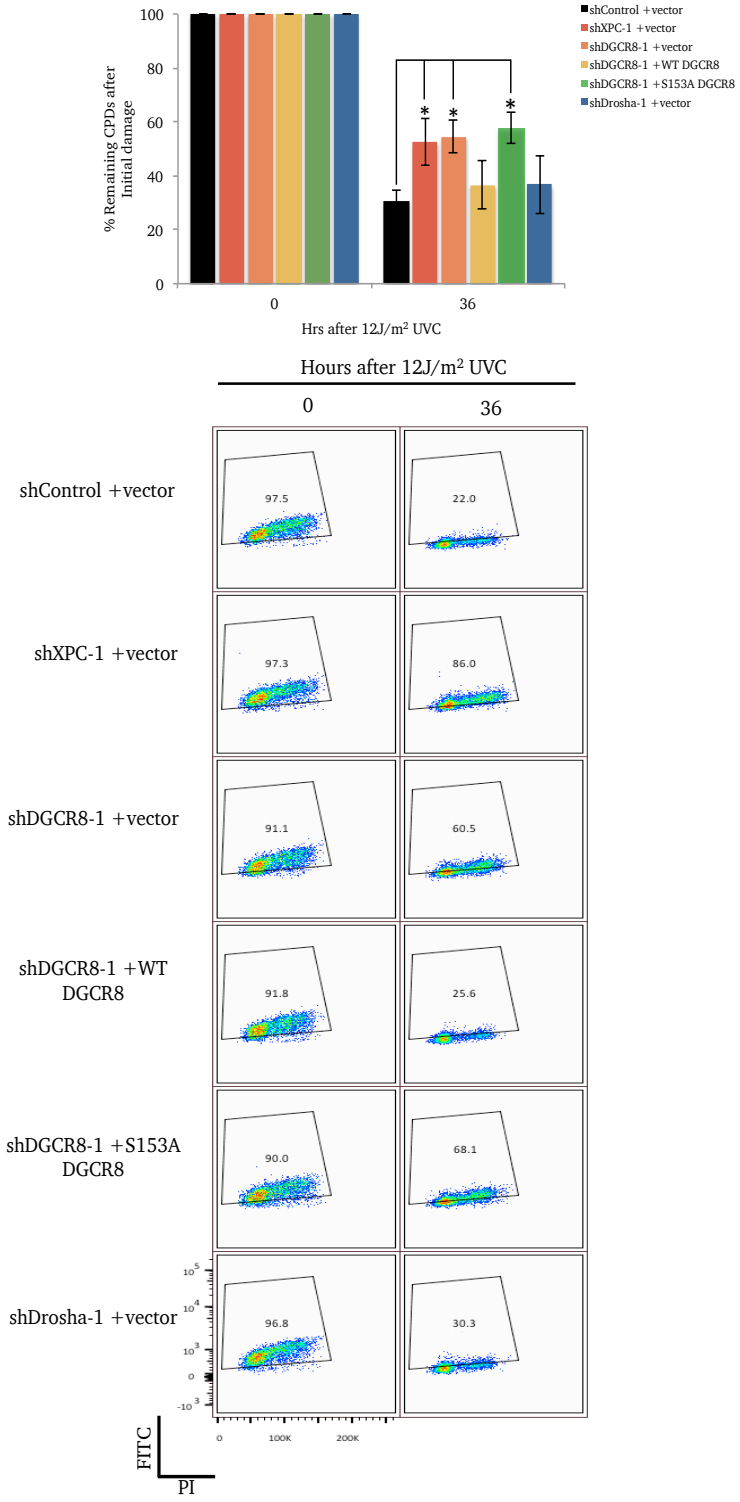

Figure 4.1 DGCR8 phosphorylation mediates the removal of cyclobutane pyrimidine dimers (CPDs). Removal of CPDs assessed by flow cytometry using anti-CPD. HCT116 cells depleted of indicated genes and complemented with indicated constructs were treated with UVC, and CPD positive cells at the indicated time points were measured. Asterisks indicate significant difference ($p<0.05$) relative to shControl +empty vector transduced cells.

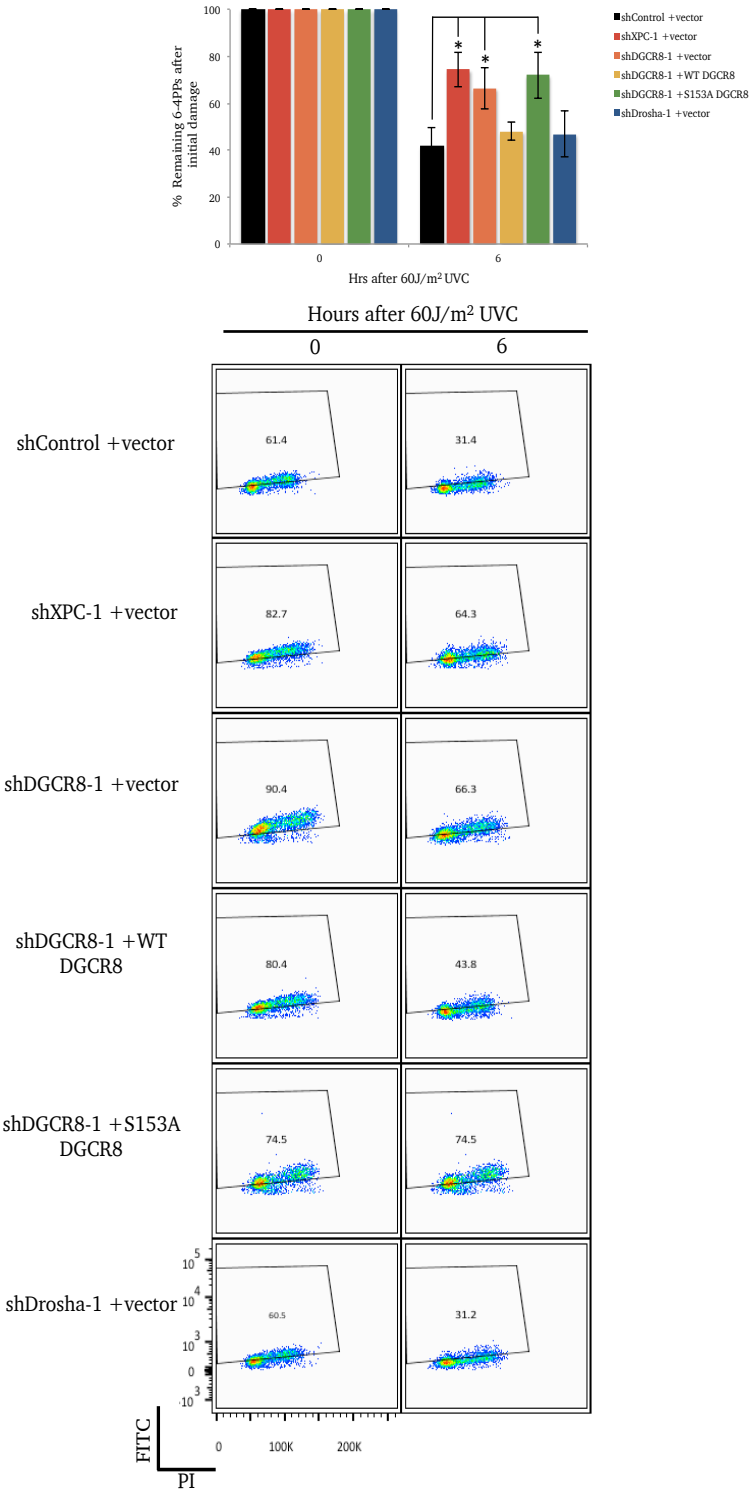

Figure 4.2 DGCR8 phosphorylation mediates the removal of 6-4 pyrimidine-pyrimidone (6-4PPs) dimers. Removal of CPDs assessed by flow cytometry using anti-6-4PPs. HCT116 cells depleted of indicated genes and complemented with indicated constructs were treated with UVC, and 6-4PPs positive cells at the indicated time points were measured. Asterisks indicate significant difference ($p<0.05$) relative to shControl +empty vector transduced cells.

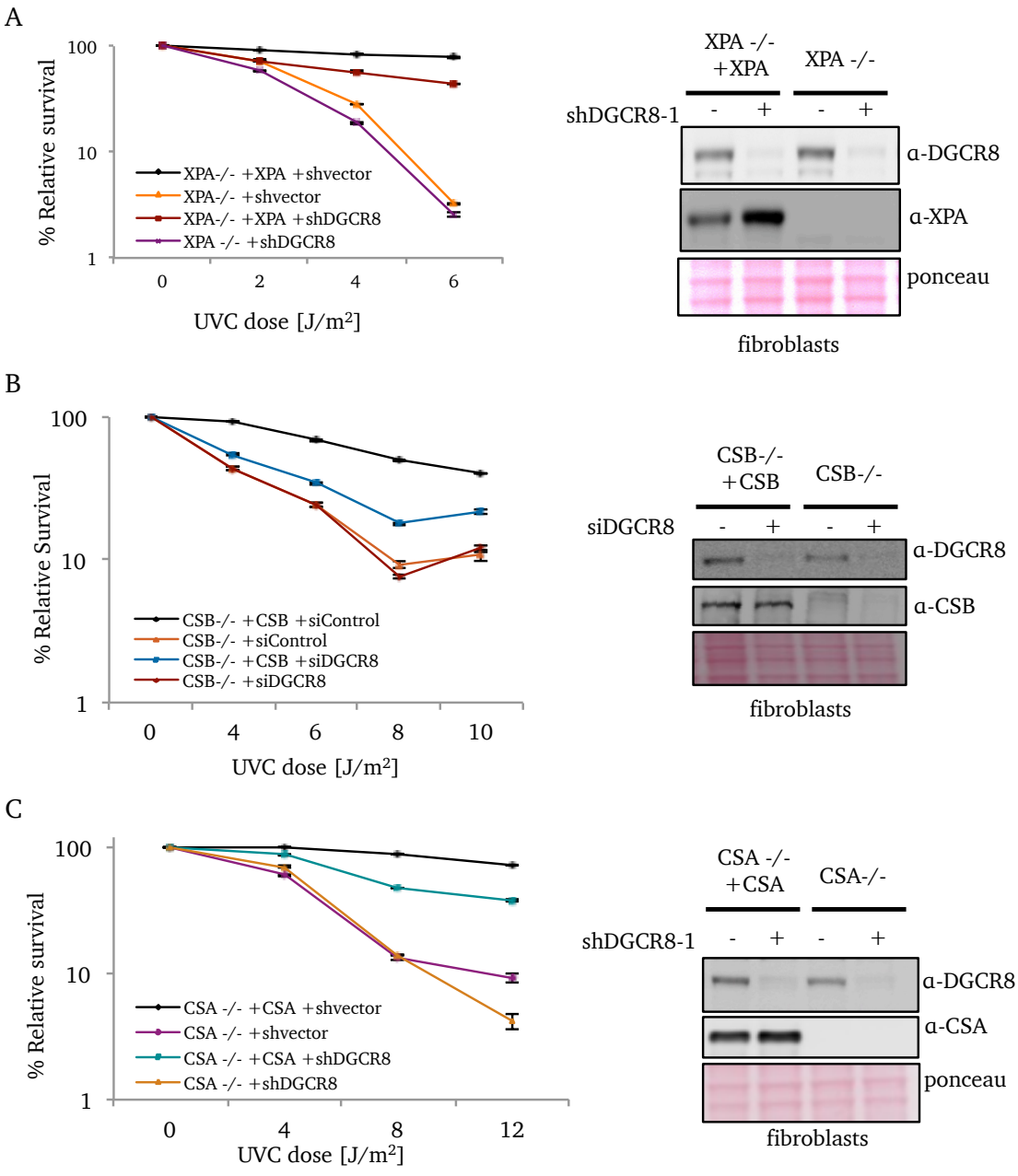

Figure 4.3 DGCR8 is functionally linked to defects in transcription-coupled nucleotide excision repair. UVC sensitivity assay. **A.** XPA-, **B.** CSB-, or **C.** CSA-deficient fibroblasts and their corrected counterparts were depleted of DGCR8, and subjected to UVC sensitivity assay.

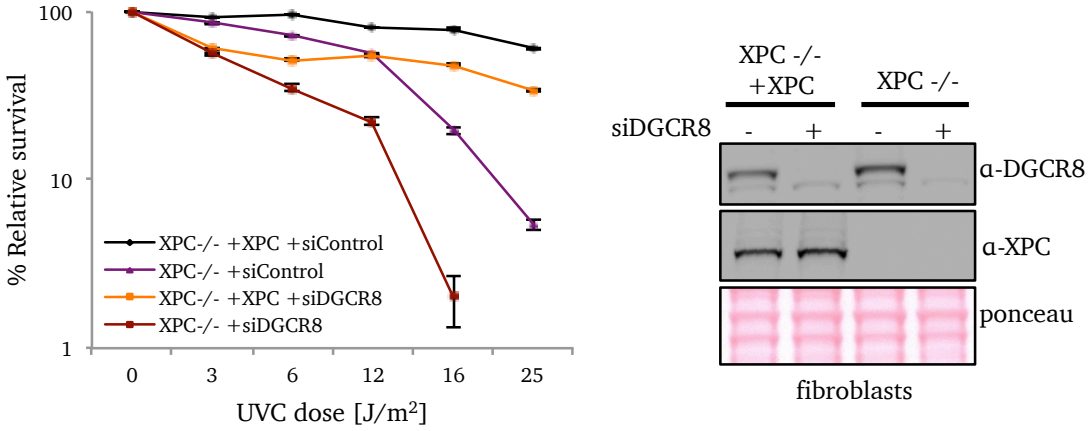

Figure 4.4 DGCR8 is not functionally linked to defects in global-genome repair. UVC sensitivity assay. XPC-deficient fibroblasts and their corrected counterparts were depleted of DGCR8, and subjected to UVC sensitivity assay.

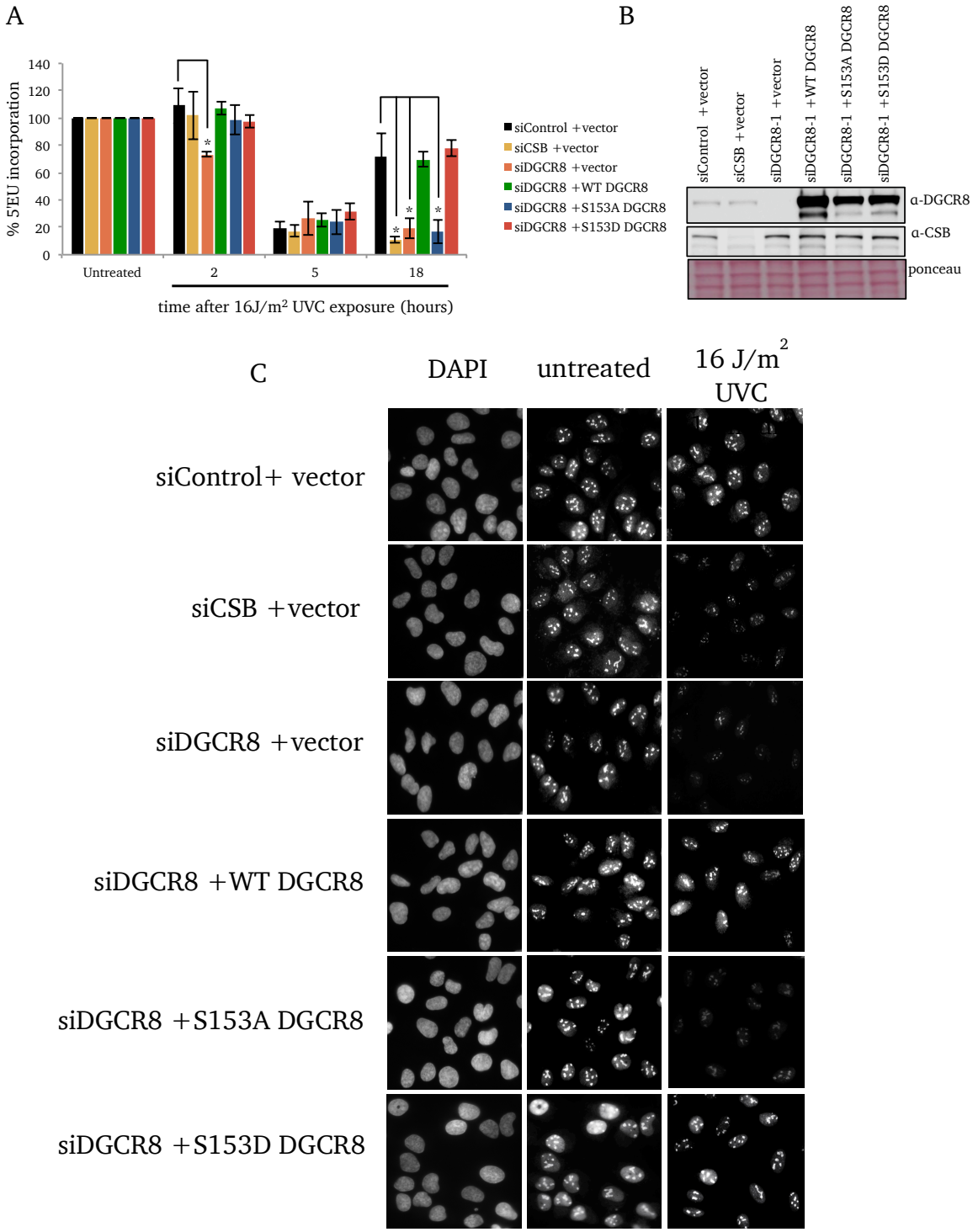

Figure 4.5 Phosphorylation of S153 on DGCR8 is required for recovery of RNA synthesis after UV radiation. A-B. Recovery of RNA synthesis (RRS) assay. 5'-ethynyuridine (5' EU) incorporation kinetics after UVC radiation. U2OS cells transfected with indicated siRNAs and cDNA constructs were subjected to the assay. Asterisks indicate significant difference ($p<0.05$) relative to siControl +empty vector transduced cells. **C.** Representative immunofluorescence images of RRS assay.

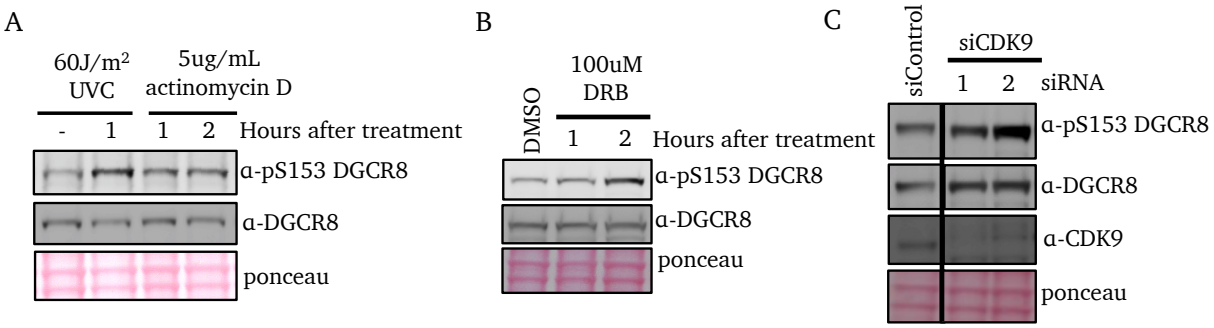

Figure 4.6 Phosphorylation of S153 on DGCR8 is induced by transcriptional inhibition. U2OS cells treated with **(A)** actinomycin D, **(B)** 5,6-Dichlorobenzimidazole 1-β-D-ribofuranoside (DRB) or **(C)** transfected with CDK9 siRNA were subjected to immunoblotting.

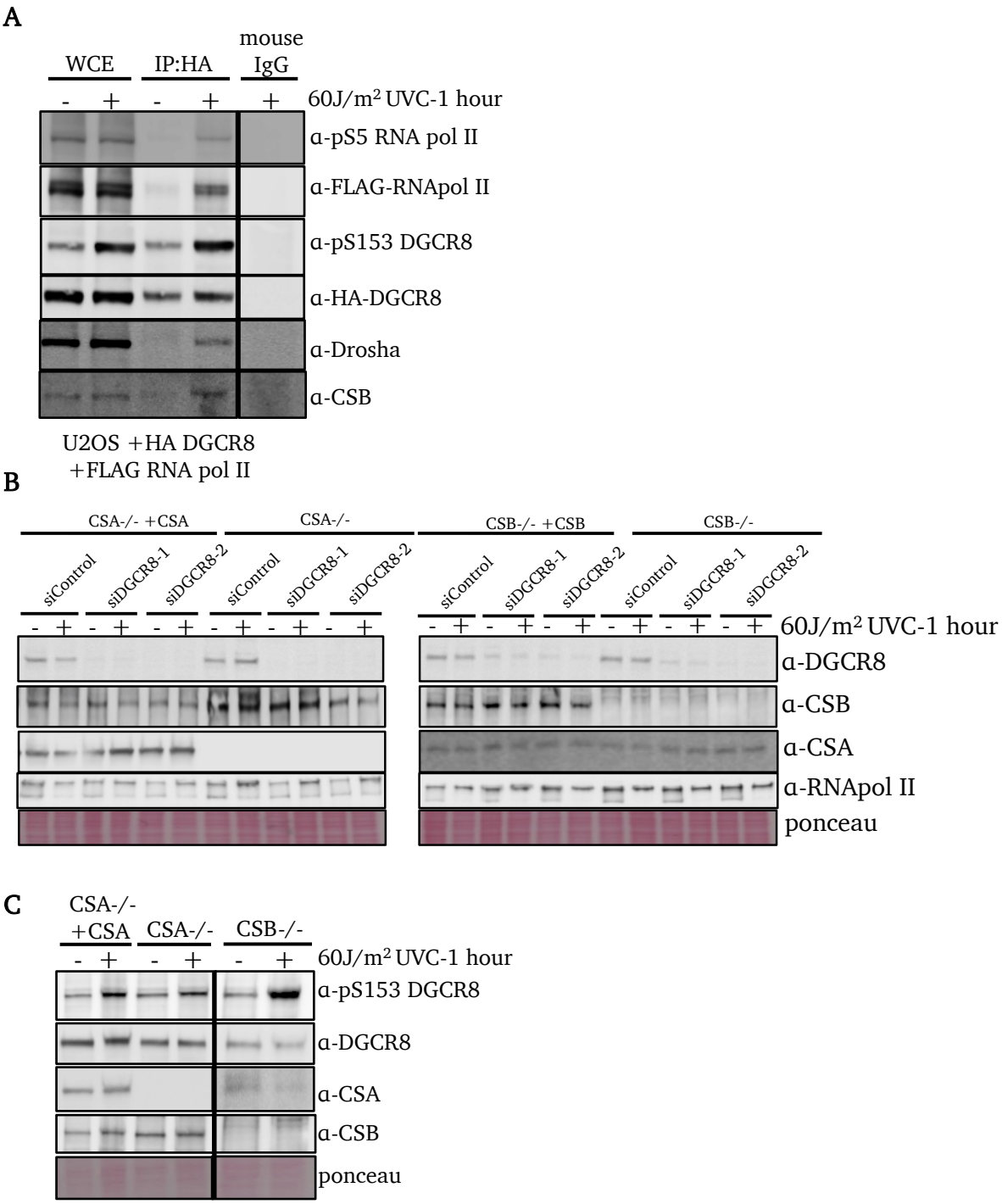

Figure 4.7 Interaction between DGCR8 and factors involved in transcription-coupled nucleotide excision. A. IP-western. Cell lysate of UV-treated (or untreated) U2OS cells transduced with the HA-tagged DGCR8 and FLAG-tagged RNAPII constructs were immunoprecipitated with anti-HA antibody or control mouse IgG. Immunoblot was done using the indicated antibodies. **B.** Immunoblot. DGCR8 depletion did not affect expression of CSA, CSB, or RNAPII. **C.** Immunoblot. CSA or CSB deficiency did not affect UV-induced phosphorylation of S153 of DGCR8.

CHAPTER FIVE

Identification of Kinase(s) that Phosphorylate S153 of DGCR8

Abstract

Kinases play a major role in cellular response to UV radiation. In earlier chapters, I demonstrate that DGCR8 is phosphorylated on S153 after UV radiation. Importantly, this phosphorylation event is required for the removal of UV-induced DNA lesions, recovery of RNA synthesis and mediates cellular resistance to UV radiation, independently of microRNA processing. However, the kinase that phosphorylates S153 of DGCR8 is unknown. Here, I describe a global approach by high-content immunofluorescence screening of a kinome siRNA library containing siRNAs against over 700 known human kinases to identify the kinase(s) that phosphorylate S153 of DGCR8. Validation using two to three independent siRNAs against many top hits revealed two promising kinases that phosphorylate S153 of DGCR8. Depletion of either Serine/Threonine Kinase 23 (STK23) or NIM1 serine/threonine protein kinase (NIM1K) delayed UV-induced S153 phosphorylation, suggesting that these kinases are involved in phosphorylating S153 of DGCR8 early in response to UV. This also suggests that other kinase(s) compensates to phosphorylate S153 of DGCR8 later after UV radiation.

In addition, I describe the results of a high-content immunofluorescence screen of siRNAs against over 300 DNA responsive genes to identify modifiers of UV-induced phosphorylation on S153 of DGCR8.

Introduction:

Ultraviolet (UV) radiation activates many kinases that phosphorylate numerous proteins which mediate cell cycle arrest, initiate DNA repair pathways and re-program gene expression to facilitate apoptosis, or survival and proliferation [7].

DGCR8 is reported to be phosphorylated at 23 phosphorylation sites, and phosphorylation of some of these sites is mediated by MAPK ERK[83]. These phosphorylation sites are important for DGCR8 protein stability, but not microRNA expression. Elucidation of each phosphorylation site of DGCR8, its functional significance and the responsible kinase(s) that phosphorylate these sites remains to be determined. In the previous chapters, I described a critical role of UV-induced phosphorylation of S153 of DGCR8 in the removal of UV-induced DNA lesions by TC-NER and in cellular survival after UV exposure. However, the kinase that phosphorylates S153 of DGCR8 in response to UV is unknown. Here, I will describe a global approach by high-content microscopy screening of over 700 known human kinases to identify the kinase(s) that is involved in the phosphorylation of S153 of DGCR8.

Results

To identify the responsible kinase(s) that phosphorylate S153 of DGCR8 after UV radiation, first we took a candidate approach and tested several kinases implicated in response to UV treatment. Depletion by siRNA or by chemical inhibition of ATR, CHK1, ATM, CK2, AMPK, MAPKs, DNA-PK, CDK1-2, CDK4, CDK6-9 and CDK11-12 did not suppress UV-induced S153 DGCR8 phosphorylation (**Fig 5.4A**). Therefore, we performed a high-content microscopy screen of a human kinome siRNA library to identify kinases that are

required for phosphorylation of S153 and included a panel of siRNAs against over 300 DNA damage responsive genes to identify additional modifiers of phosphorylation on S153 using anti-phosphoS153 DGCR8 (**Fig 5.1A**). The screen was performed on cells treated with or without hydrogen peroxide (100μM) for 1 hour. We used hydrogen peroxide instead of UV because it was technically difficult to UV irradiate cells evenly in 384-well plates and hydrogen peroxide is as potent as UV to induce phosphorylation of S153 (**Fig 2.4D**). The nuclear intensity/cell/well was captured, measured and the Z-score was calculated to determine the top hits. For example, depletion of GSK3β, like depletion of DGCR8, decreased nuclear intensity relative to control **(Fig 5.1B)**.

Since S153 of DGCR8 is basally phosphorylated **(Fig 2.3D)**, it is also important to identify kinases that phosphorylate S153 of DGCR8 in untreated conditions. From the screen, depletion of many kinases decreased **(Fig 5.2A-B)** or increased **(Fig 5.2A & C)** basal S153 phosphorylation of DGCR8. The screen also revealed depletion of many kinases decreased **(Fig 5.3A-B)** or increased **(Fig 5.2A & C)** S153 phosphorylation of DGCR8 after hydrogen peroxide treatment.

For validation, we focused on serine/threonine kinases and excluded receptor tyrosine kinases whose depletion suppressed S153 phosphorylation after hydrogen peroxide treatment. Cells depleted with two to three independent siRNAs for each target kinase of interest were treated with UV and western blotting was performed to validate the results from the screen. Many of the hits that suppressed S153 phosphorylation from the screen were not validated by western blotting using anti-phosphoS153 DGCR8, while some even increased UV-induced S153 phosphorylation or moderately decreased total

DGCR8 protein **(Fig 5.4A)**. However, depletion of serine/threonine 23 (SFRS Protein Kinase 3(SRPK3)) or NIM1 Serine/Threonine Protein Kinase (NIM1K) using two independent or three independent siRNAs, respectively, suppressed UV-induced S153 phosphorylation **(Fig 5.4B-D)**.

Lastly, analysis from screening the DNA damage responsive genes panel revealed that depletion of several factors involved in DNA damage response decreased or increased S153 phosphorylation **(Fig 5.5)**. For instance, depletion of PCNA or ATRIP, proteins involved in UV response, decreased S153 phosphorylation after hydrogen peroxide treatment. In contrast, depletion of ERCC2, MLH1 or BRCA2 increased S153 phosphorylation after hydrogen peroxide treatment.

Discussion

In the previous chapters, I describe and characterize that S153 phosphorylation is required for cellular resistance to UV by removing UV-induced DNA lesion by TC-NER pathway. Here, I described our effort to identify several candidate kinases that are involved in phosphorylation of S153 on DGCR8 using a high-content immunofluorescence microscopy screen and to identify additional candidate modifiers by screening a DNA damage responsive panel that contains many factors involved in DNA damage response and DNA repair.

After validation using two-three independent siRNAs against the top candidate kinases whose depletion reduced phosphorylation of S153 in the screen, we found that depletion of STK23 (SRPK3) or NIM1K suppressed UV-induced phosphorylation reproducibly, suggesting that these kinases may be involved in phosphorylation S153

after UV radiation. STK23 (SRPK3) or serine-arginine protein kinase 3 is an interesting candidate because it belongs to a family of kinases that phosphorylate SR motifs of its target protein and is involved in many biological processes including alternative RNA splicing, mRNA maturation, chromatin reorganization and cell cycle control[167]. Interestingly, DGCR8 has been implicated in alternative splicing independently of miRNA processing[104]. Additionally, SRPK1, a member of the SR family kinases and known binding partner of STK23 has been shown to interact with DGCR8[37, 168]. Further analysis is warranted to determine whether STK23 or other SRPKs can regulate phosphorylation of S153 on DGCR8 directly or indirectly.

In a recent report, DGCR8 has been identified to contain 23 phosphorylation sites and are phosphorylated by MAPK ERK, however it remains to be determined which of these sites are MAPK ERK1-mediated[83]. In addition, DGCR8 was immunoprecipitated with c-Jun N-terminal kinases (JNK) and it's predicted that S153 on DGCR8 is phosphorylated by NEK6[83]. Further analyses are warranted to determine whether these kinases directly or indirectly regulate phosphorylation of S153 on DGCR8.

Additionally, candidates from the DNA damage responsive panel screen also revealed promising modifiers of S153 phosphorylation, including factors involved in UV response such as PCNA[169] and ATRIP[7]. It would be interesting to determine whether S153 phosphorylation is involved in translesion DNA synthesis. Interestingly, depletion of NER factor, ERCC2, increased UV-induced S153 phosphorylation. It's intriguing to determine whether ERCC2 play a role in DGCR8-mediated UV resistance. In summary, we have identified several candidates for kinases and additional S153

phosphorylation modifiers from our screens. Further studies need to be done to determine whether they are functionally relevant in DGCR8-mediated cellular resistance to UV radiation.

Materials and Methods

Cell lines and siRNAs. U2OS was obtained from the American Type Culture Collection (ATCC) and were cultured in DMEM with 10% FBS, L-glutamine and pens/strep . siDGCR8 (5'CCUUCAACUUCUACGGAGCUUC-3'), siSTK23-1 (5'-UUUGAGGGCCACAAAGCGC-3'), siSTK23-2 (5'-AAGAACUCCCGGGAAUAGC-3') siNIM1K-1 (5'-UUCAUGAUGCAGUCGAUUC-3'), siNIM1K-2 (5'-UUUCGAAUAUGCUCU UCUG-3'), siNIM1K-3 (5'-AGUUUGGCCACGGUUUCUG-3').

Kinase library screening. Screening was done at the Quellos High Throughput Screening Core (University of Washington) utilizing their siRNA library containing 713 kinases or panel containing over 300 DNA responsive genes, all of which are collection of 3 equimolar-pooled duplexes per target, from Sigma or Monnat Lab (University of Washington), respectively. U2OS cells were plated with FluidX 384 into 384-well plates. The next day, cells were transfected with siRNA using Lipofectamine RNAiMax (Invitrogen). The transfections were carried out on the Cybio Vario liquid handler. After 48 hours, cells were treated with 100uM hydrogen peroxide (sigma) for 1hr. Then, cells were fixed and probed for anti-phosphoS153 DGCR8 using BioTek EL406 Washer and liquid handler. Nuclear intensity/cell was quantified using InCell2000 (Moon lab, University of Washington). Z-score (z=(x-mean of the population)/standard deviation of the population)) was calculated for each sample to determine the hits.

Antibodies: A rabbit polyclonal antibody against phosho-S153 DGCR8 (#5126) was generated by PhosphoSolutions. DGCR8 (10996-1-AP, Proteintech), STK23 (abcam, ab72074) and NIM1K (abcam, ab87553).

Western blot analysis. Whole-cell lysates were prepared using sample buffer (0.05 mol/L Tris-HCl (pH 6.8), 2% SDS, 6% β-mercaptoethanol), resolved by polyacrylamide gel (NuPage, Life Technologies) electrophoresis and transferred onto nitrocellulose membranes. Chemiluminescence was used for detection, and membranes were digitally scanned by Imagequant LAS 4000 (GE Biosciences).

Figures and Legends

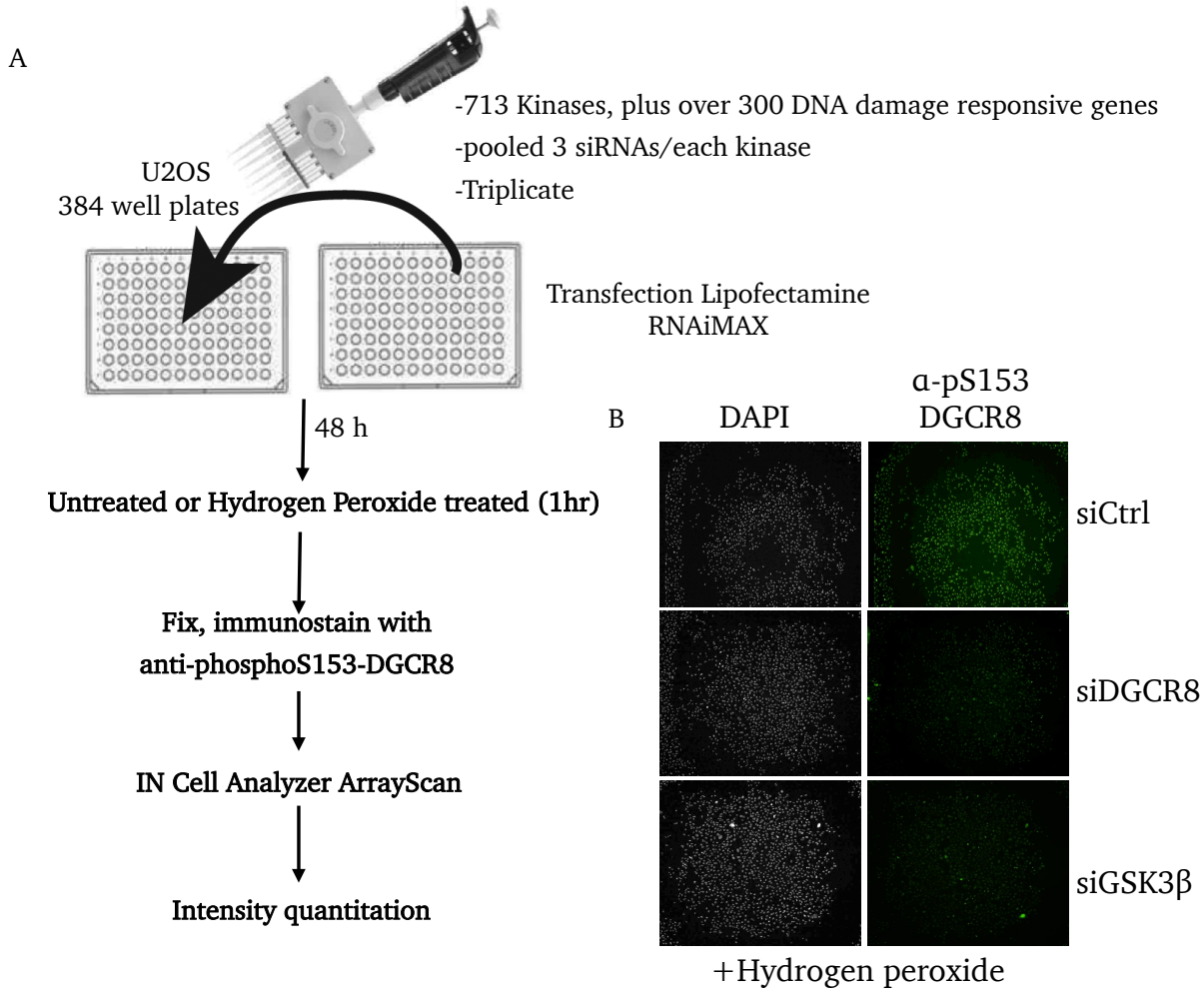

Figure 5.1 Work Flow: High-content immunofluorescence microscopy screen to identify kinases and DNA responsive genes that regulate phospho-S153. **A.** U2OS cells were plated into 384-well plates containing siRNAs against 713 known human kinases or over 300 DNA damage responsive genes. Then, cells were treated with hydrogen peroxide, fixed and immunostained with anti-phospho-S153 DGCR8. Nuclear intensity/cell was measure using In Cell Analyzer ArrayScan. **B.** Representative images of the screen. Depletion of either DGCR8 or GSK3β reduces phosphoS153 staining.

A

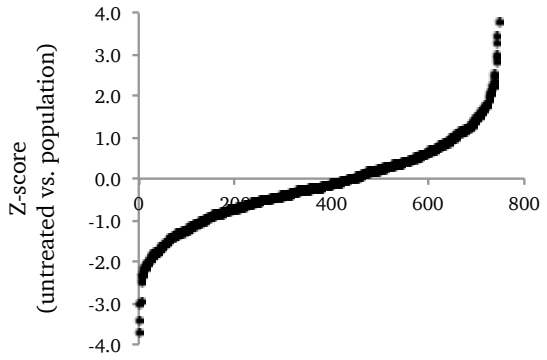

B

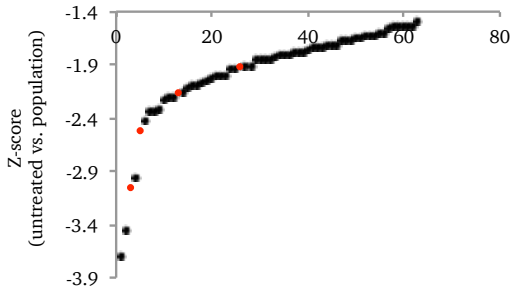

Gene symbol	Z score untreated vs. Population
ULK1	-2.35
CHKA	-2.32
PRKY	-2.24
STK4	-2.20
PIK3R2	-2.17
DGUOK	-2.13
DGKA	-2.11
DCAMKL2	-2.09
GUCY2F	-2.07
MUSK	-2.06
EEF2K	-2.01
SRMS	-2.01
CKB	-1.95
STK32A	-1.92
LOC390975	-1.92
MAPK7	-1.91
CKMT1B	-1.86
RIPK1	-1.86
BMPR2	-1.85
PGK2	-1.85
MAPK15	-1.84
C6orf199	-1.81
TP53RK	-1.81
TRIB3	-1.80
CDC2L1	-1.79
CDC2L6	-1.78

Gene symbol	Z score untreated vs. Population
LOC442075	-1.77
SLK	-1.76
PHKA1	-1.74
CSNK1G2	-1.74
UCK1	-1.74
ACVRL1	-1.71
BRD4	-1.71
MAPKAPK3	-1.68
AXL	-1.67
GPR125	-1.66
TAF1	-1.64
VRK1	-1.64
NUAK1	-1.63
MAP2K7	-1.62
CSNK1D	-1.60
CCT2	-1.56
RIPK5	-1.55
PRKACG	-1.55
TK2	-1.53
CSNK2A2	-1.53
PRKCH	-1.53
PAK7	-1.50

C

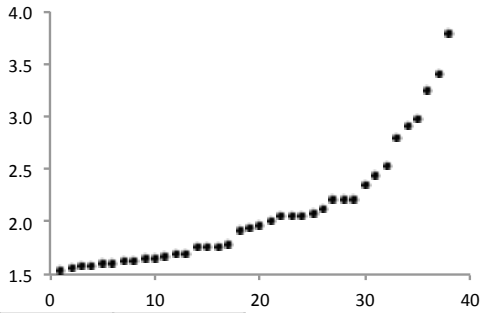

Gene symbol	Z score untreated vs. Population
TRPM7	1.54
MPP4	1.57
EPHA3	1.59
TRPM6	1.59
ROS1	1.60
GUCY2C	1.60
TBK1	1.62
MST1R	1.64
AURKA	1.64
NME3	1.66
ULK4	1.67
MPP1	1.69
SPHK2	1.70
CAMK2G	1.76
FES	1.76
PRKACA	1.76
NADK	1.78
RAPGEF4	1.91
MYO3A	1.95
DGKH	1.97
FGFR2	2.02

Gene symbol	Z score untreated vs. Population
STK39	2.05
CDC42BPG	2.05
STK16	2.06
TXK	2.08
PIK3R3	2.12
NRBP2	2.21
MPP3	2.21
BAIAP2	2.22
FLJ30698	2.34
EPHB2	2.44
DAPK2	2.54
SNRK	2.80
DAK	2.90
PIP5K1B	2.99
ABL2	3.24
ABL1	3.41
CAMK1	3.80

Figure 5.2 Candidate kinases that regulate basal S153 DGCR8 phosphorylation. **A.** Nuclear intensity/cell/well of phospho-S153 was plotted on a Z-score plot revealing candidate kinases that either suppressed or enhanced basal S153 phosphorylation. **B.** Z-score plot and table of top kinases whose depletion suppressed S153 phosphorylation z-score < -1.50. **C.** Z-score plot and table of top kinases whose depletion enhance S153 phosphorylation z-score > 1.50.

A

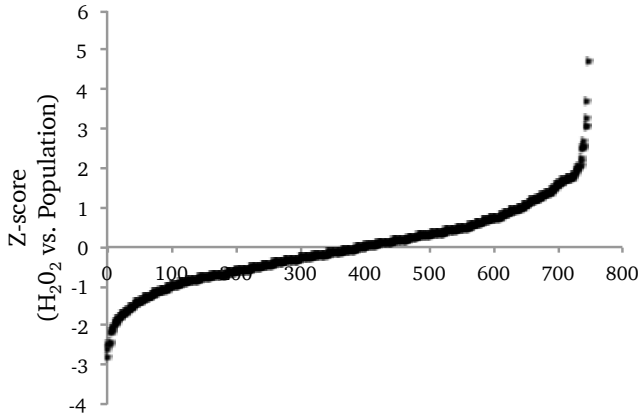

B

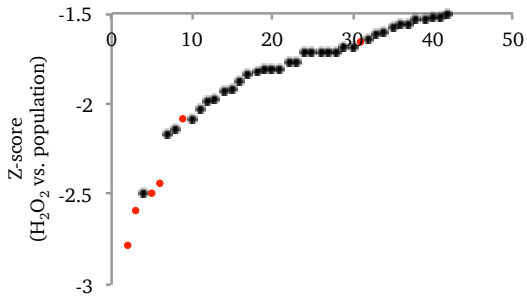

C

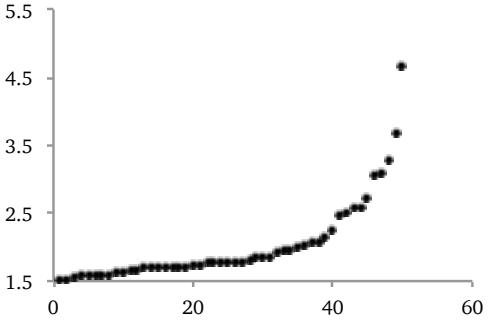

Gene Symbol	Z score H_2O_2 vs. Population
PHKG2	-2.50
CDC2L1	-2.17
ERBB3	-2.14
MGC42105 (NIM1K)	-2.08
EPHA1	-2.03
MAPKAPK3	-1.98
DCAMKL2	-1.97
ALDH18A1	-1.84
ERBB4	-1.82
ULK1	-1.81
LMTK2	-1.81
STK4	-1.81
IGF1R	-1.77
CERKL	-1.77
STK23	-1.71
GSK3B	-1.71
PRKD2	-1.68
MKNK2	-1.66
BMPR2	-1.65
DLG3	-1.62
LIMK2	-1.61
EPHA4	-1.56
MARK2	-1.56
C6orf199	-1.54
GUCY2D	-1.54
TANK	-1.51
SMG1	-1.51

Gene Symbol	Z score H_2O_2 vs. Population
PRKCA	1.53
PKD2L2	1.54
FUK	1.56
NRBP2	1.58
FRAP1	1.58
EPHB4	1.60
EPHA7	1.60
PTK9L	1.61
FLJ30698	1.64
JAK2	1.65
AMHR2	1.67
STK17A	1.68
ACVR1B	1.70
DGKI	1.70
ROR2	1.70
RET	1.71
STC1	1.71
CSNK1A1	1.71
SPHK2	1.72
BCKDK	1.74
NEK6	1.74
FLJ40852	1.76
SNF1LK2	1.76
MAP4K1	1.77
AK7	1.77
POLR3K	1.77

Gene Symbol	Z score H_2O_2 vs. Population
MGC16169	1.78
STK16	1.82
MAP3K6	1.84
NEK9	1.84
PIP5K2C	1.85
PFKFB1	1.92
SGK3	1.96
NADK	1.97
HIPK1	1.99
FGFR2	2.02
KDR	2.07
EPHB2	2.07
PRKD3	2.16
RPS6KA5	2.25
HK1	2.49
AURKA	2.51
ULK4	2.58
NME4	2.59
RBKS	2.72
MST1R	3.06
STK3	3.08
MPP4	3.29
TXK	3.69
GRK4	4.68

Figure 5.3 Candidate Kinases that regulate H_2O_2-induced S153 DGCR8 Phosphorylation. A. Nuclear intensity/cell/well of phospho-S153 was plotted on a Z-score plot revealing candidate kinases that either suppressed or enhanced H_2O_2-induced S153 phosphorylation. **B.** Z-score plot and table of top kinases whose depletion suppressed H_2O_2-induced S153 phosphorylation z-score < -1.50. "Red dots" are several siDGCR8 that served as positive controls. Kinases that we validated using two to three siRNAs are highlighted in "yellow" **C.** Z-score plot and table of top kinases whose depletion enhance H_2O_2 -induced S153 phosphorylation z-score > 1.50.

A

UV-induced S153 phosphorylation status after depletion or inhibition of the listed kinases			
No Change	Elevated Phosphorylation after UV	Decreased Total DGCR8 protein	Decreased Phosphorylation after UV
AMPK1	CDK12	CDK6	MGC42105 (NIM1K)
ATM	CDK9	CHK1	STK23
ATR	DCAMKL1	PHKG2	
CDC2L1	MAPAPK3		
CDK7			
CDK8			
CERKL1			
CHK1			
CHK2			
DNA-PK			
ERK1/2			
GSK3 alpha			
GSK3β			
JNK1/2			
LIMK2			
LMTK2			
MAPAPK2			
MARK2			
MKNK2			
p38 alpha			
p38 beta			
PRKG2			
SMG1			
STK4			
ULK1			
ULK2			
CK2			
CDK1			
CDK2			
CDK4			

B

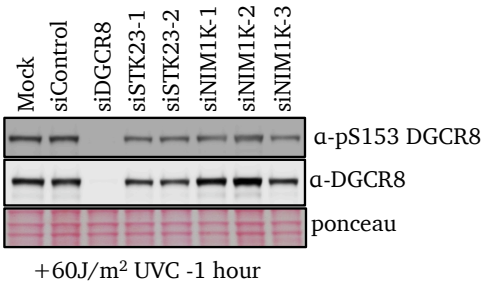

C

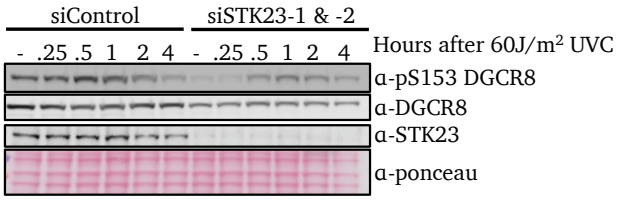

D

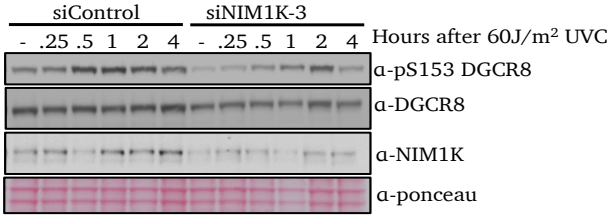

Figure 5.4 Validation of candidate kinases that are involved in phosphorylation of S153.

A. Validation results using two-three siRNAs or chemical inhibitors against the listed kinases. Some were from the kinome screen (highlighted in "yellow"), while other kinases were tested because they are known UV-inducible or proline-directed kinases. The results are divided as "No change", "Elevated phosphorylation after UV", "Decreased total DGCR8 protein" or "Decreased phosphorylation after UV." **B.** Immunoblot. Depletion of STK23 or NIM1K suppressed UV-induced S153 phosphorylation. **C.** Immunoblot of a time course experiment after UV radiation. STK23 depletion suppressed basal S153 phosphorylation and early after UV radiation. **C.** Immunoblot of a time course experiment after UV radiation. NIM1K depletion suppressed basal S153 phosphorylation and early after UV radiation.

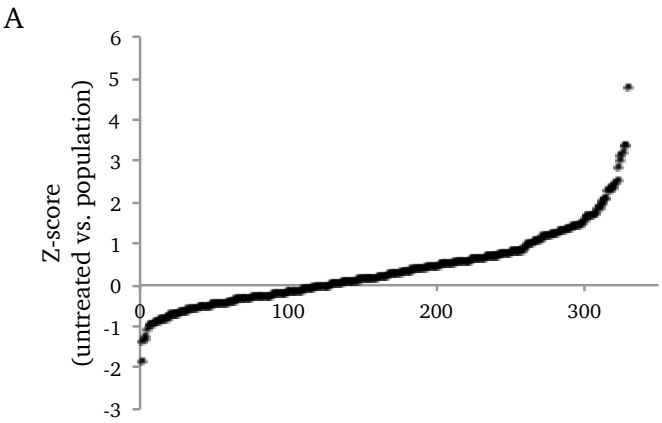

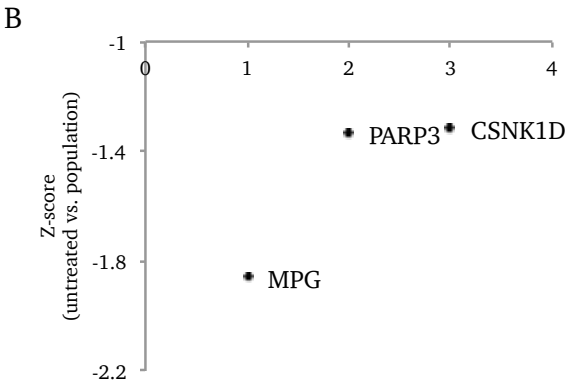

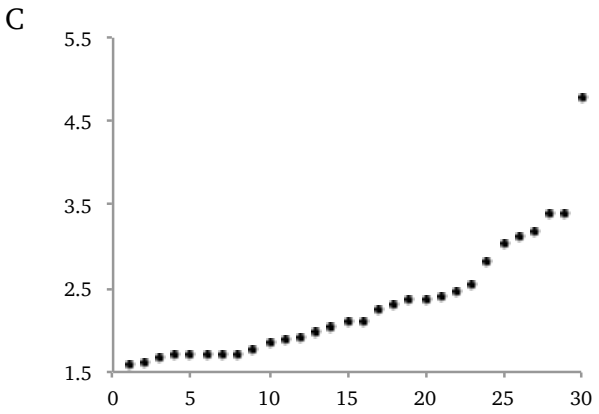

Gene Symbol	Z score H202 vs. Population
NCOA6	1.59
MRE11A	1.61
POLE	1.67
POT1	1.69
RPS9	1.69
EME2	1.71
APC	1.71
UIMC1	1.71
DHX9	1.75
YY1	1.86
SMUG1	1.88
MUS81	1.91
HSPA5	1.99
PARP4	2.03
RAD9A	2.08

Gene Symbol	Z score H202 vs. Population
APEX1	2.11
CENPE	2.26
PTTG1	2.30
MLH1	2.36
DCLRE1C	2.37
SFPQ	2.39
HIST1H2BK	2.47
NTHL1	2.56
SHFM1	2.81
NME4	3.02
RRM1	3.13
USP1	3.20
HDAC1	3.39
RAD51	3.40
RRM2	4.78

Figure 5.5 Candidate DNA responsive genes that regulate basal S153 DGCR8 phosphorylation. **A.** Nuclear intensity/cell/well of phospho-S153 was plotted on a Z-score plot revealing candidate DNA responsive genes that either suppressed or enhanced basal S153 phosphorylation. **B.** Z-score plot of top three DNA responsive genes whose depletion suppressed S153 phosphorylation z-score < -1.30. **C.** Z-score plot and table of top DNA responsive genes whose depletion enhance S153 phosphorylation z-score > 1.50.

A

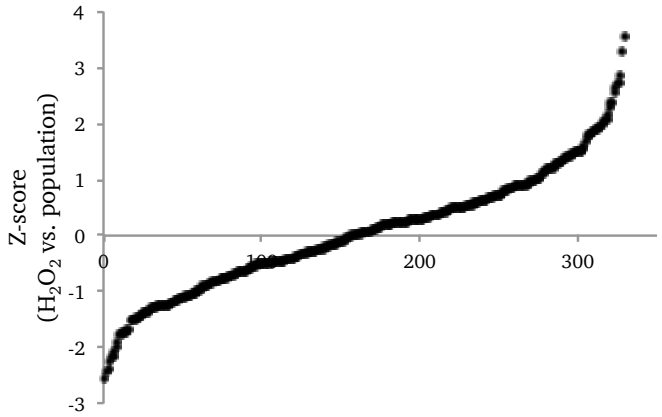

B

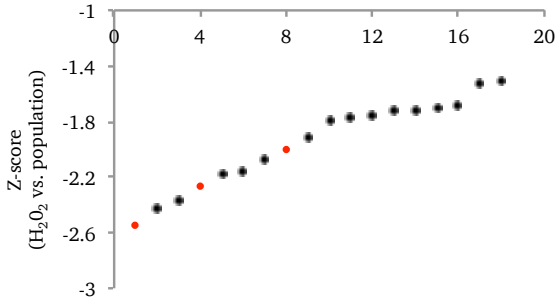

C

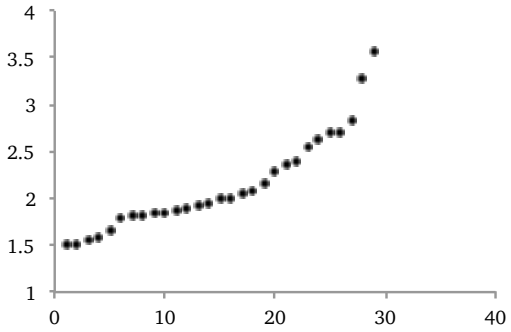

Gene Symbol	Z score H_2O_2 vs. Population
MPG	-2.42
PCNA	-2.38
ATRIP	-2.18
CSNK1D	-2.16
UHRF1	-1.90
THOC1	-1.77
CSNK1E	-1.75
RBBP8	-1.73
UNG	-1.72
BUB3	-1.70
PML	-1.68
GTF2H4	-1.52
POLD4	-1.51

Gene symbol	Z score H_2O_2 vs. Population
TFAP2A	1.50
UBE2N	1.50
TYMS	1.56
POLN	1.59
MAD2L1	1.66
RPS9	1.79
IGHMBP2	1.82
C10orf92	1.83
DDX5	1.84
TINF2	1.84
POLD1	1.88
GADD45A	1.90
MCM2	1.93
POLQ	1.96

Gene symbol	Z score H_2O_2 vs. Population
ERCC2	1.99
USP1	2.01
BRCA2	2.06
TREX2	2.07
NTHL1	2.15
NBN	2.28
TOP1	2.35
NCOA6	2.39
UBE2B	2.55
SPAG11B	2.63
APC	2.71
RPS3A	2.72
PARP1	2.84
MLH1	3.27
RRM2	3.55

Figure 5.6 Candidate DNA damage responsive genes that regulate H_2O_2-induced S153 DGCR8 Phosphorylation. A. Nuclear intensity/cell/well of phospho-S153 was plotted on a Z-score plot revealing candidate DNA damage responsive genes that either suppressed or enhanced H_2O_2-induced S153 phosphorylation. **B.** Z-score plot and table of top DNA damage responsive genes whose depletion suppressed H_2O_2-induced S153 phosphorylation z-score < -1.50. "Red dots" are several siDGCR8 that served as positive controls. **C.** Z-score plot and table of top DNA damage responsive genes whose depletion enhance H_2O_2-induced S153 phosphorylation z-score > 1.50.

CHAPTER SIX

Conclusions and Future Directions

In summary, our study identified a novel non-canonical function of human DGCR8 protein, a critical binding partner of Drosha in the microprocessor complex, in the repair of UV-induced DNA lesions by TC-NER. UV-induced phosphorylation of S153 of DGCR8 was critical for this function, but not for microRNA expression. Surprisingly, this function was not mediated by RNA-binding activity or Drosha-binding activity of DGCR8. These findings indicate that human DCGR8 has two independent functions: RNA processing and TC-NER (Fig. 6). Furthermore, Drosha was involved in cellular resistance to UV, and this function of Drosha was independent of DGCR8-binding and microRNA processing.

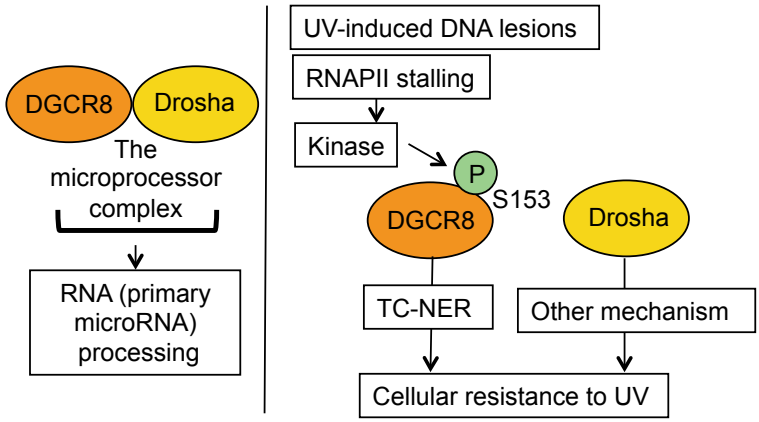

Fig. 6 Model: DGCR8 phosphorylation mediates cellular resistance to UV radiation through transcription-coupled repair

These findings establish a novel connection between the microprocessor complex and cellular resistance to UV radiation. Previous studies showed that expression of some miRNAs changes in response to UV [151] and that factors involved in miRNA silencing such as Dicer or Ago2 are required for cellular resistance to UV [151]. However, the exact mechanism remains unknown and appears to be largely dependent on miRNAs. Here, we showed that DGCR8 and Drosha are required for cellular resistance to UV

radiation. Importantly, the phosphorylation at S153 of DGCR8 is required for UV resistance independent of its RNA and Drosha binding activities. On the other hand, DGCR8 binding and RNA binding of Drosha is not required for cellular resistance to UV, suggesting that phosphorylation at S153 of DGCR8 is required for UV resistance independently of Drosha. Moreover, we showed that most miRNAs were not significantly altered by UV-induced S153 DGCR8 phosphorylation.

Elucidating the independent role of Drosha in UV resistance is an important future direction that needs to be addressed. It has been reported that the nuclear localization of Drosha is facilitated through phosphorylation by glycogen synthase kinase 3β (GSK3β)[86, 87]. Interestingly, heat and hydrogen peroxide induced N-terminal phosphorylation of Drosha by p38 MAPK resulted in nuclear export and facilitated its degradation that led to increased cell death [88]. We found that S153 of DGCR8 is phosphorylated and is required for cellular resistance after hydrogen peroxide treatment **(Fig 3.2B)**. In addition, p38 MAPK depletion or inhibition did not suppress UV-induced S153 DGCR8 phosphorylation, suggesting that phosphorylated DGCR8 and phosphorylated Drosha or Drosha, itself, may have independent roles in response to UV radiation. I speculate that Drosha may function in UV-resistance through interaction with its known[170] or unknown co-factors independent of its RNA binding activity. Another possibility is that phosphorylated Drosha could be required for cellular resistance to UV independent from phosphorylated S153 DGCR8-mediated cellular resistance.

In this study, we propose a new non-miRNA-mediated role for DGCR8 in the regulating the repair of UV-induced DNA lesions. We showed that UV-induced S153

DGCR8 phosphorylation is required for the removal of UV-induced DNA lesions and for the recovery of RNA synthesis after UV radiation. Moreover, we found that treatment of human cells with transcription inhibitors led to increased phosphorylation of S153 on DGCR8 even in the absence of UV treatment. Additionally, depletion of CDK9, a kinase known to be involved in transcription elongation also led to increased phosphorylation of S153 on DGCR8. Interestingly, we found that DGCR8 interacts with Drosha, phosphorylated RNA polymerase II and CSB. This interaction was increased after UV radiation. Also, we found that DGCR8 and NER factors, CSB, CSA and XPA, but not XPC, are epistatic in term of UV sensitivity, suggesting that DGCR8 is functionally involved with defects in TC-NER after UV radiation. Cells deficient in these factors showed that phosphorylation at S153 occurs normally, suggesting that these factors are not essential for the activation of UV-induced S153 DGCR8 phosphorylation. This also suggest that the phosphorylation occurs upstream of these factors. Altogether, these findings suggest a new function of DGCR8 in the removal of UV-induced DNA lesions by interacting with factors that initiate TC-NER to recover from stalled transcription after UV. Elucidating the exact mechanism by which S153-phosphorylated DGCR8 regulate TC-NER is another important future direction to explore. I speculate that UV-induced phosphorylated DGCR8 may facilitate in the recruitment of TC-NER factors or some other factors that mediates the removal of UV-induced DNA lesions. Another possibility is that UV-induced phosphorylated DGCR8 may sequester negative regulators for the removal of UV-induced lesions.

In fact, several reports reveal the microprocessor complex is directly associated

with transcription and in some cases, functions independent of miRNAs. First, the microprocessor complex is recruited to chromatin during transcription of the host transcript and process primary-miRNA co-transcriptionally [105, 106]. Second, Drosha was found to bind to RNAPII and at promoter regions of transcribed human genes independent of its RNA cleavage and miRNA processing activities that resulted in efficient transcription elongation and increased gene expression[159]. Third, DGCR8/Drosha along with transcription termination factors, Setx, Xrn2 and Rrp6 induces RNAPII pausing and premature termination at the HIV-1 promoter [107]. Finally, UV and transcriptional inhibitors induced DGCR8 localization to distinct speckles called P-bodies in the nucleoplasm for RNA degradation[153, 158]. These studies suggest that the microprocessor complex is involved in transcriptional regulation. It's an intriguing possibility that phosphorylated DGCR8, in addition to the function we describe in our study, could function as a general transcriptional regulator.

Cellular response to UV is triggered by the activation of signaling pathways involving kinases and phosphatases to regulate DNA repair, cell cycle, cell proliferation and survival[7]. Phosphorylation of other factors in miRNA biogenesis has been implicated in regulating subcellular localization, altered expression of a subset of miRNA expression and protein stability. Arsenite-induced phosphorylation of Ago2 by MAPAPK2 or Ago2 phosphorylation by ATK3 induced by an unknown stimulus leads to localization of Ago2 in processing bodies (P-bodies)[98] or enhanced translation repression of miRNA targets [99], respectively. Furthermore, hypoxia induced phosphorylation of Ago2 enabled disassociation of Ago2 from Dicer and as a result, reduces pre-miRNA

processing. TRBP, a binding partner of dicer, is phosphorylated by MAPK-ERK and promotes the processing of progrowth miRNAs [90].

In this study, we identified nine phosphorylation sites on DGCR8 and showed that S153 was a unique site for UV-induced phosphorylation. DGCR8 is phosphorylated by MAPK-ERK at 23 sites, including S153, that increases its stability, however global miRNA expression remained unchanged [83]. Additionally, the same study showed that DGCR8 was co-immunoprecipitated with c-Jun N-terminal kinases (JNK), but did not show whether DGCR8 was phosphorylated by JNK. Furthermore, NEK6 was predicted to phosphorylate S153 of DGCR8. Because S153 is a Serine-Proline site, we tested known UV-inducible kinases such as ATR, ATM, CHK1, CHK2, DNA-PK, MAPK kinases and several proline driven kinases including cyclin-dependent kinases (CDKs) that phosphorylate the C-terminal of the RNAPII, in addition to known UV-inducible kinases such as ATR, ATM, CHK1, CHK2, DNA-PK, MAPK kinases. We found that either depletion or chemical inhibition against these kinases did not suppress UV-induced phosphorylation at S153, suggesting that these kinases are not critical for the activation of the phosphorylation of S153. Therefore, we conducted a high-content immunofluorescence screen using a kinome library containing over 700 siRNAs against known human kinases to identify kinases that phosphorylate S153 of DGCR8. In addition, we screen another panel containing over 300 siRNAs against known DNA damage responsive genes to identify additional modifiers of S153 phosphorylation. After validation of the top hits, we found that STK23 or NIM1K suppressed basal and early S153 phosphorylation after UV radiation. Further tests are needed to determine whether

these kinases directly phosphorylate S153 after UV radiation. Additionally, further validation is needed to determine whether hits from the DNA responsive panel screening alters S153 phosphorylation and whether they are functionally relevant.

The microprocessor complex is conserved in the animal kingdom[40, 49, 171], but S153 of DGCR8 is only conserved in mammals, suggesting that phosphorylation at this site is functionally important in the evolution of mammals in response to UV radiation. In humans, there are multiple nonsynonymous polymorphisms including missense, frameshift and stop variants in DGCR8 and Drosha with some on functional protein domains[127]. DGCR8 is also one of several genes associated with a human genetic disorder called DiGeorge syndrome with a heterozygous micro-deletion in chromosome 22q11 characterized by developmental, cardiac and cognitive deficits[49]. While mouse model for this deletion showed similar phenotypes to the human disorder, changes in miRNAs was minimal, suggesting that DGCR8 may function in an alternative pathway[47]. Consistent with this study, these mice resulted in altered short-term plasticity and increase risk for schizophrenia[48, 134]. In humans, single-nucleotide polymorphisms (SNPs) in the microprocessor complex is associated with increased risk for schizophrenia[135]. It's certainly important to determine whether mutations found on DGCR8 confer cellular sensitivity to UV radiation or whether these mutations affect UV-induced S153 phosphorylation.

Genetic knockout of Drosha or DGCR8 led to early embryonic lethality in mice[46, 172]. While most of the phenotypes in these mice are likely due to decreased miRNA expression, growing evidence suggests an alternative miRNA-independent role of the

microprocessor complex. First, the microprocessor complex can cleave RNA molecules other than pri-miRNAs. For example, Drosha cleaves some mRNAs, including DGCR8 mRNA [173] and the microprocessor complex destabilizes some long-non-coding RNAs (lncRNA) and small-nucleolar RNAs (sno-RNA), while the later is DGCR8 dependent and Drosha independent[104]. In neurons, Drosha binds and cleaves the stem-loop structures in the 3'UTR of transcription factor Neurogenin2 (Ngn2) mRNA [103]. In flies, DGCR8 regulates proper neuronal morphogenesis independent of Drosha and miRNAs[50]. Phosphorylated Methyl-CpG binding protein 2 (MeCP2) binds to DGCR8, which prevents Drosha from binding resulting in the inhibition of dendritic and spine growth [85]. Further tests are needed to determine whether phosphorylation at S153 of DGCR8 is important in neurons, especially after cellular stresses and stimuli.

In human cancers, miRNAs are globally repressed[109]. One possible mechanism is the reduced processing of miRNAs by the microprocessor complex. Several studies have shown that levels of expression of Drosha and DGCR8 are altered in some cancers including ovarian[174], breast[175], skin[125], colorectal[124], and liver[176] cancers. In addition, mutations in Drosha and DGCR8 have been found in several cancer types, however additional tests are needed to delineate the functional relevance of these mutations. Several large studies recently discovered somatic mutations in the catalytic domains of Drosha and DGCR8 in a pediatric renal cancer called Wilms tumor [128-131]. These mutations in Drosha and DGCR8 result in altered expression of some miRNAs [128-131]. None of these mutations were near S153 of DGCR8, suggesting that these mutations may not affect phosphorylation of S153 nor cellular resistance to UV

radiation. Interestingly, cBioPortal for Cancer Genomics revealed several missense and nonsense mutation throughout DGCR8. Specifically, several missense mutations were flanking S153 of DGCR8 including L152F, S156N (melanoma) and G149C (stomach and lung cancer)[140, 141]. It remains to be tested whether these mutations alter phosphorylation of S153 on DGCR8. Interestingly, we found that UV-induced S153 phosphorylation was attenuated in two melanoma cell lines we treated. Further analysis of melanoma cell lines and clinical melanoma samples needs to be performed in order to determine how frequently S153 DGCR8 phosphorylation is impaired in melanoma.

In summary, we describe an entirely new function for the microprocessor complex in UV response independent of miRNAs. We identified S153 of DGCR8 as a unique site for UV-induced phosphorylation by an unknown kinase. This site is required for the removal of UV-induced DNA lesion, recovery of RNA synthesis after UV exposure and DGCR8 is functionally linked to TC-NER and not GG-NER. Lastly, we found that UV induces the interactions between DGCR8 and factors that initiate TC-NER including RNAPII and CSB. Altogether, our findings suggest a novel function of DGCR8 and highlight its functional importance in TC-NER after UV radiation.

REFERENCES

1. **Brenner, M. and V.J. Hearing,** *The protective role of melanin against UV damage in human skin.* **Photochem Photobiol, 2008. 84(3): p. 539-49.**

2. **Reichrath, J.,** *Sunlight, skin cancer and vitamin D: What are the conclusions of recent findings that protection against solar ultraviolet (UV) radiation causes 25-hydroxyvitamin D deficiency in solid organ-transplant recipients, xeroderma pigmentosum, and other risk groups?* **J Steroid Biochem Mol Biol, 2007. 103(3-5): p. 664-7.**

3. **Batista, L.F., et al.,** *How DNA lesions are turned into powerful killing structures: insights from UV-induced apoptosis.* **Mutat Res, 2009. 681(2-3): p. 197-208.**

4. **Sinha, R.P. and D.P. Hader,** *UV-induced DNA damage and repair: a review.* **Photochem Photobiol Sci, 2002. 1(4): p. 225-36.**

5. **Harper, J.W. and S.J. Elledge,** *The DNA damage response: ten years after.* **Mol Cell, 2007. 28(5): p. 739-45.**

6. **Ciccia, A. and S.J. Elledge,** *The DNA damage response: making it safe to play with knives.* **Mol Cell, 2010. 40(2): p. 179-204.**

7. **Herrlich, P., M. Karin, and C. Weiss,** *Supreme EnLIGHTenment: damage recognition and signaling in the mammalian UV response.* **Mol Cell, 2008. 29(3): p. 279-90.**

8. **Auclair, Y., et al.,** *ATR kinase is required for global genomic nucleotide excision repair exclusively during S phase in human cells.* **Proc Natl Acad Sci U S A, 2008. 105(46): p. 17896-901.**

9. **Marteijn, J.A., et al.,** *Understanding nucleotide excision repair and its roles in cancer and ageing.* **Nat Rev Mol Cell Biol, 2014. 15(7): p. 465-81.**

10. **Auclair, Y., R. Rouget, and E.A. Drobetsky,** *ATR kinase as master regulator of nucleotide excision repair during S phase of the cell cycle.* **Cell Cycle, 2009. 8(12): p. 1865-71.**

11. **Olson, E., et al.,** *RPA2 is a direct downstream target for ATR to regulate the S-phase checkpoint.* **J Biol Chem, 2006. 281(51): p. 39517-33.**

12. **Wu, X., et al.,** *Phosphorylation of nucleotide excision repair factor xeroderma pigmentosum group A by ataxia telangiectasia mutated and Rad3-related-dependent checkpoint pathway promotes cell survival in response to UV irradiation.* **Cancer Res, 2006. 66(6): p. 2997-3005.**

13. **Wu, X., et al.,** *ATR-dependent checkpoint modulates XPA nuclear import in response to UV irradiation.* **Oncogene, 2007. 26(5): p. 757-64.**

14. **Reinhardt, H.C. and M.B. Yaffe,** *Kinases that control the cell cycle in response to DNA damage: Chk1, Chk2, and MK2.* **Curr Opin Cell Biol, 2009. 21(2): p. 245-55.**

15. **Reinhardt, H.C., et al.,** *p53-deficient cells rely on ATM- and ATR-mediated checkpoint signaling through the p38MAPK/MK2 pathway for survival after DNA damage.* **Cancer Cell, 2007. 11(2): p. 175-89.**

16. **Bode, A.M. and Z. Dong,** *Mitogen-activated protein kinase activation in UV-induced signal transduction.* **Sci STKE, 2003. 2003(167): p. RE2.**

17. **Kato, T., Jr., et al.,** *CK2 Is a C-Terminal IkappaB Kinase Responsible for NF-kappaB Activation during the UV Response.* **Mol Cell, 2003. 12(4): p. 829-39.**

18. **Cao, C., et al.,** *AMP-activated protein kinase contributes to UV- and H2O2-induced apoptosis in human skin keratinocytes.* **J Biol Chem, 2008. 283(43): p. 28897-908.**

19. **Huang, C., et al.,** *Ultraviolet-induced phosphorylation of p70(S6K) at Thr(389) and Thr(421)/Ser(424) involves hydrogen peroxide and mammalian target of rapamycin but not Akt and atypical protein kinase C.* **Cancer Res, 2002. 62(20): p. 5689-97.**

20. **Carthew, R.W. and E.J. Sontheimer,** *Origins and Mechanisms of miRNAs and siRNAs.* **Cell, 2009. 136(4): p. 642-55.**

21. **Winter, J., et al.,** *Many roads to maturity: microRNA biogenesis pathways and their regulation.* **Nat Cell Biol, 2009. 11(3): p. 228-34.**

22. **Friedman, R.C., et al.,** *Most mammalian mRNAs are conserved targets of microRNAs.* **Genome Res, 2009. 19(1): p. 92-105.**

23. **Guo, L., et al.,** *Differential expression profiles of microRNAs in NIH3T3 cells in response to UVB irradiation.* **Photochem Photobiol, 2009. 85(3): p. 765-73.**

24. **Dziunycz, P., et al.,** *Squamous cell carcinoma of the skin shows a distinct microRNA profile modulated by UV radiation.* **J Invest Dermatol, 2010. 130(11): p. 2686-9.**

25. **Pothof, J., et al.,** *MicroRNA-mediated gene silencing modulates the UV-induced DNA-damage response.* **EMBO J, 2009. 28(14): p. 2090-9.**

26. **Tan, G., et al.,** *NF-kappaB-dependent microRNA-125b up-regulation promotes cell survival by targeting p38alpha upon ultraviolet radiation.* **J Biol Chem, 2012. 287(39): p. 33036-47.**

27. **Le, M.T., et al.,** *MicroRNA-125b is a novel negative regulator of p53.* **Genes Dev, 2009. 23(7): p. 862-76.**

28. **Suzuki, H.I., et al.,** *Modulation of microRNA processing by p53.* **Nature, 2009. 460(7254): p. 529-33.**

29. **Scarola, M., et al.,** *miR-335 directly targets Rb1 (pRb/p105) in a proximal connection to p53-dependent stress response.* **Cancer Res, 2010. 70(17): p. 6925-33.**

30. **Tan, G., Y. Shi, and Z.H. Wu,** *MicroRNA-22 promotes cell survival upon UV radiation by repressing PTEN.* **Biochem Biophys Res Commun, 2012. 417(1): p. 546-51.**

31. **Tan, X., et al.,** *miR-638 mediated regulation of BRCA1 affects DNA repair and sensitivity to UV and cisplatin in triple-negative breast cancer.* **Breast Cancer Res, 2014. 16(5): p. 435.**

32. **Kraemer, A., et al.,** *UVA and UVB irradiation differentially regulate microRNA expression in human primary keratinocytes.* **PLoS One, 2013. 8(12): p. e83392.**

33. **Lee, Y., et al.,** *MicroRNA genes are transcribed by RNA polymerase II.* **EMBO J, 2004. 23(20): p. 4051-60.**

34. **Han, J., et al.,** *Molecular basis for the recognition of primary microRNAs by the Drosha-DGCR8 complex.* **Cell, 2006. 125(5): p. 887-901.**

35. **Davis, B.N. and A. Hata,** *Regulation of MicroRNA Biogenesis: A miRiad of mechanisms.* **Cell Commun Signal, 2009. 7: p. 18.**

36. **Krol, J., I. Loedige, and W. Filipowicz,** *The widespread regulation of microRNA biogenesis, function and decay.* **Nat Rev Genet, 2010. 11(9): p. 597-610.**

37. **Gregory, R.I., et al.,** *The Microprocessor complex mediates the genesis of microRNAs.* **Nature, 2004. 432(7014): p. 235-40.**

38. **Yeom, K.H., et al.,** *Characterization of DGCR8/Pasha, the essential cofactor for Drosha in primary miRNA processing.* **Nucleic Acids Res, 2006. 34(16): p. 4622-9.**

39. **Han, J., et al.,** *The Drosha-DGCR8 complex in primary microRNA processing.* **Genes Dev, 2004. 18(24): p. 3016-27.**

40. **Landthaler, M., A. Yalcin, and T. Tuschl,** *The human DiGeorge syndrome critical region gene 8 and Its D. melanogaster homolog are required for miRNA biogenesis.* **Curr Biol, 2004. 14(23): p. 2162-7.**

41. **Sohn, S.Y., et al.,** *Crystal structure of human DGCR8 core.* **Nat Struct Mol Biol, 2007. 14(9): p. 847-53.**

42. **Faller, M., et al.,** *Heme is involved in microRNA processing.* **Nat Struct Mol Biol, 2007. 14(1): p. 23-9.**

43. **Barr, I., et al.,** *DiGeorge critical region 8 (DGCR8) is a double-cysteine-ligated heme protein.* **J Biol Chem, 2011. 286(19): p. 16716-25.**

44. **Barr, I., et al.,** *Ferric, not ferrous, heme activates RNA-binding protein DGCR8 for primary microRNA processing.* **Proc Natl Acad Sci U S A, 2012. 109(6): p. 1919-24.**

45. **Weitz, S.H., et al.,** *Processing of microRNA primary transcripts requires heme in mammalian cells.* **Proc Natl Acad Sci U S A, 2014. 111(5): p. 1861-6.**

46. **Wang, Y., et al.,** *DGCR8 is essential for microRNA biogenesis and silencing of embryonic stem cell self-renewal.* **Nat Genet, 2007. 39(3): p. 380-5.**

47. **Stark, K.L., et al.,** *Altered brain microRNA biogenesis contributes to phenotypic deficits in a 22q11-deletion mouse model.* **Nat Genet, 2008. 40(6): p. 751-60.**

48. **Fenelon, K., et al.,** *Deficiency of Dgcr8, a gene disrupted by the 22q11.2 microdeletion, results in altered short-term plasticity in the prefrontal cortex.* **Proc Natl Acad Sci U S A, 2011. 108(11): p. 4447-52.**

49. **Shiohama, A., et al.,** *Molecular cloning and expression analysis of a novel gene DGCR8 located in the DiGeorge syndrome chromosomal region.* **Biochem Biophys Res Commun, 2003. 304(1): p. 184-90.**

50. **Luhur, A., et al.,** *Drosha-independent DGCR8/Pasha pathway regulates neuronal morphogenesis.* **Proc Natl Acad Sci U S A, 2014. 111(4): p. 1421-6.**

51. **Rao, P.K., et al.,** *Loss of cardiac microRNA-mediated regulation leads to dilated cardiomyopathy and heart failure.* **Circ Res, 2009. 105(6): p. 585-94.**

52. **Bezman, N.A., et al.,** *Distinct requirements of microRNAs in NK cell activation, survival, and function.* **J Immunol, 2010. 185(7): p. 3835-46.**

53. **Chen, Z., et al.,** *DiGeorge syndrome critical region 8 (DGCR8) protein-mediated microRNA biogenesis is essential for vascular smooth muscle cell development in mice.* **J Biol Chem, 2012. 287(23): p. 19018-28.**

54. **Yi, R., et al.,** *DGCR8-dependent microRNA biogenesis is essential for skin development.* **Proc Natl Acad Sci U S A, 2009. 106(2): p. 498-502.**

55. **Gomez-Cabello, D., et al.,** *DGCR8-mediated disruption of miRNA biogenesis induces cellular senescence in primary fibroblasts.* **Aging Cell, 2013. 12(5): p. 923-31.**

56. **Bui, T.V. and J.T. Mendell,** *Myc: Maestro of MicroRNAs.* **Genes Cancer, 2010. 1(6): p. 568-575.**

57. **Mu, P., et al.,** *Genetic dissection of the miR-17~92 cluster of microRNAs in Myc-induced B-cell lymphomas.* **Genes Dev, 2009. 23(24): p. 2806-11.**

58. **He, L., et al.,** *A microRNA component of the p53 tumour suppressor network.* **Nature, 2007. 447(7148): p. 1130-4.**

59. **Lujambio, A., et al.,** *A microRNA DNA methylation signature for human cancer metastasis.* **Proc Natl Acad Sci U S A, 2008. 105(36): p. 13556-61.**

60. **Agirre, X., et al.,** *Epigenetic silencing of the tumor suppressor microRNA Hsa-miR-124a regulates CDK6 expression and confers a poor prognosis in acute lymphoblastic leukemia.* **Cancer Res, 2009. 69(10): p. 4443-53.**

61. **Huang, Y.W., et al.,** *Epigenetic repression of microRNA-129-2 leads to overexpression of SOX4 oncogene in endometrial cancer.* **Cancer Res, 2009. 69(23): p. 9038-46.**

62. **Brueckner, B., et al.,** *The human let-7a-3 locus contains an epigenetically regulated microRNA gene with oncogenic function.* **Cancer Res, 2007. 67(4): p. 1419-23.**

63. **Li, X., et al.,** *Gene silencing of MIR22 in acute lymphoblastic leukaemia involves histone modifications independent of promoter DNA methylation.* **Br J Haematol, 2010. 148(1): p. 69-79.**

64. **Scott, G.K., et al.,** *Rapid alteration of microRNA levels by histone deacetylase inhibition.* **Cancer Res, 2006. 66(3): p. 1277-81.**

65. **Fukuda, T., et al.,** *DEAD-box RNA helicase subunits of the Drosha complex are required for processing of rRNA and a subset of microRNAs.* **Nat Cell Biol, 2007. 9(5): p. 604-11.**

66. **Mori, M., et al.,** *Hippo signaling regulates microprocessor and links cell-density-dependent miRNA biogenesis to cancer.* **Cell, 2014. 156(5): p. 893-906.**

67. **Davis, B.N., et al.,** *SMAD proteins control DROSHA-mediated microRNA maturation.* **Nature, 2008. 454(7200): p. 56-61.**

68. **Davis, B.N., et al.,** *Smad proteins bind a conserved RNA sequence to promote microRNA maturation by Drosha.* **Mol Cell, 2010. 39(3): p. 373-84.**

69. **Kawai, S. and A. Amano,** *BRCA1 regulates microRNA biogenesis via the DROSHA microprocessor complex.* **J Cell Biol, 2012. 197(2): p. 201-8.**

70. **Watanabe, M., et al.,** *A subfamily of RNA-binding DEAD-box proteins acts as an estrogen receptor alpha coactivator through the N-terminal activation domain (AF-1) with an RNA coactivator, SRA.* **EMBO J, 2001. 20(6): p. 1341-52.**

71. **Yamagata, K., et al.,** *Maturation of microRNA is hormonally regulated by a nuclear receptor.* **Mol Cell, 2009. 36(2): p. 340-7.**

72. **Kawahara, Y. and A. Mieda-Sato,** *TDP-43 promotes microRNA biogenesis as a component of the Drosha and Dicer complexes.* **Proc Natl Acad Sci U S A, 2012. 109(9): p. 3347-52.**

73. **Morlando, M., et al.,** *FUS stimulates microRNA biogenesis by facilitating co-transcriptional Drosha recruitment.* **EMBO J, 2012. 31(24): p. 4502-10.**

74. **Sakamoto, S., et al.,** *The NF90-NF45 complex functions as a negative regulator in the microRNA processing pathway.* **Mol Cell Biol, 2009. 29(13): p. 3754-69.**

75. **Davis-Dusenbery, B.N. and A. Hata,** *Mechanisms of control of microRNA biogenesis.* **J Biochem, 2010. 148(4): p. 381-92.**

76. **Scadden, A.D.,** *The RISC subunit Tudor-SN binds to hyper-edited double-stranded RNA and promotes its cleavage.* **Nat Struct Mol Biol, 2005. 12(6): p. 489-96.**

77. **Kawahara, Y., et al.,** *RNA editing of the microRNA-151 precursor blocks cleavage by the Dicer-TRBP complex.* **EMBO Rep, 2007. 8(8): p. 763-9.**

78. **Maas, S., et al.,** *A-to-I RNA editing and human disease.* **RNA Biol, 2006. 3(1): p. 1-9.**

79. **Bahn, J.H., et al.,** *Genomic analysis of ADAR1 binding and its involvement in multiple RNA processing pathways.* **Nat Commun, 2015. 6: p. 6355.**

80. **Han, J., et al.,** *Posttranscriptional crossregulation between Drosha and DGCR8.* **Cell, 2009. 136(1): p. 75-84.**

81. **Dephoure, N., et al.,** *A quantitative atlas of mitotic phosphorylation.* **Proc Natl Acad Sci U S A, 2008. 105(31): p. 10762-7.**

82. **Olsen, J.V., et al.,** *Global, in vivo, and site-specific phosphorylation dynamics in signaling networks.* **Cell, 2006. 127(3): p. 635-48.**

83. **Herbert, K.M., et al.,** *Phosphorylation of DGCR8 increases its intracellular stability and induces a progrowth miRNA profile.* **Cell Rep, 2013. 5(4): p. 1070-81.**

84. **Wada, T., J. Kikuchi, and Y. Furukawa,** *Histone deacetylase 1 enhances microRNA processing via deacetylation of DGCR8.* **EMBO Rep, 2012. 13(2): p. 142-9.**

85. **Cheng, T.L., et al.,** *MeCP2 Suppresses Nuclear MicroRNA Processing and Dendritic Growth by Regulating the DGCR8/Drosha Complex.* **Dev Cell, 2014. 28(5): p. 547-60.**

86. **Tang, X., et al.,** *Phosphorylation of the RNase III enzyme Drosha at Serine300 or Serine302 is required for its nuclear localization.* **Nucleic Acids Res, 2010. 38(19): p. 6610-9.**

87. **Tang, X., et al.,** *Glycogen synthase kinase 3 beta (GSK3beta) phosphorylates the RNAase III enzyme Drosha at S300 and S302.* **PLoS One, 2011. 6(6): p. e20391.**

88. **Yang, Q., et al.,** *Stress Induces p38 MAPK-Mediated Phosphorylation and Inhibition of Drosha-Dependent Cell Survival.* **Mol Cell, 2015. 57(4): p. 721-34.**

89. **Hong, S., et al.,** *Signaling by p38 MAPK stimulates nuclear localization of the microprocessor component p68 for processing of selected primary microRNAs.* **Sci Signal, 2013. 6(266): p. ra16.**

90. **Paroo, Z., et al.,** *Phosphorylation of the human microRNA-generating complex mediates MAPK/Erk signaling.* **Cell, 2009. 139(1): p. 112-22.**

91. **Trabucchi, M., et al.,** *The RNA-binding protein KSRP promotes the biogenesis of a subset of microRNAs.* **Nature, 2009. 459(7249): p. 1010-4.**

92. **Zhang, X., et al.,** *The ATM kinase induces microRNA biogenesis in the DNA damage response.* **Mol Cell, 2011. 41(4): p. 371-83.**

93. **Heo, I., et al.,** *TUT4 in concert with Lin28 suppresses microRNA biogenesis through pre-microRNA uridylation.* **Cell, 2009. 138(4): p. 696-708.**

94. **Heo, I., et al.,** *Lin28 mediates the terminal uridylation of let-7 precursor MicroRNA.* **Mol Cell, 2008. 32(2): p. 276-84.**

95. **Katoh, T., et al.,** *Selective stabilization of mammalian microRNAs by 3' adenylation mediated by the cytoplasmic poly(A) polymerase GLD-2.* **Genes Dev, 2009. 23(4): p. 433-8.**

96. **Li, J., et al.,** *Methylation protects miRNAs and siRNAs from a 3'-end uridylation activity in Arabidopsis.* **Curr Biol, 2005. 15(16): p. 1501-7.**

97. **Alarcon, C.R., et al.,** *N6-methyladenosine marks primary microRNAs for processing.* **Nature, 2015. 519(7544): p. 482-5.**

98. **Zeng, Y., et al.,** *Phosphorylation of Argonaute 2 at serine-387 facilitates its localization to processing bodies.* **Biochem J, 2008. 413(3): p. 429-36.**

99. **Horman, S.R., et al.,** *Akt-mediated phosphorylation of argonaute 2 downregulates cleavage and upregulates translational repression of MicroRNA targets.* **Mol Cell, 2013. 50(3): p. 356-67.**

100. **Qi, H.H., et al.,** *Prolyl 4-hydroxylation regulates Argonaute 2 stability.* **Nature, 2008. 455(7211): p. 421-4.**

101. **Shen, J., et al.,** *EGFR modulates microRNA maturation in response to hypoxia through phosphorylation of AGO2.* **Nature, 2013. 497(7449): p. 383-7.**

102. **Rybak, A., et al.,** *The let-7 target gene mouse lin-41 is a stem cell specific E3 ubiquitin ligase for the miRNA pathway protein Ago2.* **Nat Cell Biol, 2009. 11(12): p. 1411-20.**

103. **Knuckles, P., et al.,** *Drosha regulates neurogenesis by controlling neurogenin 2 expression independent of microRNAs.* **Nat Neurosci, 2012. 15(7): p. 962-9.**

104. **Macias, S., et al.,** *DGCR8 HITS-CLIP reveals novel functions for the Microprocessor.* **Nat Struct Mol Biol, 2012. 19(8): p. 760-6.**

105. **Morlando, M., et al.,** *Primary microRNA transcripts are processed co-transcriptionally.* **Nat Struct Mol Biol, 2008. 15(9): p. 902-9.**

106. **Pawlicki, J.M. and J.A. Steitz,** *Primary microRNA transcript retention at sites of transcription leads to enhanced microRNA production.* **J Cell Biol, 2008. 182(1): p. 61-76.**

107. **Wagschal, A., et al.,** *Microprocessor, Setx, Xrn2, and Rrp6 co-operate to induce premature termination of transcription by RNAPII.* **Cell, 2012. 150(6): p. 1147-57.**

108. **Francia, S., et al.,** *Site-specific DICER and DROSHA RNA products control the DNA-damage response.* **Nature, 2012. 488(7410): p. 231-5.**

109. **Di Leva, G., M. Garofalo, and C.M. Croce,** *MicroRNAs in cancer.* **Annu Rev Pathol, 2014. 9: p. 287-314.**

110. **Costinean, S., et al.,** *Pre-B cell proliferation and lymphoblastic leukemia/high-grade lymphoma in E(mu)-miR155 transgenic mice.* **Proc Natl Acad Sci U S A, 2006. 103(18): p. 7024-9.**

111. **Nadiminty, N., et al.,** *MicroRNA let-7c is downregulated in prostate cancer and suppresses prostate cancer growth.* **PLoS One, 2012. 7(3): p. e32832.**

112. **Kasar, S., et al.,** *Systemic in vivo lentiviral delivery of miR-15a/16 reduces malignancy in the NZB de novo mouse model of chronic lymphocytic leukemia.* **Genes Immun, 2012. 13(2): p. 109-19.**

113. **Wu, Y., et al.,** *MicroRNA delivery by cationic lipoplexes for lung cancer therapy.* **Mol Pharm, 2011. 8(4): p. 1381-9.**

114. **Jin, H., et al.,** *Delivery of MicroRNA-10b with Polylysine Nanoparticles for Inhibition of Breast Cancer Cell Wound Healing.* **Breast Cancer (Auckl), 2012. 6: p. 9-19.**

115. **Wang, T.Y., et al.,** *Ultrasound-guided delivery of microRNA loaded nanoparticles into cancer.* **J Control Release, 2015. 203: p. 99-108.**

116. **Cortez, M.A., et al.,** *MicroRNAs in body fluids--the mix of hormones and biomarkers.* **Nat Rev Clin Oncol, 2011. 8(8): p. 467-77.**

117. **Boeri, M., et al.,** *MicroRNA signatures in tissues and plasma predict development and prognosis of computed tomography detected lung cancer.* **Proc Natl Acad Sci U S A, 2011. 108(9): p. 3713-8.**

118. **Arroyo, J.D., et al.,** *Argonaute2 complexes carry a population of circulating microRNAs independent of vesicles in human plasma.* **Proc Natl Acad Sci U S A, 2011. 108(12): p. 5003-8.**

119. **Huang, J.T., et al.,** *MicroRNA Machinery Genes as Novel Biomarkers for Cancer.* **Front Oncol, 2014. 4: p. 113.**

120. **Merritt, W.M., et al.,** *Dicer, Drosha, and outcomes in patients with ovarian cancer.* **N Engl J Med, 2008. 359(25): p. 2641-50.**

121. **Lin, R.J., et al.,** *microRNA signature and expression of Dicer and Drosha can predict prognosis and delineate risk groups in neuroblastoma.* **Cancer Res, 2010. 70(20): p. 7841-50.**

122. **Torres, A., et al.,** *Major regulators of microRNAs biogenesis Dicer and Drosha are down-regulated in endometrial cancer.* **Tumour Biol, 2011. 32(4): p. 769-76.**

123. **Guo, X., et al.,** *The microRNA-processing enzymes: Drosha and Dicer can predict prognosis of nasopharyngeal carcinoma.* **J Cancer Res Clin Oncol, 2012. 138(1): p. 49-56.**

124. **Kim, B., et al.,** *An essential microRNA maturing microprocessor complex component DGCR8 is up-regulated in colorectal carcinomas.* **Clin Exp Med, 2014. 14(3): p. 331-6.**

125. **Sand, M., et al.,** *Expression levels of the microRNA maturing microprocessor complex component DGCR8 and the RNA-induced silencing complex (RISC) components argonaute-1, argonaute-2, PACT, TARBP1, and TARBP2 in epithelial skin cancer.* **Mol Carcinog, 2012. 51(11): p. 916-22.**

126. **Guo, Y., et al.,** *Silencing the double-stranded RNA binding protein DGCR8 inhibits ovarian cancer cell proliferation, migration, and invasion.* **Pharm Res, 2015. 32(3): p. 769-78.**

127. **Obsteter, J., P. Dovc, and T. Kunej,** *Genetic variability of microRNA regulome in human.* **Mol Genet Genomic Med, 2015. 3(1): p. 30-9.**

128. **Wegert, J., et al.,** *Mutations in the SIX1/2 Pathway and the DROSHA/DGCR8 miRNA Microprocessor Complex Underlie High-Risk Blastemal Type Wilms Tumors.* **Cancer Cell, 2015. 27(2): p. 298-311.**

129. **Walz, A.L., et al.,** *Recurrent DGCR8, DROSHA, and SIX Homeodomain Mutations in Favorable Histology Wilms Tumors.* **Cancer Cell, 2015. 27(2): p. 286-97.**

130. **Torrezan, G.T., et al.,** *Recurrent somatic mutation in DROSHA induces microRNA profile changes in Wilms tumour.* **Nat Commun, 2014. 5: p. 4039.**

131. **Rakheja, D., et al.,** *Somatic mutations in DROSHA and DICER1 impair microRNA biogenesis through distinct mechanisms in Wilms tumours.* **Nat Commun, 2014. 2: p. 4802.**

132. **Melo, S.A., et al.,** *A genetic defect in exportin-5 traps precursor microRNAs in the nucleus of cancer cells.* **Cancer Cell, 2010. 18(4): p. 303-15.**

133. **Melo, S.A., et al.,** *A TARBP2 mutation in human cancer impairs microRNA processing and DICER1 function.* **Nat Genet, 2009. 41(3): p. 365-70.**

134. **Forstner, A.J., et al.,** *MicroRNAs as the cause of schizophrenia in 22q11.2 deletion carriers, and possible implications for idiopathic disease: a mini-review.* **Front Mol Neurosci, 2013. 6: p. 47.**

135. **Zhou, Y., et al.,** *Evaluation of six SNPs of MicroRNA machinery genes and risk of schizophrenia.* **J Mol Neurosci, 2013. 49(3): p. 594-9.**

136. **Sellier, C., et al.,** *Sequestration of DROSHA and DGCR8 by expanded CGG RNA repeats alters microRNA processing in fragile X-associated tremor/ataxia syndrome.* **Cell Rep, 2013. 3(3): p. 869-80.**

137. **Pokrishevsky, E., et al.,** *Aberrant localization of FUS and TDP43 is associated with misfolding of SOD1 in amyotrophic lateral sclerosis.* **PLoS One, 2012. 7(4): p. e35050.**

138. **Tomari, Y. and P.D. Zamore,** *MicroRNA biogenesis: drosha can't cut it without a partner.* **Curr Biol, 2005. 15(2): p. R61-4.**

139. **Jung, H.J., J.N. Hwang, and Y.R. Seo,** *The protective effect of mild hyperthermia against UV-mimetic agent 4-nitroquinoline-1-oxide (4NQO) in human colon cells.* **Res Commun Mol Pathol Pharmacol, 2004. 115-116: p. 123-33.**

140. **Gao, J., et al.,** *Integrative analysis of complex cancer genomics and clinical profiles using the cBioPortal.* **Sci Signal, 2013. 6(269): p. pl1.**

141. **Cerami, E., et al.,** *The cBio cancer genomics portal: an open platform for exploring multidimensional cancer genomics data.* **Cancer Discov, 2012. 2(5): p. 401-4.**

142. **Wallace, N.A., et al.,** *HPV 5 and 8 E6 abrogate ATR activity resulting in increased persistence of UVB induced DNA damage.* **PLoS Pathog, 2012. 8(7): p. e1002807.**

143. **Pulsipher, M., et al.,** *Subtyping analysis of Fanconi anemia by immunoblotting and retroviral gene transfer.* **Mol Med, 1998. 4(7): p. 468-79.**

144. **Wang, Y., et al.,** *MicroRNA-138 modulates DNA damage response by repressing histone H2AX expression.* **Mol Cancer Res, 2011. 9(8): p. 1100-11.**

145. **Rockstroh, M., et al.,** *Cell fractionation - an important tool for compartment proteomics.* **Journal of Integrated OMICS, 2011. 1(1): p. 135-143.**

146. **Shevchenko, A., et al.,** *Mass spectrometric sequencing of proteins silver-stained polyacrylamide gels.* **Anal Chem, 1996. 68(5): p. 850-8.**

147. **Licklider, L.J., et al.,** *Automation of nanoscale microcapillary liquid chromatography-tandem mass spectrometry with a vented column.* **Anal Chem, 2002. 74(13): p. 3076-83.**

148. **Rauch, A., et al.,** *Computational Proteomics Analysis System (CPAS): an extensible, open-source analytic system for evaluating and publishing proteomic data and high throughput biological experiments.* **J Proteome Res, 2006. 5(1): p. 112-21.**

149. **Craig, R. and R.C. Beavis,** *TANDEM: matching proteins with tandem mass spectra.* **Bioinformatics, 2004. 20(9): p. 1466-7.**

150. **Keller, A., et al.,** *Empirical statistical model to estimate the accuracy of peptide identifications made by MS/MS and database search.* **Anal Chem, 2002. 74(20): p. 5383-92.**

151. **Pothof, J., et al.,** *MicroRNA responses and stress granule formation modulate the DNA damage response.* **Cell Cycle, 2009. 8(21): p. 3462-8.**

152. **Wu, Q., et al.,** *The RNase III enzyme DROSHA is essential for microRNA production and spermatogenesis.* **J Biol Chem, 2012. 287(30): p. 25173-90.**

153. **Shiohama, A., et al.,** *Nucleolar localization of DGCR8 and identification of eleven DGCR8-associated proteins.* **Exp Cell Res, 2007. 313(20): p. 4196-207.**

154. Gong, M., et al., *Caspases cleave and inhibit the microRNA processing protein DiGeorge Critical Region 8.* **Protein Sci, 2012. 21(6): p. 797-808.**

155. Lee, Y., et al., *Drosha in primary microRNA processing.* **Cold Spring Harb Symp Quant Biol, 2006. 71: p. 51-7.**

156. Hanawalt, P.C. and G. Spivak, *Transcription-coupled DNA repair: two decades of progress and surprises.* **Nat Rev Mol Cell Biol, 2008. 9(12): p. 958-70.**

157. Macias, S., R.A. Cordiner, and J.F. Caceres, *Cellular functions of the microprocessor.* **Biochem Soc Trans, 2013. 41(4): p. 838-43.**

158. Moore, H.M., et al., *Quantitative proteomics and dynamic imaging of the nucleolus reveal distinct responses to UV and ionizing radiation.* **Mol Cell Proteomics, 2011. 10(10): p. M111 009241.**

159. Gromak, N., et al., *Drosha regulates gene expression independently of RNA cleavage function.* **Cell Rep, 2013. 5(6): p. 1499-510.**

160. Kamileri, I., I. Karakasilioti, and G.A. Garinis, *Nucleotide excision repair: new tricks with old bricks.* **Trends Genet, 2012. 28(11): p. 566-73.**

161. Yasuda, G., et al., *In vivo destabilization and functional defects of the xeroderma pigmentosum C protein caused by a pathogenic missense mutation.* **Mol Cell Biol, 2007. 27(19): p. 6606-14.**

162. Fousteri, M., et al., *Cockayne syndrome A and B proteins differentially regulate recruitment of chromatin remodeling and repair factors to stalled RNA polymerase II in vivo.* **Mol Cell, 2006. 23(4): p. 471-82.**

163. Hamperl, S. and K.A. Cimprich, *The contribution of co-transcriptional RNA:DNA hybrid structures to DNA damage and genome instability.* **DNA Repair (Amst), 2014. 19: p. 84-94.**

164. Sollier, J., et al., *Transcription-coupled nucleotide excision repair factors promote R-loop-induced genome instability.* **Mol Cell, 2014. 56(6): p. 777-85.**

165. **Nakazawa, Y., et al.,** *A semi-automated non-radioactive system for measuring recovery of RNA synthesis and unscheduled DNA synthesis using ethynyluracil derivatives.* **DNA Repair (Amst), 2010. 9(5): p. 506-16.**

166. **Jia, N., et al.,** *A rapid, comprehensive system for assaying DNA repair activity and cytotoxic effects of DNA-damaging reagents.* **Nat Protoc, 2015. 10(1): p. 12-24.**

167. **Giannakouros, T., et al.,** *Serine-arginine protein kinases: a small protein kinase family with a large cellular presence.* **FEBS J, 2011. 278(4): p. 570-86.**

168. **Varjosalo, M., et al.,** *The protein interaction landscape of the human CMGC kinase group.* **Cell Rep, 2013. 3(4): p. 1306-20.**

169. **Kannouche, P.L. and A.R. Lehmann,** *Ubiquitination of PCNA and the polymerase switch in human cells.* **Cell Cycle, 2004. 3(8): p. 1011-3.**

170. **Ha, M. and V.N. Kim,** *Regulation of microRNA biogenesis.* **Nat Rev Mol Cell Biol, 2014. 15(8): p. 509-24.**

171. **Filippov, V., et al.,** *A novel type of RNase III family proteins in eukaryotes.* **Gene, 2000. 245(1): p. 213-21.**

172. **Chong, M.M., et al.,** *Canonical and alternate functions of the microRNA biogenesis machinery.* **Genes Dev, 2010. 24(17): p. 1951-60.**

173. **Triboulet, R., et al.,** *Post-transcriptional control of DGCR8 expression by the Microprocessor.* **RNA, 2009. 15(6): p. 1005-11.**

174. **Vaksman, O., et al.,** *Argonaute, Dicer, and Drosha are up-regulated along tumor progression in serous ovarian carcinoma.* **Hum Pathol, 2012. 43(11): p. 2062-9.**

175. **Kwon, S.Y., et al.,** *Complexity in regulation of microRNA machinery components in invasive breast carcinoma.* **Pathol Oncol Res, 2014. 20(3): p. 697-705.**

176. **Kitagawa, N., et al.,** *Downregulation of the microRNA biogenesis components and its association with poor prognosis in hepatocellular carcinoma.* **Cancer Sci, 2013. 104(5): p. 543-51.**